



THE UNIVERSITY OF
SYDNEY

COPYRIGHT AND USE OF THIS THESIS

This thesis must be used in accordance with the provisions of the Copyright Act 1968.

Reproduction of material protected by copyright may be an infringement of copyright and copyright owners may be entitled to take legal action against persons who infringe their copyright.

Section 51 (2) of the Copyright Act permits an authorized officer of a university library or archives to provide a copy (by communication or otherwise) of an unpublished thesis kept in the library or archives, to a person who satisfies the authorized officer that he or she requires the reproduction for the purposes of research or study.

The Copyright Act grants the creator of a work a number of moral rights, specifically the right of attribution, the right against false attribution and the right of integrity.

You may infringe the author's moral rights if you:

- fail to acknowledge the author of this thesis if you quote sections from the work
- attribute this thesis to another author
- subject this thesis to derogatory treatment which may prejudice the author's reputation

For further information contact the University's Director of Copyright Services

sydney.edu.au/copyright

THE FUNCTIONAL SIGNIFICANCE
OF HUMAN CONNEXIN40
MUTATIONS ON ATRIAL
PHYSIOLOGY AND PROPENSITY
TO ATRIAL ARRHYTHMIA

A thesis submitted in fulfilment of the requirements for the
degree of Doctor of Philosophy in the Faculty of Medicine at the
The University of Sydney

Ajita Kanthan

March 2013

“Every day you may make progress. Every step may be fruitful. Yet there will stretch out before you an ever-lengthening, ever-ascending, ever-improving path. You know you will never get to the end of the journey. But this, so far from discouraging, only adds to the joy and glory of the climb.”

Sir Winston Churchill (1874 – 1965)

STATEMENT OF ORIGINALITY

I, Ajita Kanthan, hereby declare that this thesis contains work that has not been presented for the award of any other degree at any university. The work presented in this thesis is the result of my own investigation with the assistance from others as acknowledged herein, and contains no material previously published or written by another person except where due reference is made in the text.

Ajita Kanthan

ACKNOWLEDGMENTS

As I reflect over the years as a PhD student, it is clear that I owe a large part of my success and happiness to key individuals.

“Indebted for life” says it all when I think of my wife Yen, and children Anthony and Jasmine. They have been patient and sacrificed much so that I may succeed with my work.

I would like to thank Dr Eddy Kizana for not only being my supervisor, but also my mentor and friend. His patience, encouragement, and wisdom gave me the latitude to dream and grow.

There are a great many from Westmead Hospital – Stuart Thomas, Peter, Renuka, Jim, Tony, and Karen to mention a few. Your support is truly appreciated.

Thank you to the staff of WMI (especially Lionel, Monica, Liz, Carolyn, Medhi, Virginia, and Ross) and to Ian Alexander, Grant Logan, and the rest of the gene therapy group at the CMRI for their advice.

This work was funded by an Australian Postgraduate Award.

PRESENTATIONS, ABSTRACTS, GRANTS AND AWARDS

Kanthan A, Fahmy P, Rao R, Thomas SP, Kizana E. The Effects of the Connexin40 Mutations P88S and G38A on Cardiac Physiology in the Intact Animal. AHA Scientific Sessions 2012 (Presentation)

Kanthan A, Fahmy P, Rao R, Thomas SP, Alexander IE, Kizana E. Methods for *in-vivo* atrial gene transfer using adeno-associated virus 2/9. Heart, Lung and Circulation 2012; 21(S1):296 (Abstract)

Kanthan A, Ross J, Rao R, et al. A System for Studying Electrical Conduction in Lentivector Gene-Modified Primary Cardiomyocytes. CSANZ Conference 2011 (Presentation) and Heart, Lung and Circulation 2011; 20(S2):79 (Abstract)

Awards and Grants Related to this Thesis

AHA Travelling Fellowship, from the Cardiac Society of Australia and New Zealand (2012)

Westmead Charitable Trust Grant, Westmead Hospital (2011)

TABLE OF CONTENTS

STATEMENT OF ORIGINALITY	iii
ACKNOWLEDGMENTS.....	iv
PRESENTATIONS, ABSTRACTS, GRANTS AND AWARDS	v
TABLE OF CONTENTS	vi
LIST OF FIGURES.....	x
LIST OF TABLES.....	xi
LIST OF ABBREVIATIONS	xii
CHAPTER 1	1
Introduction and Literature Review	1
1.1 Introduction	1
1.2 Literature Review	4
1.2.1 Connexins and gap junctions	4
1.2.2 Connexins, Conduction, and Arrhythmia	21
1.2.2.1 Genetically Engineered Mice Models.....	22
1.2.2.2 Non-Genetically Engineered Animal Models	40
1.2.2.3 Human Studies.....	50
1.2.3 Summary.....	62
CHAPTER 2	65
Materials and General Methods	65
2.1 Molecular Biology.....	65
2.1.1 Chemicals, reagents, and plastic/glassware	65
2.1.2 Bacterial strains and plasmids	65
2.1.3 Bacterial growth media.....	66
2.1.4 Propagation of plasmids.....	68
2.1.4.1 Preparation of electro-competent cells	68
2.1.4.2 Bacterial transformation with plasmid DNA.....	69
2.1.4.3 Large scale preparation of plasmid DNA	70
2.1.5 Estimation of plasmid DNA concentration and purity.....	71
2.2 Cell Culture.....	73
2.2.1 Cell lines, reagents, and plastic/glassware	73
2.2.2 General cell culture methods	74
2.2.2.1 Cell counting using a haemocytometer.....	74
2.2.2.2 Subculture of adherent HEK293T cells.....	77
2.2.2.3 Short and long term storage of HEK293T cells	77
2.2.3 Neonatal rat ventricular cardiomyocyte cultures	78
2.2.3.1 Plating surface preparation	78
2.2.3.2 Isolation of neonatal rat ventricular cardiomyocytes	79
2.2.3.3 Post plating care of cardiomyocyte cultures	81
2.3 Production and Application of Lentiviral Vectors.....	82
2.3.1 Lentiviral vector plasmids.....	82
2.3.2 Vector production by lipofection	82
2.3.3 Vector purification and concentration.....	84
2.3.4 Assigning titre to vectors	85
2.3.4.1 Transduction of HEK293T cells	85

2.3.4.2 Genomic DNA extraction.....	86
2.3.4.3 Real time quantitative PCR of genomic DNA.....	87
2.3.5 Lenti-vector transduction of primary cardiomyocytes	88
2.3.6 <i>In vivo</i> lenti-vector mediated transduction of rat left atrium	89
2.4 Immunofluorescence – Staining for Connexins	91
2.4.1 Antibodies for immunofluorescence	91
2.4.2 Atrial tissue sectioning	91
2.4.3 Fixation, permeabilisation and immunostaining	93
2.4.4 Fluorescent image acquisition and processing	94
2.5 Histology – Inflammation and Fibrosis	97
2.5.1 Inflammation - Haematoxylin and Eosin staining	97
2.5.2 Fibrosis - Picro-Sirius Red staining.....	98
2.5.3 Image acquisition and processing.....	98
2.6 Immunoblotting.....	100
2.6.1 Antibodies for immunoblotting.....	100
2.6.2 Protein extraction	100
2.6.3 Protein estimation	102
2.6.4 Immunoblotting.....	103
2.7 Quantification of Tissue Connexin mRNA.....	106
2.7.1 mRNA extraction and purification	106
2.7.2 cDNA synthesis from mRNA.....	107
2.7.3 Real time quantitative PCR.....	108
2.8 Primary Cardiomyocyte Electrophysiology	110
2.8.1 The multi-electrode array	110
2.8.2 Culture recording.....	111
2.8.3 Culture stimulation	111
2.9 <i>In Vivo</i> Studies	116
2.9.1 Anaesthesia, intubation, ventilation, and positioning	116
2.9.2 Surface electrocardiography	117
2.9.3 Trans-oesophageal cardiac stimulation and recording	118
2.9.4 Thoracic surgery	119
2.9.5 Atrial tissue extraction, preparation, and storage	120
2.10 Statistics	122
CHAPTER 3	124
A System for Assessment of Lentivector Gene Modified Primary Cardiomyocytes	124
3.1 Introduction and Aims	124
3.2 Methods.....	127
3.2.1 Vector packaging and titration	127
3.2.2 Myocyte isolation, transduction and culture	127
3.2.3 Transduction optimisation	128
3.2.4 Multi-electrode array studies	128
3.3 Results	131
3.3.1 Optimal multiplicity of infections	131
3.3.2 Culture capturability	131
3.3.3 Isochronal maps and conduction velocities	133
3.4 Discussion	139
3.4.1 Assessing conduction velocities and capturability	139
3.4.1.1 Characteristics of KIR2.1 over expression.....	140
3.4.1.2 Characteristics of CX43Δ8 over expression.....	140
3.4.1.3 Characteristics of eGFP over expression	141
3.4.2 Implications of these findings	141

CHAPTER 4	143
The Human Connexin40 Mutations P88S, G38A, and A96S Alter Primary Cardiomyocyte Coupling and Conduction	143
4.1 Introduction and Aims	143
4.2 Methods.....	146
4.2.1 Vector packaging and titration	146
4.2.2 Myocyte isolation, transduction and culture	146
4.2.3 Multi-electrode array studies	147
4.2.5 Immunoblotting.....	149
4.2.6 Immunofluorescence.....	149
4.3 Results	151
4.3.1 Isochronal maps and conduction velocities	153
4.3.2 Immunofluorescence and immunoblotting	154
4.4 Discussion	161
4.4.1 Characteristics of wild-type Connexin40	161
4.4.2 Characteristics of the G38A Connexin40 Mutation	162
4.4.3 Characteristics of the A96S Connexin40 Mutation	162
4.4.4 Characteristics of the P88S Connexin40 Mutation	163
4.4.5 Other considerations	163
CHAPTER 5	166
<i>In Vivo</i> Somatic Atrial Gene Transfer of Human Connexin40 Mutations Increases the Propensity for Arrhythmia.....	166
5.1 Introduction and aims.....	166
5.2 Methods.....	169
5.2.1 Vector packaging and titration	169
5.2.2 Left atrial transduction.....	169
5.2.3 Electrophysiology studies.....	172
5.2.4 Morphometric studies.....	172
5.2.5 Immunoblotting.....	173
5.2.6 Immunofluorescence.....	173
5.2.7 Haematoxylin and Eosin staining	174
5.2.8 Picro-Sirius Red staining.....	175
5.3 Results	177
5.3.1 Electrophysiology studies.....	177
5.3.2 Immunofluorescence	182
5.3.3 Immunoblotting.....	182
5.3.4 Connexin43 mRNA	188
5.3.4 Inflammation and fibrosis	188
5.4 Discussion	191
5.4.1 <i>In vivo</i> characteristics of A96S, P88S, and G38A.....	191
5.4.2 <i>In vivo</i> characteristics of wild-type connexin40	193
5.4.3 Other considerations	194
5.4.4 Implications of somatic mutations	195
CHAPTER 6	197
Summary and General Discussion	197
6.1 <i>In Vitro</i> Ion Channel Screening Systems	198
6.1.1 Summary.....	198
6.1.2 Limitations	199
6.1.2.1 Measurement of cellular electrical activity	199
6.1.2.2 NRVM cellular electrophysiology	200

6.1.2.3 Protein interactions and toxicity	200
6.1.3 Future Directions	201
6.1.3.1 MEA technology	201
6.1.3.2 Cellular technologies	202
6.2 Connexin Mutations and Conduction	203
6.2.1 Summary	203
6.2.2 Limitations	204
6.2.2.1 Somatic mutations and <i>in vitro</i> implications	204
6.2.2.2 Germline mutations and <i>in vitro</i> implications	205
6.2.3 Future Directions	206
6.3 Connexin Mutations and Arrhythmia	207
6.3.1 Summary	207
6.3.2 Limitations	209
6.3.2.1 Mechanisms: From cells to arrhythmia	209
6.3.3. Future Directions	209
6.4 Connexin Mutations and Atrial Arrhythmia – Final Comments	211
CHAPTER 7	213
Bibliography	213

LIST OF FIGURES

Figure 1.1 Connexin structure.....	5
Figure 1.2 Gap junction structure.....	6
Figure 1.3 Action potential propagation.....	9
Figure 1.4 Human cardiac connexin isotype distributions.....	17
Figure 2.1: Left atrial transduction.....	90
Figure 2.2: Multi-electrode arrays.....	112
Figure 2.3: Multi-electrode stage.....	114
Figure 2.4: MEA recording system.....	115
Figure 3.1: NRVM's study flow diagram. (NT - Non-transduced).....	130
Figure 3.2: Transduction efficiency of eGFP transduced cultures.....	132
Figure 3.3: eGFP fluorescence of an NRVM monolayer on an MEA.....	136
Figure 3.4: Representative Isochronal maps.....	137
Figure 3.8: Graphical representation of mean conduction velocities.....	138
Figure 4.1: NRVM study flow diagram.....	148
Figure 4.2: Representative isochronal maps and mean conduction velocities.....	155
Figure 4.3: Graphical representation of conduction velocities.....	156
Figure 4.4: Co-Immunostaining of NRVM cultures.....	157
Figure 4.5: Immunoblots for connexin 40 expression in NRVM's.....	158
Figure 4.6: Immunoblots for connexin 43 expression in NRVM's.....	159
Figure 5.1: <i>In vivo</i> study groups.....	170
Figure 5.2: <i>In vivo</i> study protocol.....	171
Figure 5.3: Image processing of Picro-Sirius Red tissue staining.....	176
Figure 5.4: Representative Subcutaneous Electrocardiograms during Sinus Rhythm.....	179
Figure 5.5: Sinus Rhythm versus Atrial Fibrillation.....	180
Figure 5.6: Mean durations of atrial fibrillation.....	181
Figure 5.7: Immunofluorescence of atrial tissue sections for Cx40.....	183
Figure 5.8: Immunofluorescence of atrial tissue sections for Cx43.....	184
Figure 5.9: Immunoblots for left atrial Cx40 expression.....	185
Figure 5.10: Immunoblots for left atrial Cx43 expression.....	186
Figure 5.11: Quantitative PCR for Cx43 mRNA.....	187
Figure 5.12: Haematoxylin and eosin stains of atrial tissue.....	189
Figure 5.13: Pico Sirius Red stains of atrial tissue.....	190

LIST OF TABLES

Table 2.1: DNA Plasmids used within this Research Project	67
Table 2.2: Cell types used in cell culture experiments.....	75
Table 2.3 Plasmids for Lentiviral Vector Production	83
Table 2.4: Immunofluorescence Antibodies.....	92
Table 2.5: Filter Sets for Leica DMIL Microscope	95
Table 2.6: Excitation Wavelengths and Emission Filter Sets for the Olympus Confocal Microscope	96
Table 2.7: Secondary antibodies for immunoblotting.....	101
Table 3.1: Monolayer capturability and beat frequency	135
Table 4.1: Summary of Cx43 / Cx40 levels and conduction velocities for each group.....	152
Table 5.1: Morphometric Characteristics.	178

LIST OF ABBREVIATIONS

°C, degrees Celsius

μA, microamp(s)

μg, microgram(s)

μL, microliter(s)

μS, micro-Siemen(s)

A96S, Alanine96→Serine substitution in connexin40

Add in reference for Luna et al for HandE staining

AF, atrial fibrillation

AV, atrioventricular

CCD, charge-coupled device

cDNA, complementary deoxyribonucleic acid

cm, centimetre(s)

cm/s, centimetres per second

CMOS, complementary metal–oxide–semiconductor

CMV, cytomegalovirus

CO₂, carbon dioxide

cPPT - central polypurine tract

cPPT, central polypurine tract

cRNA, complementary ribonucleic acid

CV - conduction velocity

Cx40, connexin40

Cx43, connexin43

CX43 Δ 8, connexin43 bearing a deletion of 8 amino acid residues

DAPI, 4',6-diamidino-2-phenylindole

DEPC, diethyl pyrocarbonate

DMEM, Dulbecco's Modified Eagles Medium

DMSO, dimethyl sulfoxide

DNA, deoxyribonucleic acid

dNTP, deoxyribonucleotide triphosphate

DPBS, Dulbecco's phosphate buffered saline

dsDNA, double stranded deoxyribonucleic acid

ECG, electrocardiogram

EDTA, Ethylenediaminetetra-acetic acid

eGFP, enhanced green fluorescent protein

EPS, electrophysiology study

FBS, fetal bovine serum

Fib, fibrillatory appearing spontaneous contractile activity

G38A, Glycine38→Aspartic acid substitution in connexin40

GAPDH, glyceraldehyde 3-phosphate dehydrogenase

HBSS, Hank's Balanced Salt Solution

HEK, human embryonic kidney

HEPES, 4-[2-hydroxyethyl]-1-piperazineethanesulfonic acid

HIV, human immunodeficiency virus

HRP, horseradish peroxidase

Hz, Hertz

IMT - Institute of Microtechnology

INa, sodium current

Kir2.1, inward-rectifier potassium ion channel (KCNJ2 gene)

kV, kilovolt(s)

LB, Luria-Bertani

LDS, lithium dodecyl sulfate

LTR - long terminal repeat

LV, lentiviral vector

MEA, multi-electrode array

MEM, minimum essential media

mg, milligram(s)

MgCl, magnesium chloride

mL, millilitre(s)

mm, millimetre(s)

mM, millimolar

M-ML-VRT, Moloney Murine Leukaemia Virus Reverse
Transcriptase

MOI, multiplicity of infection

MQH-20, reagent grade water

mRNA, messenger ribonucleic acid

ms, millisecond(s)

N2A, Neuro 2A cell line

nm, nanometre(s)

NRVM, neonatal rat ventricular myocyte

NT, non-transduced

P88S, Proline88→Serine substitution in connexin40

PBS, phosphate buffered saline

PBST - Tween 20 in PBS

PC, Personal Computer

PCB, printable circuit board

PCR, polymerase chain reaction

PVC, polyvinyl chloride

PVDF - polyvinylidene fluoride

RIPA, radioimmunoprecipitation assay buffer

rpm, revolutions per minute

RRE, rev-responsive element

SA, sinoatrial

SD - Standard Deviation

SDS-PAGE - sodium dodecyl sulfate polyacrylamide gel electrophoresis

SIN - self-inactivating

siRNA, small interfering ribonucleic acid

SOC, Super Optimal broth with Catabolite repression

TB, transformation buffer

TBST, Tween 20 in Tris buffered saline

TE, Tris-EDTA

v/v, volume per volume

VSV, vesicular stomatitis virus

w/v, weight per volume

WPRE, woodchuck hepatitis virus post-transcriptional regulatory element

wtCx40, wild-type connexin40

CHAPTER 1

Introduction and Literature Review

1.1 Introduction

Atrial fibrillation (AF) is the most common cardiac arrhythmia, affecting 1% of the general population, 6% of people over the age of 65, and 9% of people over the age of 80.^{1, 2} With a squaring of the population age distribution, the overall prevalence of AF and its impact on the health system is set to increase.^{3, 4}

AF is associated with considerable morbidity and mortality. Specifically, AF is an independent risk factor for stroke, occurring in up to 19% of stroke patients over the age of 70.⁵ Furthermore, AF is associated with a 1.5 to 1.9 fold increased risk in all-cause mortality.⁶

The effectiveness of medical therapy targeting rate and/or rhythm control and stroke risk reduction is modest at best and not without side effects. In particular, warfarin anti-coagulant therapy reduces the relative risk of stroke by only 70%. Furthermore, the risk of major bleeding with warfarin use is 0.5%-1% per annum and in

those over the age of 80, this risk can rise to as high as 13% in the first year.⁷

Short of open heart surgery, the only alternative to current medical therapy is percutaneous catheter-based radiofrequency ablation which results in electrical isolation of the pulmonary veins. Pulmonary vein isolations are successful in eradicating AF in ~50% of cases. Often, patients must endure up to 3 separate ablation sittings before a 70% success rate is achieved. The risk of ablation procedures is considerable with a 6% rate of major complications that include cardiac tamponade, pulmonary vein stenosis, arteriovenous fistulas, thromboembolism, need for open heart surgery, and death.⁸

Clearly with an aging population and the sub-optimal treatment options currently available, there is a desperate need for a greater understanding of the disease process.

Over the last 2 decades, there has been mounting evidence that connexins play a significant role in cardiac myocyte electrical coupling. In particular, alterations in levels and patterns of

connexin expression in humans have been purported to facilitate the substrate required for the chronic form of AF.⁹

More recently, one germline and three somatic mutations of the gene encoding the gap junction protein connexin40 (Cx40) in patients suffering from idiopathic AF were identified by Gollob et al. and published in the New England Journal of Medicine.¹⁰ Since this first discovery, Gollob's lab has identified a further somatic mutation, this time in connexin43 (Cx43), in a patient with lone AF.¹¹ One of the major limitations of these disease-causing gene discoveries is the lack of a convincing, demonstrable, functional effect on electrical cardiac conduction that could underpin the generation of AF.

The following section will assess peer-reviewed literature on Cx40 and Cx43, with a particular focus on their functional roles in cardiac conduction. With a greater understanding of the consistencies and inconsistencies of the literature, the subsequent *in vitro* and *in vivo* research will aim to assess the functional effects of the above mentioned Cx40 mutations, in particular focusing on their propensity to cause AF.

1.2 Literature Review

1.2.1 Connexins and gap junctions

Gap Junction Structure

Connexins are a family of phosphoproteins consisting of 4 hydrophobic trans-membrane α -helices joined by 2 extracellular loops and 1 intracellular loop, and a hydrophilic cytoplasmic carboxy-terminal tail as shown in Figure 1.1.¹² Approximately 21 different connexin isotypes have been identified.¹³ The trans-membrane α -helices are relatively conserved between isotypes, while the connecting loops and tail vary widely, hence determining isotype specific properties.¹⁴

Connexins group together in hexamers to form trans-membrane hemi-channels termed connexons as shown in Figure 1.2A. In cardiac myocytes, connexons actively coalesce within the intercalated disks at sites of cadherin mediated cell-cell adhesion called gap junctions. Here, the extracellular faces of connexons dock with each other in a one to one fashion between adjacent cells forming inter-cellular communications through a central aqueous pore as shown in Figure 1.2B.¹⁴ Once formed,

Figure 1.1 Connexin structure

A connexin (pink) consists of 4 trans-membrane α -helices (M1, M2, M3, M4) linked together by 2 extracellular loops (EL1, EL2) and 1 cytoplasmic loop (CL). Both the N terminus and C terminus have an intracellular location.

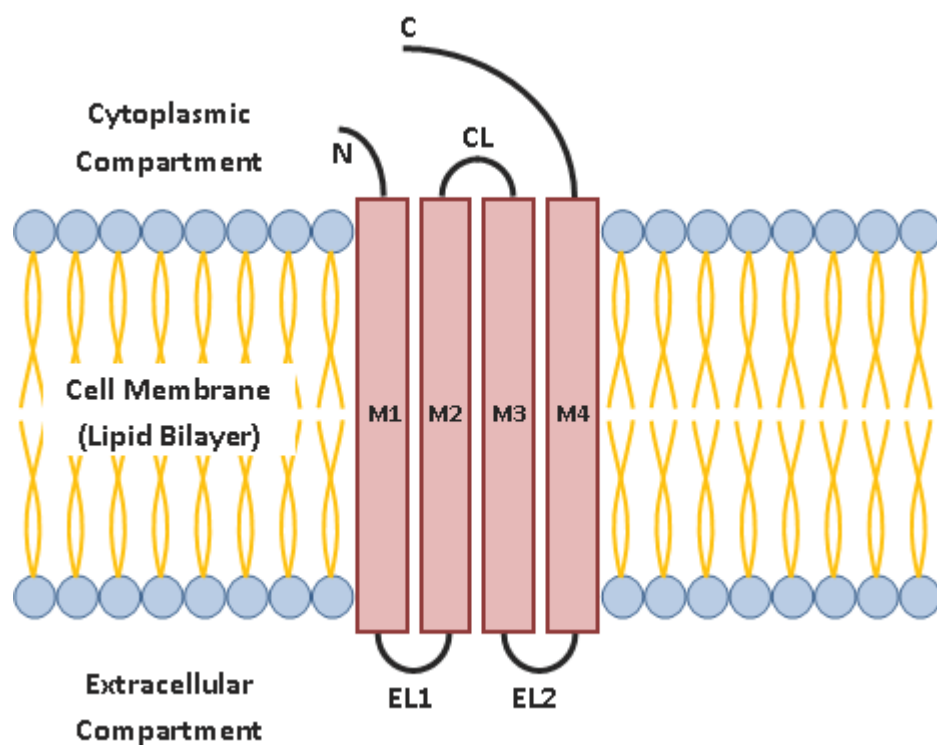
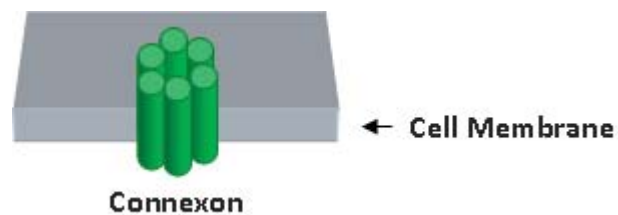


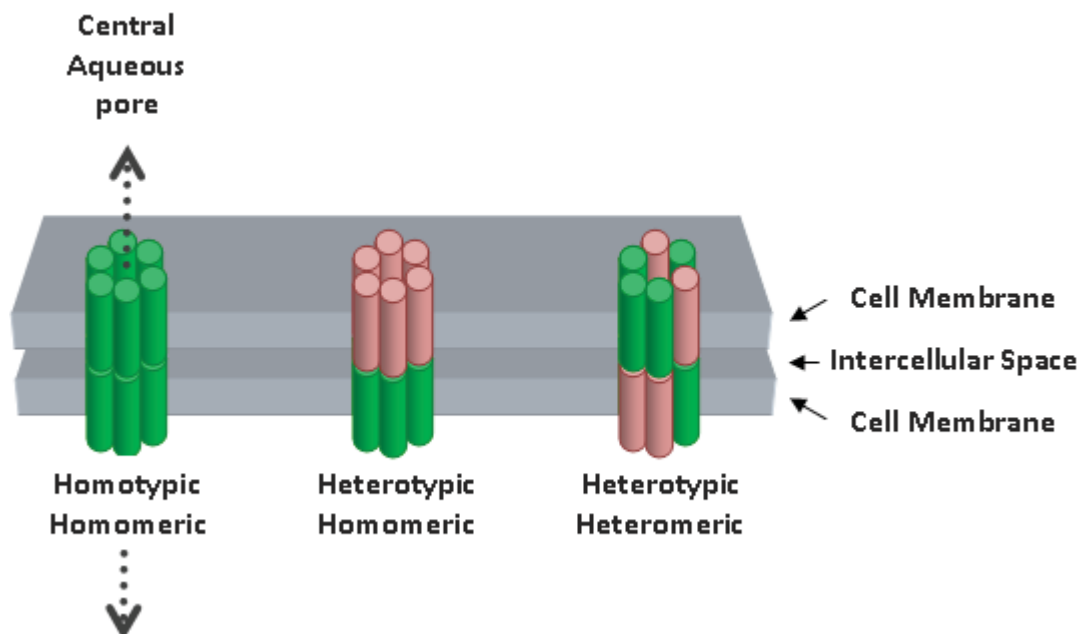
Figure 1.2 Gap junction structure

A) A connexon consisting of 6 trans-membrane connexins. B) Two cell membranes connected by docked connexons with a central aqueous pore (dotted arrow). Connexons can vary in the proportion and distribution of their constituent connexin isotypes (green and pink).

A



B



connexons have a relatively short half-life, being internalised and degraded after 1 to 5 hours.¹⁵⁻¹⁷

Connexon hemi-channels can be either homomeric, being formed from only one connexin isotype, or heteromeric, being formed from multiple connexin isotypes. Coupled connexons can be homotypic, containing the same connexins, or heterotypic, containing different connexins as shown in Figure 1.2B.¹⁴

A connexons' isotype content, degree of phosphorylation, and location, determines its functional capacity for intercellular passive ion transfer.¹⁴

Gap Junction Conductance

Action potential propagation in cardiac myocytes is dependent on the extracellular and intra cellular passive transfer of ions across an action potential wavefront between depolarised and polarised zones as shown in Figure 1.3. Transfer of ions allows the resting membrane potential to be depolarised to the thresholds required for membrane ion channel activation of action potentials.¹⁸

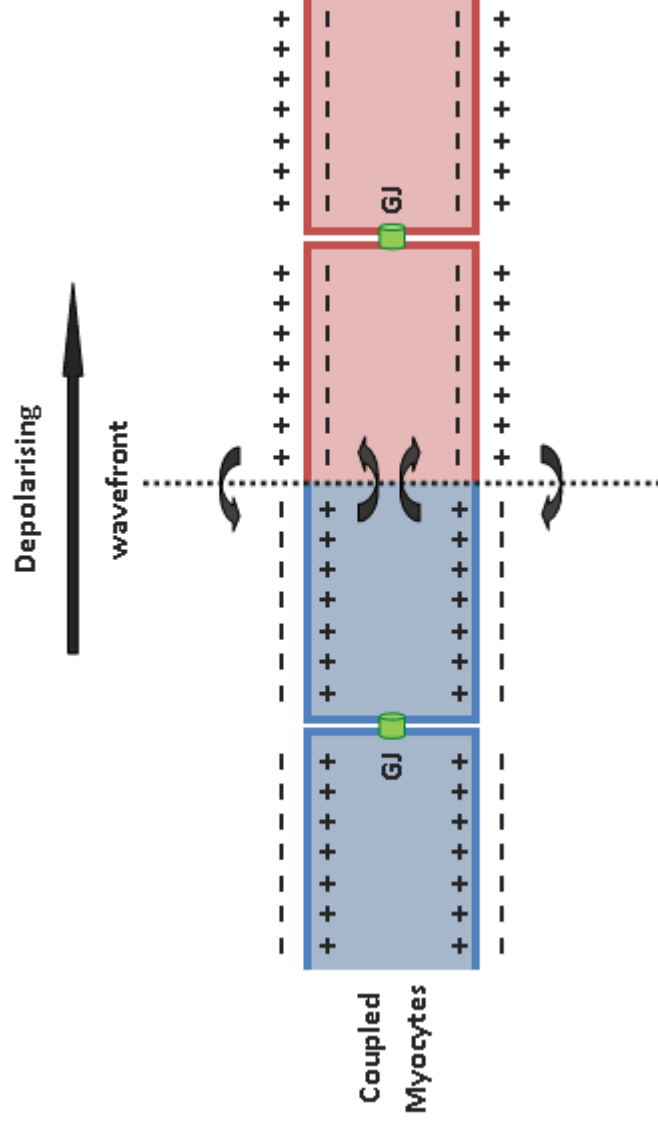
Propagation velocity is determined by the rate of passive transfer of ions between both zones. This in turn is determined by drivers of passive ion transfer and resistors to this process. The main drivers are action potential amplitude and speed of action potential generation. The main resistors are intra-cellular cytoplasmic resistance and inter-cellular gap junction coupled connexon resistance. The resistance of the central aqueous pore of cell-cell coupled connexons is inversely proportional to its conductance capacity.¹⁸

Pioneering dual whole cell voltage clamping in the study of gap junctions, Neyton et al first quantified junctional conductance and average unitary conductance's of constituent channels in rat lacrimal gland cells. The study demonstrated the presence of variable channel conductance during voltage gating with an average unitary conductance in the fully open state of 120pS.¹⁹

Using a similar method to Neyton et al, Veenstra et al demonstrated an average channel unitary conductance of 164 ± 26 pS in embryonic chicken ventricular myocytes, while Burt et al

Figure 1.3 Action potential propagation

Depolarising wavefront (dotted line) advancing across coupled myocytes from depolarised (blue) to polarised zones (red). Curved arrows show the direction of passive cation movement. Gap junctions (GJ) shown in green.



obtained a clearly different average unitary conductance of 50 ± 2 pS in neonatal rat ventricular myocytes.^{20, 21} These early studies however, did not consider the effects of differing patterns of connexin isotype expression between cell types.

Following the identification of multiple connexin isotypes, dual whole cell voltage clamping studies revealed conductance differences between homomeric homotypic channels consisting of either connexin40 (Cx40) or connexin43 (Cx43). In HeLa cells, Cx40 channels were associated with a larger average unitary conductance of 121pS to 153pS compared to the 40pS to 60pS of Cx43 channels.²²

When the voltage applied across a uniform channel is changed slowly from positive to negative, a slow symmetrical change in the absolute amplitude of ion conductance from one direction to the other is often observed and is referred to as symmetrical voltage gating. When a channel's structure is asymmetric from end to end, then different directional amplitudes of ion conductance between similar positive and negative voltages are observed, a phenomenon referred to as asymmetrical voltage gating.

Valiunas et al observed a similar pattern of average unitary conductance's to that identified in previous studies with levels of 135pS and 76pS for junctions composed of either Cx40 or Cx43 respectively, when expressed in connexin-null HeLa cells. Macroscopic junctional conductance sensitivities to voltage gating in these channels were symmetrical. Homomeric heterotypic Cx40 and Cx43 channels however demonstrated both asymmetrical unitary conductance's (~60/100pS) and asymmetrical voltage gating sensitivities. In addition, in HeLa cells, when compared to junctions composed of either Cx40 or Cx43 homomeric homotypic channels, gap junctions consisting of channels homomeric and heterotypic for connexins 40 and 43 demonstrated markedly reduced total conductances of 73% and 68% respectively.²³

Cottrell and co-workers further demonstrated that connexins 40 and 43 were capable of forming a wide variety of heteromeric/heterotypic channels when studied in Rin and A7r5 cells. Channel unitary conductances varied widely and were predominately lower than those of channels homomeric and homotypic for Cx40 (<120pS). Heteromeric/heterotypic channels higher in Cx43 content frequently possessed conductances lower than 60pS. Altered asymmetrical junctional voltage gating

sensitivities were also observed when compared to homomeric/heterotypic Cx40 and Cx43 channels.²⁴ A second study by the group involved altering the ratio of Cx40 to Cx43 in A7r5 cells from a baseline of 2.7:1 to 5.3:1 and 10.6:1 using Cx40 transfection. When these three groups of A7r5 cells were coupled to Rin43 cells, an increase in the Cx40:Cx43 ratio was associated with a non-linear reduction in unitary conductances to below that of Rin43/Rin43 coupled cells. When the three A7r5 groups were coupled to Rin40 cells, there was a small non-linear reduction in unitary conductances to below that of Rin40/Rin40 coupled cells. The results suggest a J shaped drop in conductance from that of Cx40 only channels to Cx43 channels as the ratio of Cx40 to Cx43 drops in a connexon. Unfortunately, a similar experiment using Cx43 transfected A7r5 cells was not performed.²⁵

More recently, Gollob et al demonstrated the effects of Cx40 missense mutations, identified in patients with idiopathic atrial fibrillation (AF), on gap junction conductance. Dual whole cell voltage clamping of transfected N2A cells revealed almost complete abolishment of channel activity with P88S, A96S, and G38A mutants. Immunofluorescence in each case revealed an altered pattern of gap junction expression with intracellular

accumulation of mutant connexins. When either P88S or A96S mutants were co-transfected with only wild-type Cx40 or wild-type Cx40 and Cx43 in xenopus oocytes, junctional conductance fell to well below that of their wild-type connexin only controls respectively. The results suggested that mutations in Cx40 could exert a dominant negative effect on gap junction conductance. Importantly the cellular pattern of expression of wild type Cx43 and Cx40 in oocytes was not assessed to exclude a cellular manufacturing/transport problem. This was particularly important given that an altered pattern of mutant Cx40 expression had been identified in N2A cells with immunofluorescence.

Gollobs lab went on to study the gap junctional effects of a somatic Cx43 frame-shift (932delC) mutation that was identified in a patient with lone AF. Coupled 932delC transfected N2A cells revealed a marked reduction in junctional conductance when compared to wild-type Cx43 transfected controls. Furthermore, when compared to wild-type Cx43 only junctions, there was a dominant negative effect on junctional conductance when 932delC was co-transfected with either wild-type Cx43 or wild-type Cx40. Results of studies repeated in xenopus oocytes were similar to the N2A studies except in the setting of 932delC and

Cx40 co-transfection, where there was a failure to exhibit a dominant negative effect on conductance. Co-transfection with 932delC, wild-type Cx43, and wild-type Cx40 resulted in a small but significant reduction in junctional conductance compared to wild-type only connexin co-transfection. Immunofluorescence in HeLa cells transfected with 932delC revealed only sparse gap junction formation with intracellular retention within the Golgi apparatus. This was in contrast to HeLa cells transfected with wild-type Cx43 only, which formed numerous gap junctions with co-localization. When 932delC was co-transfected with either wild-type Cx43 or Cx40 into HeLa cells, a dominant negative effect on wild-type connexin expression was observed with sparse gap junction formation and intracellular accumulation. This again was in contrast to HeLa cells co-transfected with wild-type Cx43 and Cx40, which formed numerous gap junctions with co-localization. The dominant negative effect on expression of both wild-type connexins was also observed in sections of atrial tissue using a diaminobenzidine (DAB) chromagen system. Importantly however, immunofluorescence was not performed within N2A cells and oocytes to elucidate the differences in conductance results observed between both cells types.¹¹

While gap junctions clearly have varying conductance's and hence likely varying effects on tissue conduction velocities, directional asymmetry of voltage gating sensitivities and mutations may further increase the arrhythmogenic potential of cardiac tissue. The proportional content of connexin isotypes and mutants in gap junction channels and the cellular mechanisms involved in controlling proportions during normal physiology and disease states however, have yet to be determined.

Connexins and Cardiac Distribution

Connexin isotype expression varies between the different chambers and structures of the heart as shown in Figure 1.4. Hence the role of connexin isotype expression at various areas of the heart is best appreciated by the functional conduction velocities at those areas. Of note, Davis et al demonstrated in humans that cells of the bundle branches, the fastest conducting cells of the heart, contained the largest gap junctions with abundant levels of connexins 40, 43, and 45. In contrast, the sino-atrial and atrioventricular nodal cells had the smallest gap junctions. Cells from both nodes expressed small levels of connexins 45 and 40, and atrioventricular nodal cells also

expressed Cx43. Atrial and ventricular myocytes contained moderate sized gap junctions. Atrial myocytes expressed moderate amounts of connexins 40, 43, and 45, while ventricular myocytes expressed only connexins 43 and 45.²⁶

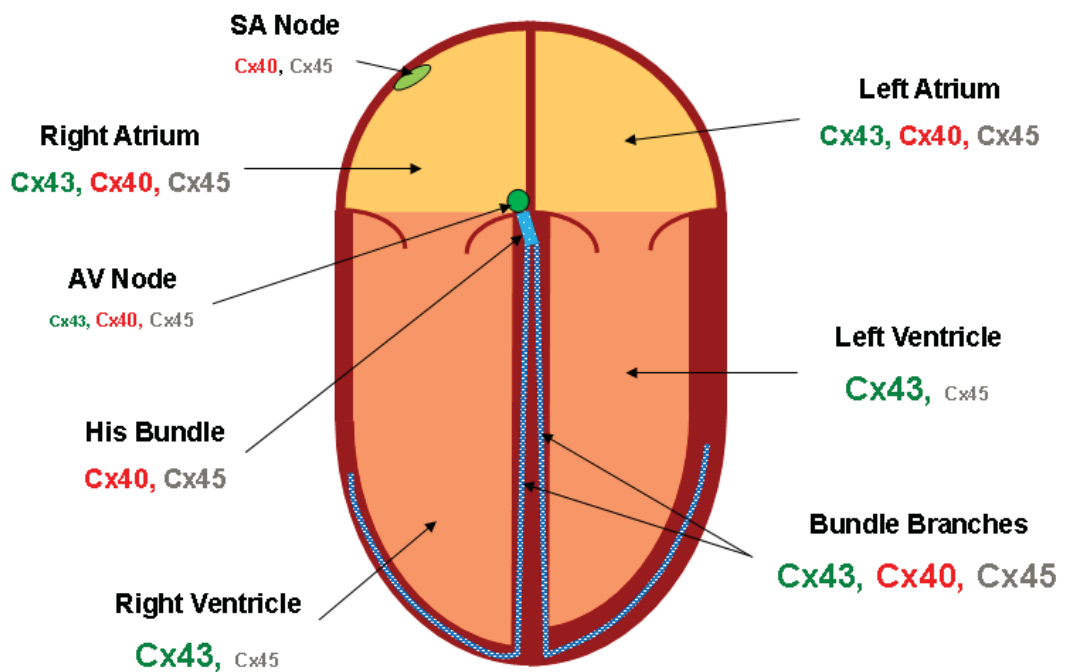
It should be noted that there is also variation of connexin isotype expression in the same areas between mammalian species. The results are best demonstrated by the differences in Cx40 distribution between guinea pig and rat hearts. Gros et al demonstrated in guinea pigs that Cx40 was only expressed within atrial myocytes, being absent from the ventricles and conducting system. In contrast, rats expressed Cx40 only within the His-Purkinje/bundle branch system. Both species clearly had a Cx40 expression profile that was also different to that of humans.^{26, 27}

Tissue Anisotropy

Anisotropic tissue conduction refers to the directional dependence of conduction velocity imparted by tissue structure. Hence when conduction velocity in one direction (such as parallel to fibre orientation) is different to another direction (such as perpendicular to fibre orientation), anisotropic conduction is said to exist. The

Figure 1.4 Human cardiac connexin isotype distributions.

The pattern of connexin isotype distribution within the human heart is illustrated below. The size of text (large, medium, small, very small) indicates the relative amount (abundant, moderate, little, minute) of each connexin isotype within various structures of the heart. (SA – sinoatrial; AV – atrioventricular)



greater this difference, the greater the degree of anisotropy.²⁸ The factors determining the degree of conduction anisotropy within tissue include myocyte morphology and coupling patterns, and the subcellular pattern of gap junction and sodium channel expression.²⁹ Differing tissue conduction anisotropy has been noted between atria and ventricles, and during specific disease states.

Saffitz and co-workers demonstrated differing patterns of tissue anisotropy between the crista terminalis and ventricles in adult canine hearts. Tissues obtained were studied using light and electron microscopy, Northern blotting, and immunohistochemistry. Individual ventricular myocytes were found to couple to approximately 11 other myocytes on average. When compared to ventricular myocytes, individual myocytes within the crista terminalis coupled to approximately 43% fewer myocytes, with more coupling in a predominantly end-to-end rather than side-to-side pattern (77% versus 53%). In addition, the crista terminalis possessed predominately small discoid gap junctions aligned in rather straight intercalated discs at their true ends. In contrast, ventricular myocytes possessed both small discoid gap junctions at the plicate segments of the intercalated discs, and

larger ribbon-shaped junctions with long axes oriented perpendicular to the cellular long axis and located in the inter-plicate regions. Hence the highly anisotropic arrangement of the crista terminalis likely contributes to the characteristic directional differences of conduction velocity compared to the ventricles, with minimal conduction in the transverse direction (longitudinal to transverse conduction velocity ratio of ~10 versus ~3 respectively).^{30, 31}

Luke and co-workers hypothesised that the slow propagation, conduction block, and fractionated electrograms identified in canine infarct models of arrhythmia were due to altered myocyte interconnections. Light and electron microscopy were used to identify an increase in intercellular collagen, reduction in large gap junctions located in the inter-plicate regions of the intercalated disks, and a reduction in the number of myocytes that an individual myocyte coupled with, this being more so with cells that were predominantly positioned side-to-side. As a result a transversely directed wavefront would encounter greater resistance to conduction and path length.³²

Peters et al demonstrated the ability of tissue anisotropy to result in arrhythmia following myocardial infarction. A total of 6 dogs received LAD infarctions and only 3 were subsequently susceptible to inducible ventricular tachycardia (VT). Figure-of-eight re-entry was observed during each VT episode and occurred over the thinnest area of viable myocardium. Immunohistochemistry revealed that the lateral walls of the central common pathway consisted of myocytes with reduced intercalated disc content of Cx43, a finding consistent with the reduced number of gap junctions observed by Luke et al. The roof and floor of the central common pathway were formed by the epicardium and non-viable myocardium respectively. An increase in lateralised membranous Cx43 expression in myocytes was noted but its functionality was not investigated.³³

1.2.2 Connexins, Conduction, and Arrhythmia

Based on the tissue specific distribution of connexin isoforms and their properties in gap junctions, alteration of location specific conduction velocities might be expected as individual isoform expression is altered.

The results of investigations however, into the role connexins play in electrical propagation and arrhythmia in the heart, have been inconsistent. Two main techniques have been used by investigators to assess these roles. The first has involved the knockout of connexin expression with subsequent assessment of conduction. Outcomes assessed have included measures representative of conduction velocity acquired through cutaneous electrocardiograms and functional electrophysiological studies, and tissue conduction velocity itself via surface electrode arrays and optical mapping systems. Interpretation of the results of genetically engineered animal studies is however hampered by the high rate of congenital malformations associated with connexin knockout.³⁴⁻³⁶ The second technique involves the study of differences in connexin expression between sinus rhythm and an arrhythmia such as AF, with subsequent correlation of

differences with conduction parameters. Interpretation of the results however must be made within the context of the method used to generate the arrhythmia, or the disease process setting in which the arrhythmia occurs.

1.2.2.1 Genetically Engineered Mice Models

Cutaneous Electrocardiographic Studies

Simon et al examined the effects of alterations in Cx40 expression levels on the electrocardiogram (ECG) durations of P waves, PR intervals, and QRS complexes. Heterozygous and homozygous Cx40 knockout mice were bred through mating 129/Sv strains with C57BL/6 strains. Conventional three lead ECG's were produced using limb needle electrodes during pentobarbital intra-peritoneal anaesthesia. The P, PR, and QRS intervals were similar between wild-type and heterozygous knockout mice. However there were significantly increased P wave durations of 13.4ms versus 12.3ms, PR intervals of 41.2ms versus 34.1ms, and QRS durations of 15.5ms versus 11.6ms between homozygous knockout and wild-type mice respectively. No spontaneous arrhythmias were observed.³⁷ Based on previously described patterns of cardiac tissue distribution of Cx40, it was suggested

that Cx40 was an important determinant of both atrial and His-Purkinje conduction velocities.³⁸ Closer examination of immunofluorescence images however reveals an absence of Cx40 expression within the atria of wild-type mice and hence would not explain the P wave prolongation that occurred in homozygous knockout mice. While ventricular chamber size was studied, no data was provided on atrial size. It is possible that homozygous knockout mice possessed developmentally related atrial dilation, a feature that would result in P wave prolongation.

Using a similar method to Simon et al, both Kirchhoff et al and Hagenfordff et al achieved similar patterns of alteration in ECG parameters with Cx40 knockout mice. However both groups noted more pronounced prolongation in P wave durations and also observed high frequency re-entrant atrial arrhythmias, intermittent sino-atrial block, and intermittent atrio-ventricular block in homozygous knockout mice. When compared to wild-type mice, P waves in homozygous knockout mice were prolonged by 57% and 56% in their studies respectively. Of note, Kirchhoff et al demonstrated the presence of Cx40 in wild-type atria. Connexins 43 and 45 were also demonstrated within the atria of null Cx40 mice, however immunostaining within wild-type atria were not

performed to assess for possible changes in levels of expression. Both studies came from the same lab, using 129/Sv/C57BL/6 mice and intra-peritoneal Avertin for anaesthesia.^{39, 40} Bearing in mind the genetically engineered nature of the mice used, the results suggested that reduced Cx40 expression could produce a suitable substrate to precipitate re-entry.³⁴ The presence of sino-atrial and atrio-ventricular block was unexpected but may have been due to altered coupling between the atria and these regions or altered levels of vagal tone under anaesthesia.

P wave prolongation by 25% in addition to QRS widening was also observed by Verheule et al in 129/Sv/C57BL/6 Cx40 homozygous knockout mice. The QRS widening was abolished when the ventricles were stimulated from the epicardial surface rather than being activated through the intrinsic His-Purkinje system, confirming that Cx40 participated in His-Purkinje conduction. No spontaneous atrial arrhythmias were observed, an absence of which may again have been due to less pronounced P wave prolongation in homozygous knockouts compared to Kirchhoff et al and Hagenfdorff et al. Surprisingly, PR intervals were not significantly prolonged in this study suggesting normal coupling of the atrioventricular node to surrounding structures.

Assessment of connexin expression was not made to elucidate this difference, and sample sizes were smaller compared to Kirchhoff et al. Mice in this study were anaesthetised with urethane.⁴¹

Interestingly, Cx40 heterozygous knockout mice possessed ECG parameters similar to wild-type mice in the 4 above mentioned studies. Levels of connexin expression, both 40 and 43, in atria heterozygous for Cx40 were not assessed however.

More recently, Bagwe et al demonstrated, using both 6 lead surface ECG's in conscious mice and volume conducted ECG's of Langendorff perfused hearts, prolongation of P wave, PR, and QRS durations in Cx40 homozygous knockout mice compared to wild-type mice. Aberrant P waves within all homozygous knockout mice were observed regardless of the method of ECG acquisition. The presence of aberrant P waves was suggestive of an atrial ectopic rhythm rather than sinus rhythm, and hence Cx40 was considered to be important in sinus node function as well.⁴² Cx43 levels within whole hearts and atria were similar between both groups with Western blotting and immunofluorescence. Differences in ECG acquisition with fewer leads may have

accounted for the lack of observation of P wave aberrancy in the prior detailed ECG studies.

Other potential confounding factors for result variances between the five studies included potential definition differences, the use of knockout mice, litter variances, and differing anaesthetic agents. Pentobarbital has been shown to alter conduction and automaticity in canine models while Avertin is a known cardio-depressant in mice.^{43, 44}

Thomas et al demonstrated that reduced Cx43 expression within the atria of Cx43 heterozygous knockout mice did not result in atrial conduction slowing as evidenced by similar P wave durations to that of wild type mice. When compared to wild-type mice however, quantitative densitometry of immunoblots for atrial Cx43 revealed an approximately 60% reduction in expression. There were no significant alterations in Cx40 levels. These results suggested that Cx40 was the main determinant of conduction velocity within the atria. Conversely, reduced ventricular levels of Cx43 expression assessed by Western blotting were associated with slow ventricular conduction. In particular, heterozygous knockouts possessed 72% wider mean QRS intervals compared

to wild-type mice, indicating that Cx43 was the main determinant of conduction velocity within the ventricles. Genetically engineered mice were of C57BL/6 origin and studied under pentobarbital and ketamine anaesthesia.⁴⁵

It should be noted that Morley et al failed to identify a difference in mean QRS width between wild-type and Cx43 heterozygous knockout mice. Interval definitions used by Morley et al were similar to Kirchhoff and anaesthetised wild-type mice possessed similar QRS durations of 14.5ms and 17.1ms between both studies. Mice were anaesthetised with ketamine and acepromazine.⁴⁶

In an attempt to explain the findings of Morley et al, Eloff et al compared epicardial electrogram QRS complexes with optically recorded action potentials using mice hearts. While the onset of QRS complexes coincided with action potential onset, the timing of QRS offset was more difficult to discern with electrocardiography and may have explained the QRS width discrepancies between Thomas et al and Morley et al. The width of QRS complexes were not reported by Eloff et al however.⁴⁷

Functional Electrophysiological Measurements

Electrophysiological studies complement electrocardiograms, allowing assessment of electrical conduction, refractoriness, and arrhythmia vulnerability at specific locations within the heart. Assessment includes function of the sinus node, atrio-ventricular node, and His-Purkinje system through sinus node recovery times, AH intervals, and HV intervals respectively. Atrial and ventricular refractory periods can also be assessed.⁴⁸

In addition to electrogram studies, Hagendorff and co-workers performed limited electrophysiology studies via trans-oesophageal pacing and recording on Cx40 deficient and wild-type mice. Mean sinus node recovery times were 41% longer and both sinus node entry and exit block were observed in Cx40 deficient mice. Furthermore, significantly longer minimum 1:1 atrioventricular (AV) nodal conduction times of 13% were demonstrated in Cx40 homozygous knockout mice. These findings provide further evidence that Cx40 is involved in the electrophysiology of the sinus and AV nodes. Without His electrograms it was not possible to determine if the His-Purkinje system was affected as well by Cx40 knockout. Increased propensity to arrhythmia, both

spontaneous and stimulated was demonstrated in Cx40 homozygous knockout mice. Arrhythmias displayed features of either re-entry or AF.⁴⁰

Building on the results of Hagendorff et al, *in vivo* electrophysiological studies were also performed by Verheule et al in similar Cx40 deficient and wild-type mice. Measurements and stimuli were facilitated however, with 0.03mm fine wire epicardial surface electrodes placed via a thoracotomy. Similar to Hagendorff et al, corrected sinus node recovery times and AV Wenckebach times were prolonged in Cx40 homozygous knockout mice. Effective refractory periods of the atria and ventricles were similar between Cx40 homozygous knockout and wild-type mice. This time only induced re-entrant type arrhythmia was observed.⁴¹

Thomas et al performed intra-cardiac electrophysiology studies (EPS) in Cx43 heterozygous knockout mice. Atrial effective refractory periods, sinus node recovery times, and AV Wenckebach times were similar to wild-type mice. There was a 38% prolongation in the ventriculo-atrial Wenckebach time suggesting impaired 1:1 coupling between the ventricles and AV

node. Ventricular effective refractory periods were non-significantly prolonged. Of note, small sample sizes were used and wide standard deviations observed. The results provided further evidence that the major determinant of electrophysiology of the atria was likely to be Cx40 and not Cx43.⁴⁵

Direct Conduction Velocity

Consistent with electrogram studies and knowledge of Cx40 tissue distribution, Verheule et al demonstrated 30% slower intra-atrial and unaltered intra-ventricular conduction velocities during pacing at a cycle length of 100ms in Cx40 homozygous knockout mice compared to wild-type mice. *In vivo* measurements were made and stimuli delivered using a hand held probe consisting of 2 stimulus electrodes at one end oriented perpendicular to a linear array of 4 unipolar electrodes. No details were provided regarding the method used for consistent probe orientation over each chamber.⁴¹

Bagwe and co-workers further assessed, with optical mapping, the role of Cx40 on right atrial electrical excitation and conduction using Langendorff-perfused hearts from wild-type and Cx40

homozygous knockout mice. Perfusate containing Tyrodes solution and the voltage sensitive dye di-4-ANEPPS was maintained at 37-38°C. No mechanical or pharmacological motion reduction technique was used during the experimental protocol. Two Dalsa high resolution CCD cameras acquiring at 920 frames per second were used for recording. A translational motion tracking and correction algorithm based on a template matching technique was applied offline to eliminate mechanical errors. Optical mapping revealed that spontaneous beating originated from ectopic sites within the right atrium of knockout mice, a finding that explained the aberrant P wave morphologies observed on their ECG's. In addition there was a shift towards heterogeneously slower conduction velocities with some areas of extremely delayed activation suggesting conduction block. Successive ablations of ectopic pacemaker sites until the sinus node was the leading pacemaker site revealed that the sinus node possessed a longer cycle length compared to wild-type mice. Atrial pacing at 10Hz revealed a uniform reduction in conduction velocity of approximately 36% across the atria of knockout mice, without evidence of conduction block. However as pacing frequency was increased up to 25Hz, increasing areas of conduction block became evident. This increasing inability to

maintain 1:1 conduction suggested a reduced safety factor for atrial conduction in Cx40 knockout mice, a substrate property postulated to allow for fibrillation of the atria.⁴⁹ Microelectrode techniques excluded alterations in membrane properties as a cause for the observed results. In particular, there were no changes in resting membrane potential and action potential parameters including maximal dV/dT , amplitude, and duration.⁴²

Using high resolution optical mapping, Tamaddon et al extended the assessment of the effects of Cx40 homozygous knockout to the bundle branches of the ventricular conducting system. Results were compared to wild-type mice hearts. Langendorff perfused mice hearts were maintained without motion reduction techniques at 37°C to 38°C and perfused with Tyrodes solution. A Dalsa CCD camera was used, sampling at 912 frames per second with 12 bit resolution. During sinus rhythm and atrial pacing at cycle length of 120 milliseconds, right ventricular activation was grossly delayed with only mildly delayed left ventricular activation in Cx40 knockout hearts. Ventricular epicardial pacing revealed no differences in conduction velocities, indicating that the activation delays from atrial pacing were due to conduction slowing within the ventricular conduction system. Direct imaging of the right

bundle of the ventricular conduction system revealed conduction slowing within this branch. Comparisons of bundle activation times with volume conducted ECG's revealed no significant conduction delay within the left bundle of knockout hearts. The results suggested that Cx40 was the main determinant of conduction within the right bundle of the ventricular conducting system, but not the left.⁵⁰

Guerrero et al studied the effect of reduced Cx43 on ventricular conduction velocity in neonatal and adult Cx43 heterozygous knockout mice hearts. Results were compared to wild-type hearts. Velocities were measured using an electrode array placed in a consistent manner on the epicardial surface parallel to the left anterior descending artery of superfused neonatal and perfused adult hearts that were cooled to 31°C and paced at 200 beats per minute. A temperature of 31°C was chosen to slow the spontaneous beat frequency of hearts enough to facilitate ventricular pacing. Spontaneous beat frequency was similar between Cx43 heterozygous knockout and wild-type hearts. The results of ventricular pacing revealed that Cx43 heterozygous knockout reduced conduction velocity by 30% and 44% in neonatal and adult hearts respectively. There was no difference in

ventricular effective refractory periods. Furthermore, assessment during spontaneous beating in neonatal hearts revealed no difference in AV conduction times between knockout and wild-type hearts. Histological analysis of adult mice hearts revealed no obvious difference in myocardial fibre orientation or curvature of the anterior left ventricular free wall between Cx43 knockout and wild-type groups. Furthermore fibres were parallel to the orientation of the recording array indicating that maximum conduction velocities were recorded. The results suggested that Cx43 was a major determinant of ventricular myocyte conduction.⁵¹

Thomas et al also studied the effects of reduced Cx43 on atrial and ventricular conduction in adult mice heterozygous for Cx43. Epicardial surface recordings were performed with a linear array on superfused adult mice hearts cooled to 31°C and paced at 200 beats per minute. Atrial assessment was performed on both isolated and intact atria. A recording electrode array was placed on the right atrial appendage longitudinal to its long axis, and a stimulating electrode was placed at the distal most tip of appendage. In both isolated and intact atria, no difference was identified between wild-type and Cx43 heterozygous knockout

mice. Ventricular assessment was performed in a similar way to Guerrero et al. A significant 38% reduction in ventricular conduction velocity was observed in heterozygous mice.⁴⁵

Using optical mapping, Morley et al failed to identify a difference in ventricular conduction velocities between wild-type and heterozygous Cx43 mice. Excised hearts were perfused as Langendorff preparations between 37°C and 39°C. Fluorescence associated with mechanical artefact was inhibited by adding diacetyl monoxamine to the perfusate. Conduction velocities were measured with the assistance of the voltage sensitive dye di-4-ANEPPS, and recorded via a CCD video camera. Two CCD cameras were used during the study. One was a Dalsa camera with a frame rate of 1500 frames per second and the other was a Cohu camera with a frame rate of 240 frames per second (1000 frames per second after implementation of a synchronous acquisition system). The inability of linear epicardial surface electrodes to sample more than one dimensional conduction, to detect breakthrough activation and wavefront collision, and its dependence on stimulation electrode positioning was used to account for the differences between this study and earlier epicardial electrode array studies.⁴⁶

Eloff and co-workers repeated the work of Morley et al, but used mice of both congenic and mixed genetic origins to control for the possible developmental defects known to occur in Cx43 deficient mice.³⁶ Similar Langendorff preparations were used with diacetyl monoxamine and di-4-ANEPPS. An optical mapping system with a higher temporal resolution, sampling at a rate of 3400 samples per second, and a higher voltage resolution by virtue of a photodiode optical mapping array was used. In addition, algorithms were used to eliminate virtual electrode effects and errors caused by sub-epicardial breakthrough. Subsequent action potentials recorded had a time course of membrane potential change comparable to action potentials recorded with microelectrodes by Zhou et al⁵². An approximately 25% reduction in conduction velocity was subsequently observed in mixed and congenic mice heterozygous for Cx43 compared to wild-type mice. Based on weight, no differences in tissue oedema were found in hearts used for this study. Using light microscopy, fibre orientation was similar between wild-type and genetically engineered mice. Lower voltage and temporal resolutions, and lack of compensation for the virtual electrode effect were postulated as the reason for the failure of Morley et al to detect a

difference in conduction velocities between wild-type and heterozygous Cx43 knockout mice.⁴⁷

To avoid the confounding effects of congenital cardiac malformations in traditional Cx43 knockout mouse models, Gutstein et al used cardiac restricted inactivation of Cx43 in a conditional knockout mouse model to study conduction velocity and propensity to arrhythmia. Cardiac restricted inactivation of Cx43 was performed using the Cre/loxP system. Immunofluorescence revealed almost complete abolishment of Cx43 from ventricular myocytes in conditional knockout mice at 4 weeks of age. Immunoblots revealed up to 95% reduction in Cx43 expression with no change in Cx40 levels in the ventricles of conditional knockout mice compared to littermate controls. Histological examination revealed no microscopic differences between groups and echocardiography did not reveal any structural or functional differences. Knockout mice possessed high death rates within the first 2 months of life, and telemetry revealed terminal spontaneous ventricular arrhythmias. Langendorff preparations and optical mapping was performed in a manner similar to Tamaddon et al to assess ventricular conduction.⁵⁰ Knockout hearts displayed a 55% and 42% reduction in

conduction velocities in the transverse and longitudinal directions respectively during ventricular epicardial pacing. They were also highly susceptible to spontaneous ventricular arrhythmia compared to controls which had none.⁵³

Leaf et al studied the pattern of atrial Cx40 expression in wild-type and knockout mice using a combination of epicardial optical mapping during pacing, RNA expression, and protein expression. When conduction velocities were assessed in wild-type mice, left atrial appendage velocities were higher than right. This difference was abolished in both heterozygous and homozygous knockout mice. When genotypes were compared, there was only a mild reduction in conduction velocities of the left atrial appendage between wild-type and heterozygous knockout mice. Cx40 mRNA expression was highest in the left atrial appendage compared to the right in wild-type mice. This difference was again abolished in heterozygous knockout mice. There was no change in Cx43 mRNA expression between right or left atrial appendages of all three genotypes. Subjective assessment of immunofluorescence and band densitometry of Western blots revealed no significant differences in Cx40 expression between the left and right atria however. When wild-type and heterozygous mice were compared,

there was a significant reduction in Cx40 mRNA and protein levels. Wild-type and knockout embryonic mice atrial appendages were also studied with optical mapping at 13.5 days post coitum and 15.5 days post coitum. At 15.5 days post coitum, results revealed similar atrial conduction velocity trends to that of adult mice except that conduction velocity was faster within the right atria compared to left of wild-type embryos. This heterogeneity was not evident at 13.5 days post coitum. Furthermore, at day 13.5 post coitum, spontaneous atrial rhythm originated from the sinus node in all embryos. By day 15.5 post coitum, spontaneous atrial rhythm originated from multiple ectopic sites in knockout mice compared to wild-type mice which remained in sinus rhythm.⁵⁴

Beauchamp and co-workers studies the effects of connexin 40 and 43 knockout on conduction velocities in an *in vitro* model of neonatal mouse atrial myocytes. High resolution optical mapping was used to assess conduction velocities in atrial cultures. Homozygous knockout of Cx43 resulted in conduction slowing. Although there was also a reduction in junctional Cx40 with immunofluorescence, it was inferred that the proportional increase in Cx40 to Cx43 was responsible for conduction slowing.

Homozygous knockout of Cx40 resulted in an increase in conduction velocity. Although there was an increase in junctional Cx43 with immunofluorescence, it was inferred that the proportional decrease in Cx40 to Cx43 was responsible for increased conduction velocities. The increase in junctional Cx43 with Cx40 knockout was not observed in adult rat hearts however. Although the results were consistent with the findings in human atria by Kanagaratnam et al, they must be interpreted with caution. Firstly, results were confounded by differing quantities of the remaining connexin isotype between knockout and wild-type atria. Secondly, differences in associated binding affinities and relative fluorescence's of the antibodies used, meant that results could not be directly compared to the conductance findings of previous patch clamping studies.⁵⁵

1.2.2.2 Non-Genetically Engineered Animal Models

Observational Studies

As part of a study into radiofrequency ablation of pacing induced AF in dogs, Elvan et al used 3 dogs to study the effects of chronic pacing alone on Cx43 expression. Dogs underwent endocardial high frequency burst pacing of the right atrium for up to

approximately 15 weeks to induce AF. When the right atria of dogs in AF were compared to sinus rhythm controls, immunofluorescence revealed an increase in the level of membranous Cx43, while immunoblotting revealed an increase in total cellular Cx43.⁵⁶

Van Der Velden et al studied the distribution of connexin40 and 43 in atrial appendages of goats before and 2 months after induction of sustained AF via epicardial pacing. Epicardial mapping using a 244 lead electrode array with an inter-electrode distance of 2.25mm was also performed with atrial pacing to assess conduction velocities before and after AF induction. Just prior to the second mapping session, hearts were defibrillated to sinus rhythm. Electrode mapping revealed similar epicardial conduction velocities before and after induction of AF. PCR and Western blotting revealed no difference in cellular Cx40 and Cx43 mRNA or protein levels before and after induction of AF. Immunofluorescence however revealed patches of cells varying in diameter from 150µm to 600 µm that were almost devoid of Cx40 interspersed between areas of cells with normal Cx40 levels 2 months after induction of AF. There was no difference in the pattern of Cx43 distribution before and after AF induction. The

results suggested that heterogenous Cx40 distribution may reduce the safety factor for conduction without altering the overall conduction velocities and that the resolution of mapping was not high enough to pick up altered conduction velocities within areas of reduced Cx40 expression.⁵⁷

Van Der Velden et al subsequently used a similar model to assess the time course for connexin changes in the left and right atria of goats subject to atrial pacing. Goats however this time received endocardial burst pacing. Paced goats were assessed either at 1, 2, 4, 8, or 16 weeks from commencement of pacing and compared to non-paced goats that remained in sinus rhythm. Prior to sacrifice, goats were considered to be in stable AF if spontaneous termination did not occur within the preceding 3 hours with the pacemaker switched off. There was an increased incidence of stable AF as pacing time increased, with all goats at 16 weeks possessing stable AF. Immunofluorescence of atria from each time point revealed increasingly heterogeneous Cx40 distribution on myocytes and increasingly greater areas of myocytes almost devoid of this protein. Increasing levels of myolysis paralleled the decrease in Cx40 expression. The pattern of Cx43 expression however remained unchanged.

Immunoblotting revealed a reduction in cellular Cx40. While there was no difference in cellular Cx43, there was a shift towards greater phosphorylated Cx43 over time. There was no change in mRNA levels for connexins 40 and 43 however. Changes in Cx40 expression also varied between left and right atria. The results suggested that longer atrial burst pacing resulted in greater changes in Cx40 heterogeneity which in turn resulted in an increasing propensity for AF.⁵⁸

Pharmacotherapy Studies

Further evidence that connexins played a role in conduction and arrhythmia came from the study of compounds that modulate gap junction function. The effect of Rotigaptide on atrial conduction and the propensity for AF in dogs was studied by Guerra et al. Three groups of dogs were used. The first consisted of control animals that had no surgical intervention. The second consisted of dogs with mitral regurgitation secondary to valve avulsion. The last consisted of dogs with ventricular pacing induced heart failure. Baseline epicardial electrode array mapping and AF induction was performed on all animals, specifically at 6 weeks after valve avulsion, and at 4 weeks after onset of ventricular

pacing. Studies were repeated on all animals during the same sitting, before and 20 minutes after commencement of infusions of Rotigaptide designed to achieve serum concentrations of 10, 50, and 200nmol/L. At baseline, epicardial conduction velocities tended to be slower in the valve avulsion and pacing groups and were associated with increased vulnerability for burst pacing induced AF when compared to control animals. Following administration of Rotigaptide, there was an increase in left and right atrial conduction velocities of the control and valve avulsion groups. In the pacing group however, there was no change in conduction velocity in the left atrium and a mild increase in the right atrium. AF vulnerability within the valve avulsion group was normalised following administration of Rotigaptide to serum concentrations of 10 and 50nmol/L. This reduction however dropped off with Rotigaptide serum concentrations of 200nmol/L. Rotigaptide did not alter AF vulnerabilities within the pacing group. Although spatial distributions of Cx40 and Cx43 were similar between all three groups with immunofluorescence, there was an approximately 3 fold increase in the percentage of fibrosis in atrial sections from the pacing group when compared to the other two groups. This may have accounted for the lack of response to Rotigaptide within the pacing group.⁵⁹

Shiroshita-Takeshita et al also studied the effects of Rotigaptide on conduction and propensity to arrhythmia but in 3 different canine models of AF. The first model consisted of atrial pacing with assessment at 3 weeks and 6 weeks. The second consisted of the ventricular pacing heart failure model with assessment at 2 weeks. The third consisted of acute atrial ischemia. EPS and mapping via epicardial electrode arrays were performed prior to and after administration of Rotigaptide and compared to respective instrumented but not paced sham controls. Rotigaptide had no effects on effective refractory periods and conduction velocities in all sham controls. At 3 and 6 weeks, atrial pacing resulted in longer effective refractory periods. Rotigaptide had no effect on effective refractory periods, but slightly increased conduction velocities in this group. Ventricular pacing did not alter effective refractory periods. Like the atrial pacing group however, Rotigaptide had no effect on effective refractory periods, and mildly increased conduction velocities. Atrial ischemia did not change effective refractory periods as well. There was however significant conduction slowing within ischemic areas. While Rotigaptide again had no effect on effective refractory periods, there was a significant attenuation of conduction slowing within ischemic areas at 3 and 5 hours. Conduction heterogeneity

indexes of localised conduction slowing were significantly increased in the ischemia and ventricular pacing models compared to sham controls. Rotigaptide significantly attenuated conduction heterogeneity index changes in the setting of ischemia, but not ventricular pacing induced heart failure. AF durations were prolonged in all groups compared to controls, and Rotigaptide significantly attenuated these durations. This reduction was small within the atrial pacing group. However within the ischemic group, AF duration was reduced to sham control levels.⁶⁰

A more recent study of the gap junction modifier GAP-134 was performed by Rossman et al. Initially, the effect of the gap junction modifier GAP-134 on atrial conduction velocity and propensity for AF in the setting of stress was studied. Two models were assessed. In the first, strips of left atrial tissue were perfused with regular Tyrodes buffer. Stress was induced by altering perfusate to non-oxygenated, glucose free Tyrodes buffer. Stress was assessed in the presence and absence of GAP-134. Conduction velocities, measured by two electrodes oriented parallel to the long axis of the strips, rapidly dropped off with stress in the absence of GAP-134, while they were maintained at baseline

levels in the presence of GAP-134. Further study was performed using a canine model of sterile pericarditis. Conduction velocity was significantly increased in the presence of GAP-134. Furthermore, there was a reduction in duration and vulnerability of pacing induced AF after the administration of GAP-134. This effect was not observed in animals that did not receive GAP-134. Immunoblotting for Cx43 in the left atrium of both groups did not demonstrate any effect of GAP-134 on cellular expression levels.⁶¹

Gene Therapy Studies

Bikou et al was the first to utilise acute somatic gene transfer techniques to study the role Cx43 played in a porcine, pacing induced model of AF. Animals were assigned to receive an adenovirus encoding either GFP or Cx43 followed by 14 days of burst pacing to induce AF. Viral vector was applied by multiple direct injections into the left and right atria followed by electroporation at the atrial surface. A third group of pigs received no vector or pacing and acted as a sinus rhythm control. At day 14, all animals that underwent GFP transduction were in persistent AF as defined by greater than 48 hours of continuous

AF. Conversely, all animals that underwent Cx43 transduction were predominantly in sinus rhythm. Paroxysmal AF was observed in 3 animals within the Cx43 group. Animals with persistent AF had a 62% reduction in cellular Cx43 compared to sinus rhythm controls as determined by Western blotting. A significant decrease was not observed in the Cx43 gene transfer group. Immunohistochemistry revealed a 2.0 fold increase in membranous Cx43 levels, primarily at the intercalated discs, in animals from the Cx43 group compared to the GFP group. Cx43 therapy did not alter the levels of Cx40. Atrial surface conduction velocities, assessed *in vivo* by an epicardial electrode array, were 62% greater in the Cx43 group compared to the GFP group. Left ventricular ejection fractions, assessed by echocardiography mirrored the conduction velocity findings. The study did not assess other factors such as inflammation or fibrosis. Furthermore, no sinus rhythm controls with GFP therapy and no pacing controls without GFP therapy were used to assess for the possible effects of GFP therapy itself on Cx43 expression and epicardial conduction velocities. This study however was the first to suggest the possibility of reducing AF vulnerability with Cx43 up regulation.⁶²

Also using acute somatic gene transfer techniques, Igarashi et al assessed the effects of Cx40 and Cx43 overexpression in a pacing induced porcine model of AF. Thirty swine were divided into 2 groups, namely, a sinus rhythm group, and a burst pacing induced AF group. Each group was further divided into 3 subgroups, namely, a sham operated control subgroup, or one of two gene therapy subgroups receiving either Cx40 or Cx43 via an adenoviral vector. Baseline EPS's were performed followed by the atrial application of a viral vector to the appropriate subgroups. A camel hair brush was used to apply a gel mix containing vector, poloxamer, and trypsin, to the epicardial surface. Pacemakers were inserted into the groups targeted for burst pacing induction of AF. Swine were observed daily and a final EPS was performed on day 7 followed by cardiac extraction for optical mapping, histology, Western blotting, and immunohistochemistry. As expected, all control animals within the burst pacing group were in continuous AF by day 7, while no animal within the sinus rhythm group developed AF. Animals within the burst pacing group that received gene transfer had a lower percentage of time in AF at day 7 compared to sham operated controls. Compared to sinus rhythm sham controls, AF sham controls possessed a significant reduction in total and phosphorylated Cx43 levels and unchanged

Cx40 levels by Western blotting, an almost 50% reduction in the percentage of membranous Cx43 located at the intercalated disc on immunofluorescence, and longer P wave durations, inter-atrial conduction times, and surface conduction velocities with electrophysiological assessment. Cx43 gene transfer to animals within the burst pacing group virtually normalised these parameters. Interestingly Cx40 gene transfer did not alter Cx40 or Cx43 intercalated disc levels within the burst pacing group. Cellular levels of Cx40 were however increased by Cx40 gene transfer. Importantly, no vector control group was used within this study to confirm that adenovirus itself was not responsible for the results observed, particularly within the Cx40 group. Nevertheless, the Cx43 findings were similar to that of Bikou et al.^{62, 63}

1.2.2.3 Human Studies

Kanagaratnam and co-workers attempted to identify a correlation between the relative expression of connexins 40 and 43 and atrial conduction velocity in humans. During coronary artery bypass surgery, electrophysiology studies were performed via a grid of epicardial electrodes (16 X 7 array, 3.5mm inter-electrode spacing) attached to the right atrium. Biopsies were taken to

quantitate connexin isotype expression levels with immunofluorescence. During sinus rhythm, an increase in Cx40 levels and the ratio of Cx40 to summed Cx40 and Cx43 levels was associated with conduction slowing. Furthermore, during sinus rhythm, while an increase in Cx43 levels was not associated with alterations in conduction velocity, an increase in the ratio of Cx43 to summed Cx40 and Cx43 was associated with an increase in conduction velocity. These correlations were abolished however, with a reduction in the coupling interval by atrial pacing from the area of the sinus node. Interestingly, relative Cx40 expression correlated with rate related changes in conduction velocity, suggesting a role in rate adaptation. Interpretation of results within this study were however limited. Firstly, the mapped area was large with low spatial resolution and likely subject to 3D-wave propagation error. This may have also accounted for the alteration in conduction velocities observed between pacing and sinus rhythm. Secondly, differences in associated binding affinities and relative fluorescence's of the antibodies used, meant that results could not be directly compared to the conductance findings of previous patch clamping studies.⁶⁴

Dupont et al studied right atrial appendage expression of Cx40 and Cx43 in humans with and without sustained acute AF following coronary artery bypass grafting. All patients had no prior history of AF. Analysis of a limited set of possible confounding factors such as atrial size and left ventricular ejection fraction revealed no significant difference between groups. Analysis however did not include underlying medical history or medication use. Compared to patients without AF, mRNA and total cellular protein levels for Cx40 were elevated in patients with AF. There however was no difference in Cx43 mRNA and protein levels between both groups. Although the results suggested that increased total cellular Cx40 expression increased the risk of developing AF, no assessment was made to see if this increase translated into an increase in Cx40 at the intercalated discs where intercellular conduction is facilitated. Interestingly, immunofluorescence revealed heterogeneous expression of Cx40 within the atria of both groups. Cx43 expression was homogenous in both groups. No histological assessments were performed however for ischemia, inflammation or fibrosis. This is particularly important given the background of an ischaemic disorder in all patients, and the rapid occurrence of sterile pericarditis on

pericardial instrumentation, both of which have the ability to alter connexin distribution.⁶⁵⁻⁶⁷

Polontchouk et al subsequently compared the expression of connexins 40 and 43 in the right atrial appendages of patients with and without chronic AF at the time of open heart surgery. The reasons for surgery were coronary artery bypass grafting and/or correction of a valvular defect. The proportion of patients undergoing each type of surgery appeared similar between both groups. Immunoblotting revealed an increase in cellular Cx40 levels and no change in cellular Cx43 levels in patients with AF. Analysis of the membranous distribution of connexins with immunofluorescence revealed no difference in connexin 40 and 43 levels at the outer end quarters of myocytes between patients with and without AF. However there was an increase in connexin 40 and 43 levels in the mid half of myocytes indicating lateralisation in patients with AF. The implications of the observed changes in connexin expression were then assessed using a model of pacing induced acute AF in rats. Acute AF was generated by atrial pacing explanted Langendorff perfused right atria for 24 hours. Two control groups were used. The first consisted of right atria not subjected to Langendorff perfusion, and

the second consisted of right atria subjected to Langendorff perfusion for 24 hours without pacing. Following 24 hours of pacing, AF was present in all atria for up to 5 minutes at most. Non-paced Langendorff perfused hearts remained in sinus rhythm. Surface conduction velocities were assessed with atrial pacing at the edge of a linear array of 4 electrodes (3mm inter-electrode spacing) placed transversely and subsequently longitudinally to surface fibre orientation. There was a non-significant ($p=0.1$) increase in transverse fibre conduction velocity from 5cm/s to 8cm/s in the pacing group. There were no differences in longitudinal conduction velocities between groups. Immunoblotting and immunofluorescence revealed differences in connexin expression between sinus rhythm and AF that were similar to the human studies. The findings suggested that connexin lateralisation improved transverse conduction, reduced conduction anisotropy, and hence increased the propensity for AF. The results must be interpreted however in the setting of the method used to assess conduction velocity, which was likely subject to angulation error and limited in its ability to detect 2 and 3 dimensional conduction.⁶⁸

The pattern of Cx40 and Cx43 expression between different regions of the right atrium of humans with and without chronic AF was assessed by Kostin et al. All patients with AF underwent a mini-Maze procedure. Although patients with sinus rhythm were matched to patients with AF by right and left atrial sizes, the reasons for their surgery was not specified. Patients with AF tended to have more valvular heart disease. Biopsies of the atrial appendage and free wall of the right atrium were assessed with immunofluorescence. Consistent with earlier studies, results revealed a marked lateralisation of connexins 40 and 43 in both atrial areas of patients with AF compared to sinus rhythm. In addition, patients from both groups possessed heterogenous expression of Cx40 with areas of lower levels of expression to adjacent regions of normal Cx40 levels. However the total area of heterogeneity was lower in patients with sinus rhythm. Cx43 expression was homogenous in both groups. The total level of membranous Cx43 expression was reduced by approximately 57% in both biopsy areas of patients in AF compared to sinus rhythm. Total membranous Cx40 expression was reduced by 54% in atrial appendages, but trended towards a 16% increase in the free walls of patients with AF when compared to controls. Increased fibrosis was also noted in patients with AF.⁶⁹

Nao et al studied patterns of connexin 40 and 43 expression in humans with chronic AF in the setting of mitral valve disease. Right atrial appendage tissue was collected from patients at the time of open heart surgery. Two control groups were used, the first being patients in sinus rhythm with mitral valve disease, and the second being patients in sinus rhythm without mitral valve disease and undergoing coronary artery bypass grafting. Results revealed a reduction in Cx40 protein by immunoblotting and mRNA levels by PCR in the setting of chronic AF. There was however an increase in serine phosphorylation of Cx40 within the AF group compared to both controls. No significant difference between groups was found in Cx43 mRNA, protein or phosphorylation levels. Immunofluorescence revealed a pattern of heterogenous Cx40 expression in patients with valvular heart disease, being worse in patients with AF. Furthermore, total membranous signal was lower in patients with mitral valvular disease. Due to ethical reasons, epicardial conduction velocity assessment was not performed.⁷⁰

Kanagaratnum et al subsequently studied the relationship between right atrial connexin 40 and 43 expression and epicardial surface activation in the setting of acute and chronic AF. Acute AF

(lasting longer than 30 seconds) was studied in patients in sinus rhythm, without a history of AF, and undergoing coronary artery bypass surgery. Acute AF was generated at the time of surgery through burst pacing of the right atrium. Chronic AF was studied predominately in patients undergoing valvular replacement, with only 1 patient undergoing coronary artery bypass grafting, and another undergoing an atrial septal defect repair. The pattern of epicardial activation was assessed using a rectangular array of 112 electrodes (with 3.75mm spacing) or 225 electrodes (2.25mm spacing). Complexity of activation was assessed based on the number simultaneous wavefronts seen to pass over the area of the array in consecutive windows of a 2 second time period. Mapping revealed no difference in the complexity of epicardial activation between patients with acute or chronic AF. Immunofluorescence revealed heterogenous Cx40 expression in all chronic AF patients and only 60% of patients in the acute AF group. The degree of Cx40 heterogeneity was the same between patients with heterogeneity in both groups. There was no difference in Cx43 signal between both groups and homogenous expression was always observed. In patients with chronic AF, complexity of activation was inversely associated with Cx40 signal and the ratio of Cx40 to summed Cx40 and Cx43 signals. This

relationship however, was not observed in acute AF patients and Cx43 levels did not correlate with complexity in either group. The results suggested that changes in other factors associated with the underlying disease process may also be required before alterations in Cx40 and Cx43 ratios produced meaningful correlations with AF.⁷¹

The pattern of ion channel expression in addition to connexins 40 and 43 in patients with and without AF was studied by Gaborit et al. Three groups of patients were used. The first consisted of patients in sinus rhythm in the setting of coronary artery disease. The second consisted of patients in sinus rhythm with valvular heart disease. The last consisted of patients in AF with valvular heart disease. Gene microarray analysis revealed a significant up regulation of Cx43 and down regulation of Cx40 in patients with valvular heart disease compared to patients with coronary artery disease. Two way hierarchical analyses however revealed no differences of both connexins between patients with AF and sinus rhythm in the setting of valvular heart disease. Real time PCR for Cx40 and Cx43 mRNA was consistent with the gene array results. Protein levels assessed with Western blotting mirrored the gene expression results. Importantly there were significant differences

in other ion channels including that of potassium and calcium at the gene, protein, and patch clamping levels between patients with and without AF in the setting of valvular heart disease. The findings confirmed that factors such as ion channel expression were also altered in AF, supporting the idea that a threshold of conduction heterogeneity was required for the genesis of AF. The results also highlighted the importance of appropriate controls when assessing differences to ensure an accurate understanding of the significance of results.⁷²

Wetzel et al also studied the pattern of Cx40 and Cx43 expression in the atria of patients with and without AF. Study groups consisted of patients in sinus rhythm in the setting of either valvular or coronary heart disease, patients with lone AF undergoing intra-operative radiofrequency ablation, or patients with AF in the setting of mitral valve disease. Patients with lone AF were significantly younger while patients with AF and valvular disease had significantly larger left atria. Tissue samples were obtained from the left atrium. The only exception were patients with sinus rhythm undergoing coronary artery bypass grafting where right atrial appendage tissue was used. Quantitative densitometry of Western blots revealed a small but significant

increase in Cx40 levels and a large increase in Cx43 levels in patients with AF when compared to sinus rhythm controls. Further analysis revealed that the increase in Cx40 was due to patients with lone AF, while the increase in Cx43 was due to patients with AF in the setting of valvular disease. When the results of patients with the lone AF and valvular AF groups were further divided into paroxysmal or chronic AF, there was no difference in the levels of Cx40 and Cx43 when compared to patients in sinus rhythm. In addition, there was no difference in connexin levels between patients with and without valvular heart disease. Based on the findings of Kostin et al and Leaf et al where connexin expression varied between different sections of atrial, the results were difficult to interpret given that origin of tissue samples in 60% of sinus rhythm controls were different to patients with AF.^{54, 69, 73}

Rucker-Martin et al studied the pattern of expression of Cx40 and Cx43 in the right atrial appendages from patients undergoing open heart surgery. Study groups consisted of patients in sinus rhythm with normal sized atria and underlying coronary artery disease, patients with chronic AF and atrial dilation in the setting of valvular heart disease, and patients in sinus rhythm with dilated atria in the setting of predominately valvular heart disease. Compared to the

non-dilated atrial control group, atrial tissue from patients with dilated atria demonstrated lateralisation of Cx40 and Cx43 on immunofluorescence. In addition, there was a decrease in the cellular ratio of phosphorylated to non-phosphorylated Cx43, and a decrease in Cx40 expression on Western blotting. Importantly however, no loading controls for western blot analysis were used making the significance of the Cx40 results difficult to interpret.⁷⁴

The results of the preceding human studies suggest that a variable and complex inter-related threshold of tissue heterogeneity comprised not only of alterations in Cx40 and Cx43 ratios, but also other factors such as connexin phosphorylation and lateralisation, ion channel expression, and fibrosis must be reached to create a substrate suitable for supporting AF. It is also likely that the differing patterns of connexin alterations observed within each of these studies are affected by the underlying disease processes of the recruited patients. While valvular heart disease is likely to result in heart failure secondary to volume overload, ischaemic heart disease can alter atrial connexin expression directly through lack of tissue oxygenation and indirectly through ventricular failure^{74, 75}.

1.2.3 Summary

In summary, based on the preceding literature review, it is clear that connexins have the ability to modulate tissue conduction velocity and anisotropy, and through aberrant expression also have the ability to lower tissue vulnerability thresholds for the development of arrhythmia.

Connexin expression is clearly dynamic and subject to many intracellular and extracellular factors. Macroscopic junctional conductance is affected by cell type and has a non-linear relationship to connexon isotype composition. Other influential factors of conductance include the degree of connexin phosphorylation, connexin location, and total junctional connexin content. These factors vary from location to location within the same cardiac chamber, and are subject to further influences including blood supply, chamber pressures, and beat frequency. An added layer of complexity occurs when changes such as genetic engineering, somatic gene transfer, or arrhythmia induction are applied.

One of the biggest problems with human and animal studies has been the use of controls from different disease states. Clearly patients with sinus rhythm and ischemia are not adequate controls for patients with AF and valvular heart failure. Appropriate vector controls need to be used with somatic gene transfer techniques so as to fully understand the outcomes. Genetically engineered models need to be adequately assessed to explain discrepancies such as the presence of AV synchrony despite the apparent knockout of all connexins within the His bundle. Clearly such an animal must either still be a chimera with an incomplete level of connexin knockout in the His bundle, or have a congenital accessory AV pathway. Lastly, when assessing outcomes such as conduction velocities and foreknowing the scale of heterogeneity, mapping systems with high enough resolution should be utilised.

A striking feature upon reviewing this literature is the considerable variation and often opposing patterns of connexin expression between similar study models. This highlights the difficulty, but also necessary importance of choosing the right model and considering all factors that may influence conduction, when designing a study into connexins.

Based on the above-mentioned considerations, the technique of somatic gene transfer presents itself as the best way to assess the true functional significance of relative connexin isotype expression levels, and of connexin mutations. With appropriate controls including a vector control, and a wild-type connexin control, the confounding factors and problems identified within this literature review can be avoided.

CHAPTER 2

Materials and General Methods

This chapter describes the general methods employed within this research project. Specialised methods or variations of these general methods are described in their respective results chapters.

2.1 Molecular Biology

2.1.1 Chemicals, reagents, and plastic/glassware

Only analytical grade chemicals and reagents were used and the suppliers of these are indicated throughout the text. In addition, only reagent grade water (MQH₂O) was used when solution production required water. All plastic and glassware were washed, rinsed with MQH₂O, and autoclave sterilised prior to use.

2.1.2 Bacterial strains and plasmids

Only the *Escherichia coli* bacterial strain JM109 (genotype: endA1, recA1, gyrA96, thi, hsdR17 (r_k⁻, m_k⁺), relA1, supE44, Δ(lac-proAB), [F', traD36, proAB, laqI^qZΔM15]; source: Promega) was

used to propagate plasmid DNA. The plasmids used within this research are described in Tables 2.1 and 2.2. Each plasmid possessed an ampicillin resistance gene.

2.1.3 Bacterial growth media

Escherichia coli was grown in Luria-Bertani (LB) broth or on solid LB-agar. Fresh broth was prepared when required using 0.5% (w/v) yeast extract (Sigma-Aldrich), 1% (w/v) tryptone (Sigma-Aldrich), and 1% (w/v) sodium chloride (Sigma-Aldrich) dissolved in MQH₂O. Bacteriological agar 1.5% (w/v) was added to fresh broth when LB-agar was required. All media was autoclave sterilised at 121°C for 20 minutes. To facilitate selective growth of successfully transformed JM109 cells during propagation, ampicillin (100µg/mL) was added to media once cooled. In the case of LB-agar, this was at approximately 55°C, prior to pouring into 10cm petri dishes.

Table 2.1: DNA Plasmids used within this Research Project

Plasmid	Description	Source
Lentiviral Vector (LV) plasmids	See Table 2.3	Inder Verma, USA
pPPT.CX40	LV plasmid encoding cDNA for rat connexin40 (Cx40)	Vector plasmids produced by Eddy Kizana prior to research program based on pRRLSin18.cPPT.CMV.eGFP.W
pPPT.P88S	pPPT.Cx40 bearing a missense 882C→T mutation in the Cx40 coding region	
pPPT.G38A	pPPT.Cx40 bearing a missense 113G→A mutation in the Cx40 coding region	
pPPT.A96S	pPPT.Cx40 bearing a missense 286G→T mutation in the Cx40 coding region	
pPPT.KIR2.1	LV plasmid encoding cDNA for rat inward-rectifier potassium ion channel 2.1	
pPPT.CX43Δ8	LV plasmid encoding cDNA for rat connexin43 bearing a 24 bp deletion	
pUC18	Transformation control plasmid	Thermo Scientific

2.1.4 Propagation of plasmids

2.1.4.1 Preparation of electro-competent cells

From a glycerol stock, non-transformed *Escherichia coli* (JM109) was streaked onto a fresh LB-agar plate and incubated at 37°C. The following afternoon, a single bacterial colony was used to inoculate 5mls of LB-broth. This was incubated overnight at 37°C on an orbital shaker set to 220rpm. The resulting bacterial suspension was added to 500mL of LB broth and incubated at 37°C on an orbital shaker until the cultures reached a mid-log phase of growth as determined by spectrophotometry, (absorbance of 0.4 at 600nm). This was approximately 3 hours. The bacterial suspension was transferred to 2 polypropylene centrifuge bottles and centrifuged at 3000 x g at 4°C for 2 minutes. The supernatant was discarded and the cells gently resuspended in 250mls of ice cold Transformation Buffer (TB) buffer. The cells suspension was incubated on ice for 30 minutes before centrifuging again at 3000 x g at 4°C for 2 minutes. The supernatant was discarded and the cells were resuspended in 1ml of 10% w/v glycerol (Sigma-Aldrich). Cell suspension aliquots of 40µL were put into microcentrifuge tubes, snap frozen in liquid nitrogen, and stored in a -80°C freezer. The transformation

efficiency was assessed by transforming a known quantity of plasmid DNA into an aliquot of cells and counting the colonies grown on selective LB-agar plates. The efficiency of these cells was $>2.0 \times 10^7$ transformants per μg of DNA.

2.1.4.2 Bacterial transformation with plasmid DNA

A 40 μL aliquot of JM109 electro-competent cells and plasmid stock were thawed on ice. One microliter of plasmid stock, containing between 50 to 500ng of DNA, was added to the bacterial cells. The mixture was transferred to a pre-chilled electroporation cuvette. The cells were pulsed once with 200 Ω resistance and capacitance of 960 μF at 1.7kV using a Bio-Rad Gene Pulser II electroporator. This produced a time constant of approximately 4.5ms. Immediately following electroporation, 200 μL of SOC medium was added to the cuvette. The cell suspension was transferred to a microcentrifuge tube and incubated at 37°C for 1 hour. A 10 fold dilution with SOC medium was performed and a 100 μL aliquot was plated onto LB agar for incubation overnight at 37°C.

2.1.4.3 Large scale preparation of plasmid DNA

A starter culture was produced by inoculating 5mL of LB broth with a single colony of transformed cells in a 14mL polypropylene tube and incubating the resulting suspension on an orbital shaker for 8 hours at 37°C. The starter culture was added to 150mL of LB broth in a 1L conical flask and incubated on an orbital shaker at 220rpm at 37°C overnight. The following morning, a glycerol stock was made by gently mixing 850µL of the resulting bacterial suspension with 150µL of glycerol (Sigma-Aldrich) and subsequently stored in a -80°C freezer. The rest of the suspension was pelleted at 6000 x g for 15 minutes at 4°C. The supernatant was discarded and the bacterial pellet processed with the alkaline lysis method, using a commercially available Qiagen HiSpeed Plasmid Maxi Kit according to the manufacturer's protocol. The cell pellet was resuspended in 10mL of buffer P1 containing RNase A. Lysis was enacted with the addition of 10mL of buffer P2 and subsequent incubation for 5 minutes at room temperature. Genomic DNA, protein, and cell debris were precipitated with the addition of 10mL of chilled buffer P3 and subsequent incubation for 10 minutes at room temperature. During the incubation period, a HiSpeed Maxi Tip was equilibrated

with 10mL buffer QBT. The lysate was filtered with a QIAfilter cartridge onto the HiSpeed Maxi Tip and allowed to pass through the resin by gravity flow. The HiSpeed Maxi Tip was washed with 60mL of buffer QC and the DNA eluted using 15mL of buffer QF into a 50ml polypropylene tube. DNA was precipitated by incubation with 10.5mL of 100% (v/v) isopropanol (Sigma-Aldrich) for 5 minutes. The eluate/isopropanol mixture was filtered through a QIAprecipitator. The QIAprecipitator was washed with 2mL of 70% (v/v) ethanol (Fronine) and air dried. DNA was subsequently eluted with 1mL of TE buffer. DNA concentration and purity of the new plasmid stock was assessed with spectrophotometry prior to storage in a -80°C freezer. The yield of plasmid DNA varied between 0.5mg to 1.5mg.

2.1.5 Estimation of plasmid DNA concentration and purity

Spectrophotometry was routinely used to assess plasmid DNA samples. Absorbances at wavelengths of 260nm and 280nm were used to determine plasmid DNA concentration and purity. This method assumed that 50µg of dsDNA has an absorbance of 1.0

at 260nm while pure dsDNA has a 260/280 absorbance ratio of 1.8.

2.2 Cell Culture

2.2.1 Cell lines, reagents, and plastic/glassware

The cell lines used during this project are listed in table 2.2.

Cell culture media was freshly supplemented with the cell culture grade reagents specified in Table 2.2 prior to the commencement of individual experimental protocols.

For subculture and other manipulations, HEK293T cells were washed with Dulbecco's Phosphate Buffered Saline (DPBS) lacking calcium and magnesium (Lonza) and detached and disaggregated using 0.05% Trypsin/0.5mM EDTA solution (Sigma-Aldrich).

Sterile filtered fetal bovine serum (FBS; SAFC Biosciences), was stored at -20 °C and heat inactivated prior to use by warming to 37°C for 30 minutes.

Cell culture plastic ware including culture flasks and serological pipettes were obtained from Falcon and Corning and used only

once. Glassware was washed, rinsed with MQH₂O and autoclave sterilized prior to each use.

2.2.2 General cell culture methods

Published cell culture methods were employed in this research project.⁷⁶ Cells were grown in disposable polystyrene flasks/dishes (Falcon or Corning) or sterile glassware containing their respective media as detailed in Section 2.2.1. All cultures were grown in a 5% CO₂ environment at 37°C.

2.2.2.1 Cell counting using a haemocytometer

Cell suspensions were counted at a concentration of 10⁵ to 10⁶ cells per millilitre. A 100uL aliquot of cells was mixed with an equal volume of 0.5% trypan blue (Sigma-Aldrich). A 15uL aliquot was applied beneath each side of a cover slipped haemocytometer (Brand). Live cells were counted using a 10X objective of an inverted microscope (Olympus CK2). The number of cells in the 4 major outer corners of each of the 2 chambers (8 squares in total) was averaged, corrected for dilution, and multiplied by 10⁴ to give the number of cells per mL.

Table 2.2: Cell types used in cell culture experiments

Cell Type	Description	Source	Medium
HEK293T	Transformed human embryonic kidney cells	ATCC number: CRL-11268	1
NRVM	Primary Day 2-3, neonatal rat ventricular myocytes	Adult Sprague Dawley rats, Animal Resources Centre, Western Australia	2,3,4,5

1. Dulbecco's Modified Eagles Medium (DMEM; Invitrogen) supplemented with 10% (v/v) FBS (SAFC Biosciences) and 2mM glutamine (Invitrogen)
2. Hank's Balanced Salt Solution (HBSS; Invitrogen)
3. HBSS with 1mg/ml Ultrapure Trypsin (Trypsin 4.066 USP u/mg, Chymotrypsin 12.13 USP u/mg; USB Corporation)

4. HBSS with 1mg/ml Collagenase Type 2 (245u/mg; Worthington)

5. Medium 199 (Invitrogen) supplemented with 1% HEPES Buffer Solution (Invitrogen), 1% MEM Non-Essential Amino Acids (Invitrogen), 1.75g Glucose (Sigma-Aldrich), 2mM L-Glutamine (Invitrogen), 1.5µm/L Vitamin B12, 20U/mL Penicillin solution (Sigma), and 2% or 10% (v/v) FBS (SAFC Biosciences).

2.2.2.2 Subculture of adherent HEK293T cells

When cultures became confluent or were required for experimentation, cells were subcultured by enzymatic detachment and replating. Culture media was aspirated from the flask and the cells were washed once with PBS. A total of 2mL of 0.05% Trypsin/EDTA solution was added to the culture and placed at 37 °C for 2 minutes to allow cell detachment. Trypsin was subsequently inactivated by the addition of culture media. The media was pipetted up and down approximately 5 times to further dislodge cells and then transferred to a polypropylene tube for centrifugation at 1500 revolutions per minute for 5 minutes. Media was decanted and the pellet resuspended in fresh culture media. An aliquot of the cell suspension was seeded into a new culture flask according to the dilution required. Cells were split 2 to 3 times per week depending on their growth characteristics.

2.2.2.3 Short and long term storage of HEK293T cells

Cells to be frozen were detached by trypsinisation during exponential growth and pelleted by centrifugation (300 x g, 5 minutes). Media was aspirated and the cells resuspended at 1-2 X

10^6 per mL in storage media consisting of culture media with 20-50% FBS and 10% (v/v) DMSO (Sigma-Aldrich). Cell suspension aliquots of 1mL were placed in sterile cryovials (Nunc) and stored at -80 °C. Cells for long term storage were moved to liquid nitrogen the following day.

Cells to be recovered from short and long term storage were thawed rapidly in a 37°C water bath. To remove DMSO, the contents of a cryo-vial was mixed with 9mls of warmed (37°C) culture media, pelleted at 300 x g for 5 minutes and resuspended in fresh culture media following aspiration of the supernatant.

2.2.3 Neonatal rat ventricular cardiomyocyte cultures

2.2.3.1 Plating surface preparation

On the day of ventricular harvesting from rat pups, surfaces intended for cardiomyocyte culturing were sterilised with ultraviolet light for 1 hour. Following sterilization, surfaces were coated at room temperature using a fresh 25mg/ml solution of fibronectin powder (BD Biosciences) dissolved in MQH₂O that had been previously filter sterilised with a 0.45µm PVDF syringe driven filter

unit (Millipore). The fibronectin solution was aspirated from culture surfaces just prior to the plating of cardiomyocytes.

2.2.3.2 Isolation of neonatal rat ventricular cardiomyocytes

Ethics approval was received prior to dissection. Two litters of rat pups were used for each dissection. Pups were sprayed with 70% ethanol, decapitated with a large pair of straight surgical scissors (Roboz Surgical Instrument Co), and their chests opened with angled delicate scissors (Roboz Surgical Instrument Co). Ventricles were excised, placed into ice cold HBSS, and quartered. Following 2 rinses with ice cold HBSS, ventricular tissue was transferred to a glass jar containing 40mL of trypsin/HBSS solution, and agitated on an orbital shaker at 75rpm at 4°C for 16 hours. Following trypsinization, the media was aspirated and discarded. Warm 10% serum culture media was added and gently agitated in a 37°C water bath for 4 minutes. The media was then aspirated and discarded. Fresh collagenase/HBSS (8mL) was added to the tissue and gently agitated in a 37°C water bath for 1 minute. The collagenase/HBSS solution was aspirated and discarded. A fresh 8mL of

collagenase/HBBS solution was again added to the tissue and gently agitated in a 37°C water bath for 1 minute. The tissue and media was pipetted up and down once with a 10mL serological pipette to assist with myocyte dissociation. The media was aspirated and added to ice cold HBSS and kept on ice. A further 8mL of collagenase/HBBS was added to the tissue and the process repeated 3 times. The 4 aliquots of HBSS solution containing dissociated cells were pelleted at 50 x g at 4°C for 8 minutes. The supernatant was aspirated and the pellets resuspended in 8mL of ice cold HBSS. The cell suspension was filtered with a 40µm cell strainer (BD Biosciences) and the filtrate centrifuged at 50 x g at 4°C for 6 minutes. Again the supernatant was aspirated and discarded. The pellet was resuspended in warm 10% serum culture media, pre-plated into a 150cm² tissue culture flask, and incubated at 37°C at 5% CO₂ for 2 hours. This pre-plating step allowed for the removal of fibroblasts. Following incubation, media containing non-attached cardiomyocytes was aspirated and placed into a 50ml polypropylene tube. The tissue culture flask was rinsed gently with 10% serum culture media and the rinse also added to the 50ml polypropylene tube. The media was gently pipetted up and down once with a 25mL serological pipette just prior to assessing the cell density of the solution. Cells

were counted as described in section 2.2.2.1. Further 10% serum culture media was added to the cell suspension to achieve a final density of 7×10^5 cardiomyocytes/mL. At this density, a confluent monolayer was always achieved at 24 hours post plating.

2.2.3.3 Post plating care of cardiomyocyte cultures

Approximately 24hrs after plating cardiomyocytes, media was aspirated and the cardiomyocytes washed once with PBS pre-warmed to 37°C. Fresh 10% serum culture media pre-warmed to 37°C was added to the cardiomyocytes and the cells returned to the incubator. To prevent the growth of fibroblasts, media was replaced with fresh 2% serum culture media pre-warmed to 37°C at 48hrs and 90hrs post plating.

2.3 Production and Application of Lentiviral Vectors

2.3.1 Lentiviral vector plasmids

Third-generation, lentiviral constructs based on the human immunodeficiency virus Type 1 (HIV-1) were used throughout this research project.⁷⁷⁻⁸¹ The plasmids included the self-inactivating (SIN) long terminal repeat (LTR), the central polypurine tract (cPPT) and the woodchuck hepatitis virus post-transcriptional regulatory element (WPRE). The four plasmids (see Table 2.3) required for vector production were kindly supplied by Professor Inder Verma from the Salk Institute.

2.3.2 Vector production by lipofection

Vector was produced by Lipofectamine 2000 reagent (Invitrogen) mediated lipofection of the four lentiviral plasmids into HEK293T cells. Seven 75 cm² tissue culture flasks were used per vector production run. Cells were grown to 80% confluence and on the morning of transfection, media was aspirated and 10mL of fresh culture media added. Approximately 6 hours later, the media was aspirated again and replaced with the transfection mix. For each

Table 2.3 Plasmids for Lentiviral Vector Production

Plasmid	Abbreviation	Description	Size (bp)
pRRLsin18.cPPT.CMV.eGFP.WPRE	PPT.CMV.eGFP	Vector	7425
pMDL.g/p RRE	MDL.RRE	Packaging	8895
pMD2.VSV.G	VSV.G	Envelope	5824
pRSV-REV	REV	Regulator	4174

75 cm² flask of HEK293T cells, 10 mL of transfection mix containing a total of 40 µg of plasmid DNA was prepared. The DNA was made up of the 4 plasmids in equimolar ratio. The plasmid DNA and 75 µL of Lipofectamine 2000 reagent were initially incubated in 2 separate polypropylene tubes containing 1.9 mL of Opti-MEM 1 media (Invitrogen) each, for 5 minutes at room temperature. Plasmid and Lipofectamine aliquots were subsequently mixed and co-incubated for a further 20 minutes at room temperature. A total of 6.2 mL of 10% DMEM/FBS was gently added to the plasmid/Lipofectamine mix to produce the final transfection mix. Approximately 16 hours later, media was removed from each flask and replaced with 10 mL of fresh DMEM/FBS media. A further 24 hours later, media was removed and replaced with 10 mL of fresh DMEM/FBS media. Vector-containing supernatant was then collected 24 hours later.

2.3.3 Vector purification and concentration

Vector containing supernatant was purified with a 0.45 µm polyvinylidene fluoride (PVDF) syringe driven filter unit (Millipore) immediately after collection and subjected to concentration. Unconcentrated supernatant was added to a sterile Centricon Plus-

70 (Millipore) sample filter cup, and spun in a swing bucket centrifuge at 720 x g at 10 °C for 120 minutes. The filtrate and its collection cup were subsequently discarded, and the device re-centrifuged at 720 x g at 10 °C for a further 2 minutes with a concentrate collection cup attached. Concentrated viral supernatant was divided into 50µL and 100 µL aliquots and stored in microcentrifuge tubes at -80 °C.

2.3.4 Assigning titre to vectors

Lentiviral titre was assigned by assessing genomic DNA integration in transduced HEK293T cells using a quantitative PCR-based method as described by Sastry et al.⁸²

2.3.4.1 Transduction of HEK293T cells

Suspensions of 5×10^4 HEK293T cells in 2mL of 10% DMEM/FCS were prepared in polypropylene tubes. Polybrene (Millipore) 8 µg/mL was added to enhance transduction efficiency. To these, 4 serial 10-fold dilutions of an initial 10µL of thawed concentrated vector were added in triplicate. Resulting suspensions were incubated at 37°C in 6-well plates for 4 days. Subsequent individual well cultures were washed with PBS and

dislodged after incubation with 100µL of 0.05% trypsin for 2 minutes. Trypsin was deactivated with 10% DMEM/FBS and the cell suspensions collected in microcentrifuge tubes. Cells were pelleted at 300 x g for 5 minutes, and resuspended in 200µL of fresh PBS after decantation of the supernatant.

2.3.4.2 Genomic DNA extraction

Genomic DNA was isolated from the samples using a QIAamp DNA Mini kit (Qiagen) according to the manufacturer's protocol. Qiagen Protease (20µL) was added to each sample and cell lysis was initiated by the addition 200µL of buffer AL. Samples were mixed with pulse-vortexing for 15 seconds and incubated at 56°C for 10 minutes. Genomic DNA was precipitated with 200µL of 100% ethanol (Fronine) and mixed again with pulse-vortexing for 15 seconds. The sample mixture was added to a QIAamp Mini spin column and centrifuged at 6000 x g at 20°C for 1 minute. The filtrate cup was replaced and the column was washed with 500µL of buffer AW1 centrifuged though at 6,000 x g at 20°C for 1 minute. After discarding the filtrate, a second column wash was performed with 500µL of buffer AW2 centrifuged through at 20,000 x g at 20°C for 3 minutes. The column was spun again at

20,000 x g at 20°C for a further 1 minute using a clean filtrate cup to ensure complete removal of buffer AW2. A total of 50µL of buffer AE was added to the column and allowed to incubate at room temperature before the genomic DNA was eluted by centrifugation at 6000 x g at 20°C for 1 minute. The concentration and purity of genomic DNA was assessed as described in section 2.1.5. Samples were stored at -80°C.

2.3.4.3 Real time quantitative PCR of genomic DNA

Sequences for the lentiviral probe (5'-FAMAGCTCTCTCGACGCAGGACTCGGC-TAMRA), forward primer (ACCTGAAAGCGAAAGGGAAAC), and reverse primer (CACCCATCTCTCTCCTTCTAGCC) were used as described by Sastry et al and manufactured by Sigma Aldrich.⁸² A total of 50ng of genomic DNA was used in each PCR reaction. Genomic DNA was diluted in 3 µL TE buffer and added to 22µL of a PCR master mix consisting of TaqMan buffer A (Applied Biosystems), 3.5mM MgCl (Applied Biosystems), 200µM of each dNTP (Applied Biosystems), 320nM of forward primer, 320nM of reverse primer, 200nM of lentiviral probe and 0.025units/µL of AmpliTaq Gold polymerase (Applied Biosystems). For a negative template

control, 3 μ L of H₂O was used. All reactions were carried out in triplicate and amplifications were performed with 1 cycle of 95°C for 10 minute, 35 cycles of 95°C for 15 seconds, and 60°C for 2 minutes using a Rotor-Gene 6000 PCR cycler (Corbett). Concurrent standard curves were generated using 7 serial 10 fold dilutions from 10⁸molecules/ μ l of the plasmid pRRLsin18.cPPT.CMV.eGFP.WPRE. Plasmid standards were spiked with genomic DNA (50ng/3 μ L) from non-transduced HEK293T cells to control for any inhibitory effect of genomic DNA on the PCR reactions. The number of vector DNA molecules in each sample reaction was calculated by comparing threshold cycle values of samples to the standard curve. To determine the final viral vector titre, the number of vector DNA molecules of each sample reaction was corrected for dilution and the number of cells plated, and then averaged.

2.3.5 Lenti-vector transduction of primary cardiomyocytes

Vector stock stored at -80 °C was thawed rapidly in a 37 °C water bath prior to transduction. Cardiomyocytes were suspended in media containing Polybrene 8 μ g/mL at the required cell density.

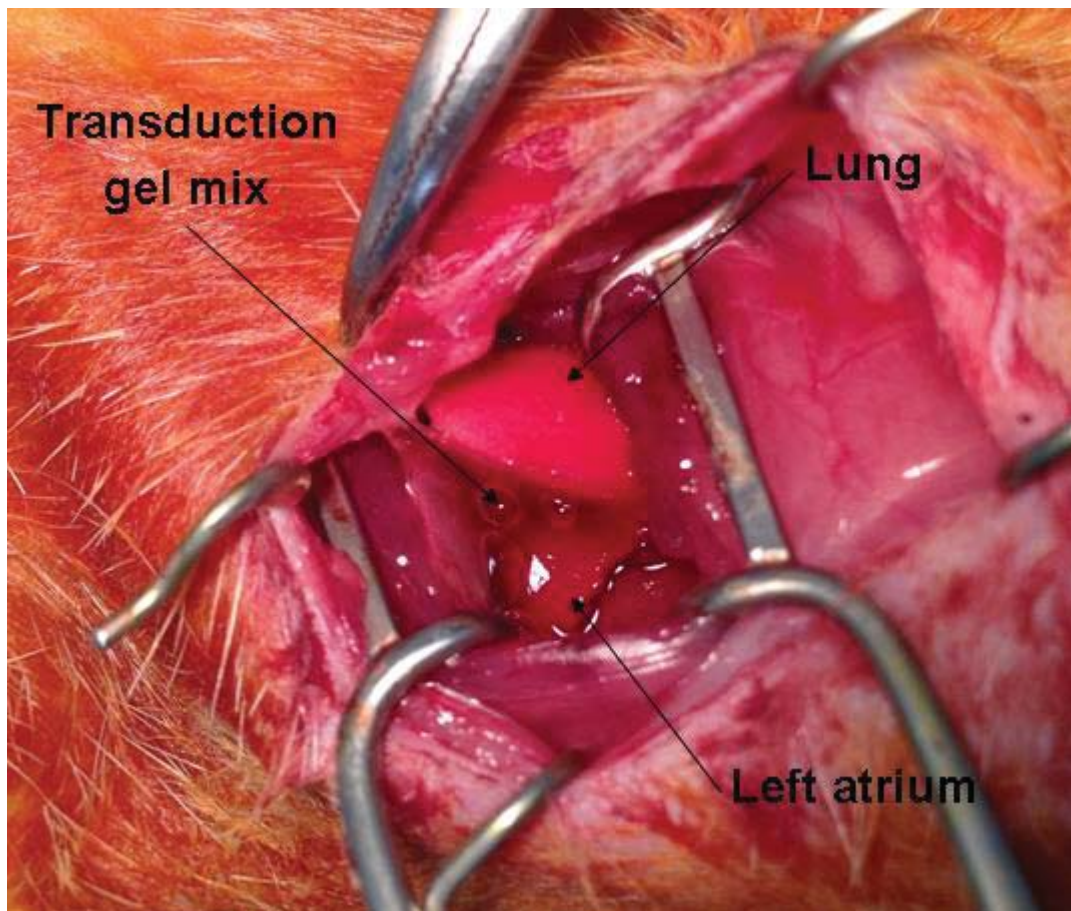
Vector stock was added at the required multiplicity of infection and the suspension gently pipetted once up and down with a serological pipette. The cell suspension was then plated and incubated at 37°C. Media was subsequently changed as described in section 2.2.3.3. Assessment of transduced cardiomyocytes was performed 96 hours post plating.

2.3.6 *In vivo* lenti-vector mediated transduction of rat left atrium

Vector stock stored at -80 °C was thawed rapidly in a 37 °C water bath prior to transduction. Following direct exposure of the left atrium, as per method 2.9.4, a mix of viral vector / 20% (wt/vol) Pluronic F127/ 0.05% Trypsin / Polybrene (160µg/mL) was produced, allowed to gel at room temperature, and applied to the left atrium with a camel hair brush as shown in Figure 2.1. Atria were left exposed for 20 minutes to allow viral adsorption.

Figure 2.1: Left atrial transduction

Transduction gel mix applied to the epicardial surface of the left atrium of a rat via a left thoracotomy.



2.4 Immunofluorescence – Staining for Connexins

2.4.1 Antibodies for immunofluorescence

Primary and secondary antibodies used during experiments are listed in table 2.4. Antibodies that required storage at -20°C were divided into 10µL aliquots using microcentrifuge tubes to minimise freeze-thaw cycles.

2.4.2 Atrial tissue sectioning

All cryo-sectioning was performed with a Microm HM 505E microtome cryostat. The temperature of the cooling chamber was always set to -21°C prior to the commencement of tissue handling. Frozen atrial tissue embedded in OCT compound (obtained as detailed in section 2.9.5) were mounted on a cryostat chuck pre-cooled with dry ice, and placed on the cryostat arm. A fresh microtome knife was used to initially trim the specimen, and then cut 7µm sections of atria that were transferred to glass slides (Superfrost Ultra Plus; Thermo Scientific) and kept on dry ice.

Table 2.4: Immunofluorescence Antibodies

Primary Ab Specificity		Host Species	Source	Dilution
Connexin40		Rabbit, polyclonal	Millipore	1 in 1000
Connexin43		Mouse, monoclonal	Millipore	1 in 250
Secondary Ab Specificity	Fluorophore			
Mouse Fc	Alexa Fluor 488	Goat, F(ab') ₂ fragment	Invitrogen	1 in 1000
Rabbit Fc	Alexa Fluor 594	Goat, F(ab') ₂ fragment	Invitrogen	1 in 2000
Mouse Fc	Alexa Fluor 594	Goat, F(ab') ₂ fragment	Invitrogen	1 in 2000

2.4.3 Fixation, permeabilisation and immunostaining

Atrial tissue sections and cell cultures were fixed, permeabilised and immunostained using the same method. Samples were fixed with 4% (w/v) paraformaldehyde for 15 minutes at room temperature and then washed 3 times with PBS. As the primary antibody epitopes were intracellular antigens, samples were then subject to permeabilisation by with 0.1% (v/v) Triton X-100 (Sigma-Aldrich) in PBS for 15 minutes followed by 3 gentle washes with 0.05% (v/v) Tween 20 (Sigma-Aldrich) in PBS (PBST) for 5 minutes each on an orbital shaker. A blocking solution consisting of 2% goat serum and 0.1% cold fish skin gelatine in PBST was applied for 1 hour. Samples were then incubated with primary antibody diluted in blocking solution overnight at 4°C. The following morning, samples were washed gently 3 times with PBST for 5 minutes each on an orbital shaker. Secondary antibody, diluted with 0.1% (v/v) cold fish skin gelatine in PBST, was added to samples for 1 hour at room temperature in the dark, followed by 3 gentle washes with PBST for 5 minutes each on an orbital shaker in the dark. Samples were cover slipped (Deckgläser; Menzel-Gläser) mounted with Prolong Gold anti-fade

reagent with DAPI (Life Technologies) and allowed to set in the dark, overnight at 4°C.

2.4.4 Fluorescent image acquisition and processing

Imaging of slides was performed under oil immersion using either an upright wide field fluorescent microscope (Leica DMBL) with a 100X objective (Leica 100X/1.30 Oil FLUOTAR 506195) or a confocal laser scanning microscope (Olympus FV 1000) using a 60X objective (Olympus 60X/1.35/0.15 (WD) Oil UPLSAPO). Imaging of cultures was performed using an inverted wide field fluorescent microscope (Leica DMIL) with a 20X objective (Leica 20X/0.305 Ph1 α /0.2 506272 HI plan 1). Digital images from the Leica DMBL microscope were acquired into PC based software (Spot Advanced version 4.1) using a digital camera (Spot RT KE) fitted to the microscope. Digital images from the confocal microscope were directly acquired into PC based software (Olympus FV10-ASW Version 1.7). Digital images from the Leica DMIL microscope were acquired into PC based software (Leica Application Suite Version 2.6.0 R1) using a digital camera (Leica DFC 490) fitted to the microscope.

Table 2.5: Filter Sets for Leica DMIL Microscope

Filter Sets	Exciter (nm)	Emitter (nm)
DAPI	315 - 420	385 - 515
GFP	430 - 510	475 - 575
DsRed	480 - 570	565 ALP

**Table 2.6: Excitation Wavelengths and Emission Filter Sets
for the Olympus Confocal Microscope**

Filter Sets	Excitation (nm)	Emission (nm)
WU2	BP 330 - 385	BA 420
NIBA3	BP 470 - 495	BA 510 - 550
WIG3	BP 530 - 550	BA 575 IF

2.5 Histology – Inflammation and Fibrosis

2.5.1 Inflammation - Haematoxylin and Eosin staining

Fresh atrial tissue sections were produced as described in sections 2.4.2 and 2.9.5. The technique of Haematoxylin and Eosin staining as described by Luna et al was performed with a Shandon Linear Stainer. Atrial sections were immersed in Haematoxylin for a total of 4 minutes, Scott's Bluing solution for 1 minute, and 0.1% Eosin for 1 minute. A 1 minute wash with tap water was performed following each step. Prior to coverslip mounting with a hydrophobic mounting agent, Ultramount No4 with colourfast (Fronine), samples were dehydrated with absolute ethanol for 30 seconds and placed in xylene clearing solution. Slides were allowed to set overnight. Following image acquisition as described in section 2.5.3, images were assessed manually for inflammation by two independent observers. The technique described by Igarashi et al was used to grade inflammation on a scale of 1 to 5. Images were assigned a score of 1 if inflammation was not present, a score of 2 if occasionally present, a score of 3 if diffusely affecting less than 50% of the image, a score of 4 if diffusely present throughout more than 50% of the image, and a score of 5 if near complete presence in the entire image.

2.5.2 Fibrosis - Picro-Sirius Red staining

Atrial tissue sections produced as described in section 2.4.2 were fixed with 4% paraformaldehyde for 15 minutes followed by 3 washes in PBS for 5 minutes. Sections were placed in Picro-Sirius red solution (0.1% Direct Red 80 (Sigma), 0.1% Fast Green FCF (Sigma), Saturated Picric Acid (Sigma)) for 1 hour in the dark on an orbital shaker set to 50rpm. One wash with MQH₂O was performed followed by 3 washes in 100% ethanol for 1 minute each to dehydrate the sections. Samples were allowed to air dry for 1 hour and then immersed in xylene clearing solution for 5 seconds before cover slip mounting with a hydrophobic mounting agent, Ultramount No4 with colourfast (Fronine). Slides were allowed to set overnight. Sections were then processed with custom made software designed to objectively calculate the relative areas of red (collagen) and green staining (myocytes).

2.5.3 Image acquisition and processing

Samples were visualised initially using an upright microscope (Leica DMBL). A 20X objective (Leica 20X/0.40 N plan \times /0.17/D 506096) was used for image acquisition of 8 random areas of

each section under oil immersion. The PC based software, Spot Advanced version 4.1, was used to directly acquire digital images from a Spot RT KE camera fitted to the microscope.

2.6 Immunoblotting

2.6.1 Antibodies for immunoblotting

Primary antibodies used during experiments are listed in table 2.4. Secondary antibodies used during experiments are listed in table 2.7. Antibodies that required storage at -20°C were divided into 10µL aliquots using microcentrifuge tubes to minimise freeze-thaw cycles.

2.6.2 Protein extraction

Cell culture

Six well plates with confluent cells were placed on ice. A 50µl mix of ice cold lysis solution (RIPA buffer (Sigma-Aldrich), 1% phosphatase inhibitor cocktail 2 (Sigma-Aldrich), and 4% protease inhibitor cocktail (Sigma-Aldrich)) was added to each well. Cells were dislodged from the plate surface with a plastic scraper. The resulting suspension was placed in ice cold microcentrifuge tubes and incubated on ice for 30 minutes. Suspensions were then centrifuged at 300 x g for 5 minutes at 4°C. The supernatant decanted into a second ice cold microcentrifuge tube and kept on ice ready for protein estimation.

Table 2.7: Secondary antibodies for immunoblotting

Secondary Ab Specificity	Label	Host Species	Source	Dilution
Mouse Fc	HRP	Rabbit	Sigma	1 in 10000
Rabbit Fc	HRP	Goat	Sigma	1 in 10000

Atrial Tissue

Frozen atrial tissue was placed into an ice cold round bottom microcentrifuge tube and kept on ice. An ice cold steel ball (Qiagen) was inserted into the tube along with 300 μ l of ice cold lysis solution (RIPA buffer (Sigma-Aldrich), 1% (v/v) phosphatase inhibitor cocktail 2 (Sigma-Aldrich), and 4% (v/v) protease inhibitor cocktail (Sigma-Aldrich)). The tissue was then subjected to disruption with bead milling for 4 minutes using a TissueLyser (Qiagen) set to 20Hz. Suspensions were then centrifuged at 300 x g for 5 minute at 4°C. The supernatant was decanted into a second ice cold microcentrifuge tube and kept on ice ready for protein estimation.

2.6.3 Protein estimation

Protein estimation was performed using the Bradford method. All standards and samples were assayed in triplicate. Bovine serum albumin (1mg/mL) was added, in 1mL increments from 1mL to 10mL, to different wells of a 96 well plate, and used to generate a standard curve. Extracted protein samples were diluted 10 fold with MQH₂O and added to wells in quantities of either 1 μ L or 2 μ L. Protein assay dye reagent concentrate (Bio-Rad) was diluted 4

fold and added in 200 μ L quantities to each well. The absorbance at a wavelength of 595nm was then measured for each well using a Victor² Multilabel Counter (PerkinElmer life Sciences). The amount of protein added to each sample well was calculated by comparing its absorbance to the standard curve. To determine the original protein concentration of an individual lysis supernatant, the protein amount within each well corresponding to the respective supernatant sample was corrected for dilution and then averaged.

2.6.4 Immunoblotting

Precast polyacrylamide 4-12% gradient Bis-Tris gels (NuPAGE; Invitrogen) were placed in a gel electrophoresis chamber (XCell SureLock Min-Cell; Invitrogen) containing running buffer (MOPS, NuPAGE; Invitrogen). For each sample, 20mg of protein was diluted in a microcentrifuge tube to a final volume of 20 μ L with 2 μ L of reducing agent (NuPAGE; Invitrogen), 5 μ L of LDS sample buffer (NuPAGE; Invitrogen), and MQH₂O. Diluted samples were heated to 95°C for 10 minutes to denature proteins and then loaded into separate gel wells. A constant 200V current gradient was applied to the gel for 1 hour. A pre-stained protein ladder

(PageRuler Plus; Thermo Scientific) was used to assess protein separation and approximate protein sizes. Following electrophoretic separation, protein was transferred from the gels to a membrane using the IBLOT gel transfer system (Invitrogen). Gels were placed in a gel transfer stack (Invitrogen) and the IBLOT's default 7 minute transfer protocol was used. Membranes were subsequently blocked with a solution of 5% skim milk in TBST (0.05% Tween 20, Tris-Buffered Saline) for 1 hour. Membranes were then incubated with primary antibody diluted in blocking solution, with gentle agitation on an orbital shaker, overnight at 4°C. The following morning, membranes were washed 3 times in TBST for 5 minutes each, and incubated with secondary antibody diluted in blocking solution for 1 hour, with gentle agitation on an orbital shaker. Three TBST washes for 5 minutes each was performed again followed by 5 minutes of incubation with Amersham ECL Western blotting detection reagents, which had been mixed in a 1 to 1 ratio according to the manufacturer's instructions. Membranes were transferred to an autoradiography cassette (Hypercassette; Amersham Biosciences). In a dark room, chemiluminescence film (Hyperfilm ECL; Amersham) was exposed to the protein membranes in the autoradiography cassette. The time of exposure was dependant

on the demands of the experiment. Following exposure, film was processed with an AGFA film processor according to the manufacturer's protocol.

2.7 Quantification of Tissue Connexin mRNA

2.7.1 mRNA extraction and purification

mRNA extraction was performed using an RNAeasy Mini Kit (Qiagen) according to the manufacturers protocol. Atrial tissue was transferred frozen to an ice cold round bottom microcentrifuge tube. A stainless steel bead (Qiagen), along with 350 μ L of buffer RTL (Qiagen), was placed within the microcentrifuge tube. The tissue was then subjected to simultaneous disruption and homogenisation with bead milling for 4 minutes using a TissueLyser (Qiagen) set to 20Hz. Following milling, the lysate was centrifuged at 20,000 x g for 3 minutes at 21°C. All subsequent centrifugation steps were performed at 8,000 x g at 21°C. The supernatant was carefully aspirated and placed in a fresh microcentrifuge tube. A 450 μ L volume of 70% ethanol was added to the supernatant and mixed with pipetting. The resulting solution was transferred to an RNAeasy spin column in 2 successive 450 μ L aliquots which were centrifuged for 15 seconds each. The column was washed using 700 μ L of buffer RW1 with centrifugation for 15 seconds. The column was then washed twice using 500 μ L of buffer RPE, with centrifugation for 15 seconds for the first wash and 2 minutes for the second wash.

The RNeasy spin column was then centrifuged for 1 minute using a new collection tube to eliminate any possible carryover of buffer RPE. The RNeasy spin column was transferred again to a new collection tube. A 30µL volume of RNase-free water was added to the column and used to elute the RNA with centrifugation for 1 minute. RNA samples were placed on ice. RNA concentration and purity was assessed with spectrophotometry as described in section 2.1.5, however with the assumption that 40µg of mRNA had an absorbance of 1.0 at 260nm and pure mRNA had a 260/280 absorbance ratio of 1.8.

2.7.2 cDNA synthesis from mRNA

mRNA was converted to cDNA with a Moloney Murine Leukaemia Virus Reverse Transcriptase (M-ML VRT) first-strand synthesis system (Promega). A mix containing 2µg of mRNA and 0.5 µg of random primers (Invitrogen) was diluted to 10 µL using DEPC-treated water. The RNA/primer mixture was incubated at 70°C for 5 minutes to melt secondary template structures and then placed on ice. Following incubation, a reaction mix consisting of 5 µL M-MLV 5X reaction buffer, 1.25 µL of each dNTP, 25 Units of Recombinant RNasin Ribonuclease Inhibitor, and 200 Units of

M-MLV RT was added to the RNA/primer mixture and diluted with DEPC-treated water to a final volume of 25 μ L. The resultant mixture was gently flicked and incubated at 42°C for 60 minutes. The reaction was then terminated with 5 minutes incubation at 70°C. The sample was placed on ice ready for cDNA concentration assessment as described in section 2.1.5.

2.7.3 Real time quantitative PCR

The Cx43 forward and reverse primer sequences were AGCCTGAACTCTCATTTTTCTT and CCATGTCTGGGCACCTCT respectively. The Cx40 forward and reverse primer sequences were CAGAGCCTGAAGAAGCCAAC and CATCTTGCCAAGTGTTGGAG respectively. The GAPDH forward and reverse primer sequences were TGGGAAGCTGGTCATCAAC and GCATCACCCCATTTGATGTT respectively. A total of 8 μ L of cDNA, 10 μ M primers (0.75 μ L), 2X Sybr min (10 μ L), and water (0.5 μ L) were used in each PCR reaction. All reactions were carried out in triplicate and amplifications were performed with 1 cycle of 50°C for 2 minutes, 1 cycle of 95°C for 2 minutes, and 40 cycles of 95°C for 15 seconds alternated with 60°C for 45 seconds, using a Rotor-Gene

6000 PCR cycler (Corbett). Results for each triplicate were averaged. Connexin RNA levels were normalised to GAPDH.

2.8 Primary Cardiomyocyte Electrophysiology

2.8.1 The multi-electrode array

Custom made multi-electrode arrays (MEA) were obtained from 2 sources as shown in Figure 2.2. The first, obtained from the Institute of Microtechnology (IMT; University of Neuchâtel, Switzerland), utilised a PECVD silicon nitride passivated glass chip with platinum electrodes that was mounted onto an open PCB with epoxy. The usable transparent area was delimited by a glass ring with an internal diameter of 20mm which formed the walls of the culture well. Recording electrodes had a diameter of 60 μ m and a centre to centre inter-electrode distance of 500 μ m. The second manufactured by Lowe Electronics Limited (China) using conventional printed circuit board (PCB) technology. Its surface consisted of polyimide, and electrodes were gold plated. The usable semi-transparent area was delimited by a Perspex (poly-methyl-methacrylate) ring with an internal diameter of 16mm which formed the walls of the culture well. Recording electrodes had a diameter of 75 μ m and a centre to centre inter-electrode distance of 700 μ m. Two stimulation electrodes with an inter-electrode (stimulation to stimulation and stimulation to recording) distance of 1000 μ m were placed on each of the 4 sides of the

recording array of both MEA's. Both MEA's possessed 52 recording electrodes and 8 stimulation electrodes

2.8.2 Culture recording

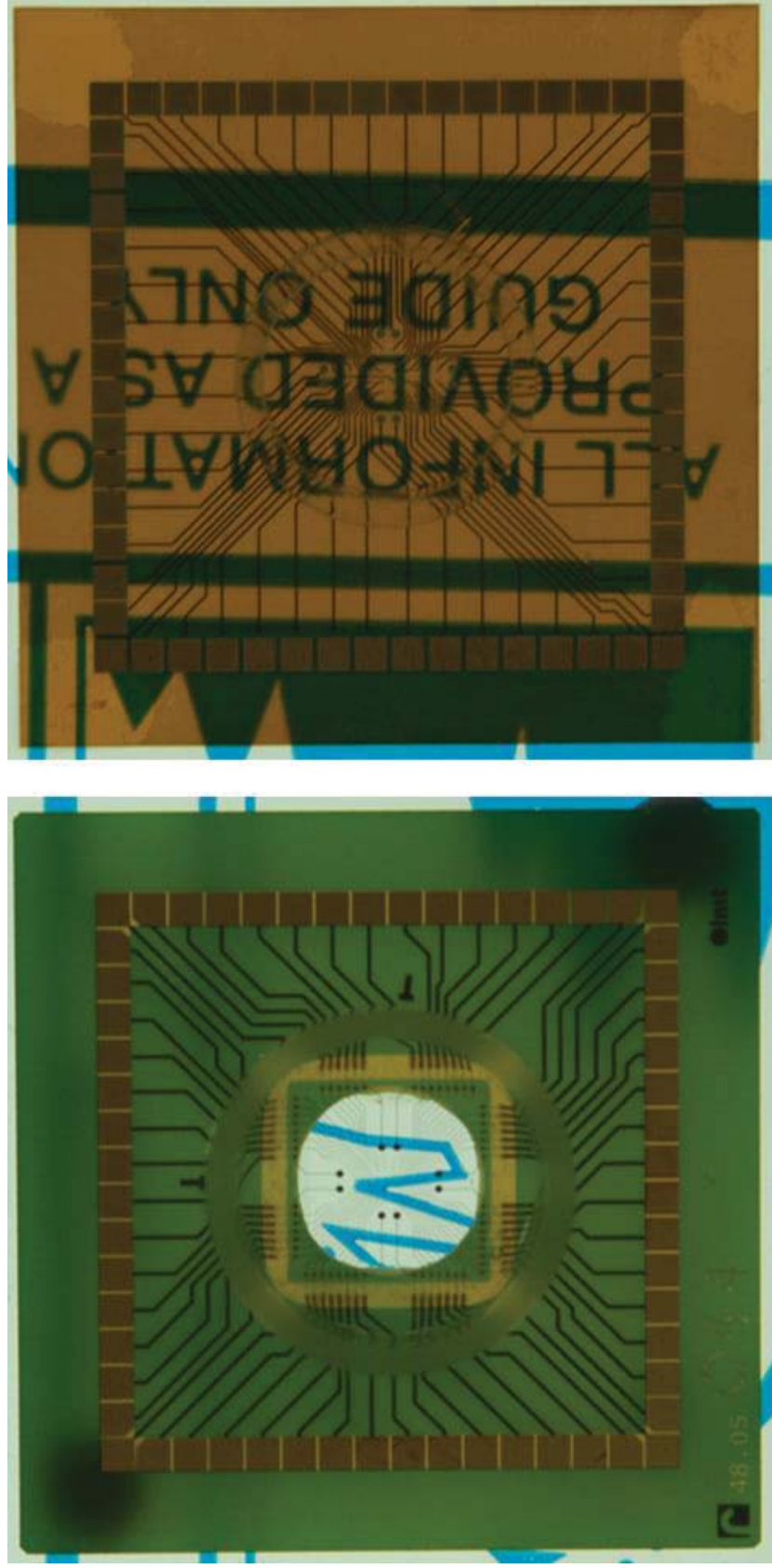
Multi-electrode arrays containing cardiomyocyte cultures were mounted into a commercial recording stage fitted internally with an amplifier (MEA1060 Amplifier; Multichannel Systems) as shown in Figure 2.3. After amplification, the electrical activity of cultures detected by the 52 recording electrodes were simultaneously digitised at 10kHz with a PXI platform (National Instruments), transferred to a PC based laptop computer (Dell) via an express card (NI ExpressCard-8360; National Instruments), and recorded using LabView (Version 10.0.1; National Instruments) as shown in Figure 2.4. Data was processed using the commercially available software CEPAS (Cuoretech).

2.8.3 Culture stimulation

An isolated pulse stimulator (Model 2100; A-M Systems) was used to deliver constant current stimuli at a frequency of 2Hz to cardiomyocyte cultures. Cultures grown on MEA's sourced from

Figure 2.2: Multi-electrode arrays

Silicon nitride passivated glass MEA chip mounted onto PCB on the left. Polyimide plastic MEA chip on the right.



IMT were stimulated by the stimulating electrodes incorporated into the array and required approximately $50\mu\text{A}$ for cardiomyocyte capture. Due to the capacitance properties of the polyimide MEA's, stimulation was performed via a separate custom made bipolar electrode device which when fitted to the top of culture wells, placed its electrodes in close proximity to the culture. This method required approximately $200\mu\text{A}$ for cardiomyocyte capture.

Figure 2.3: Multi-electrode stage.

MEA 1060 stage with internal amplifier (Multichannel Systems). The weighted stimulation electrode device is seen sitting above the well of an MEA placed within the stage.

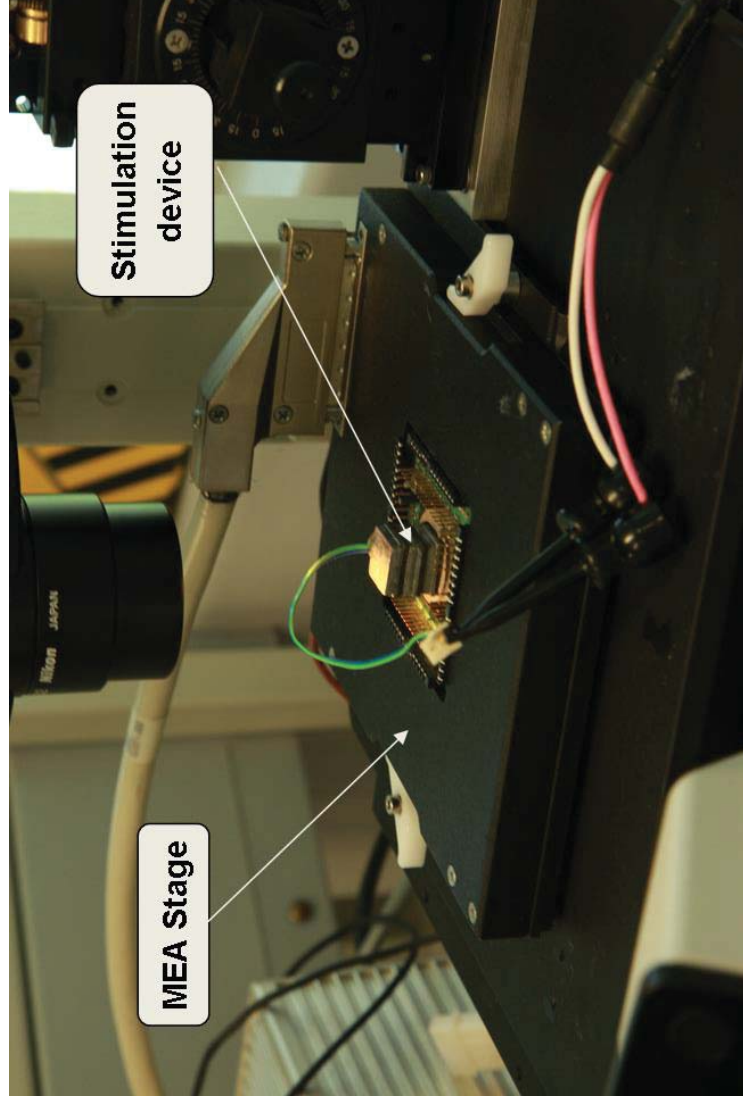
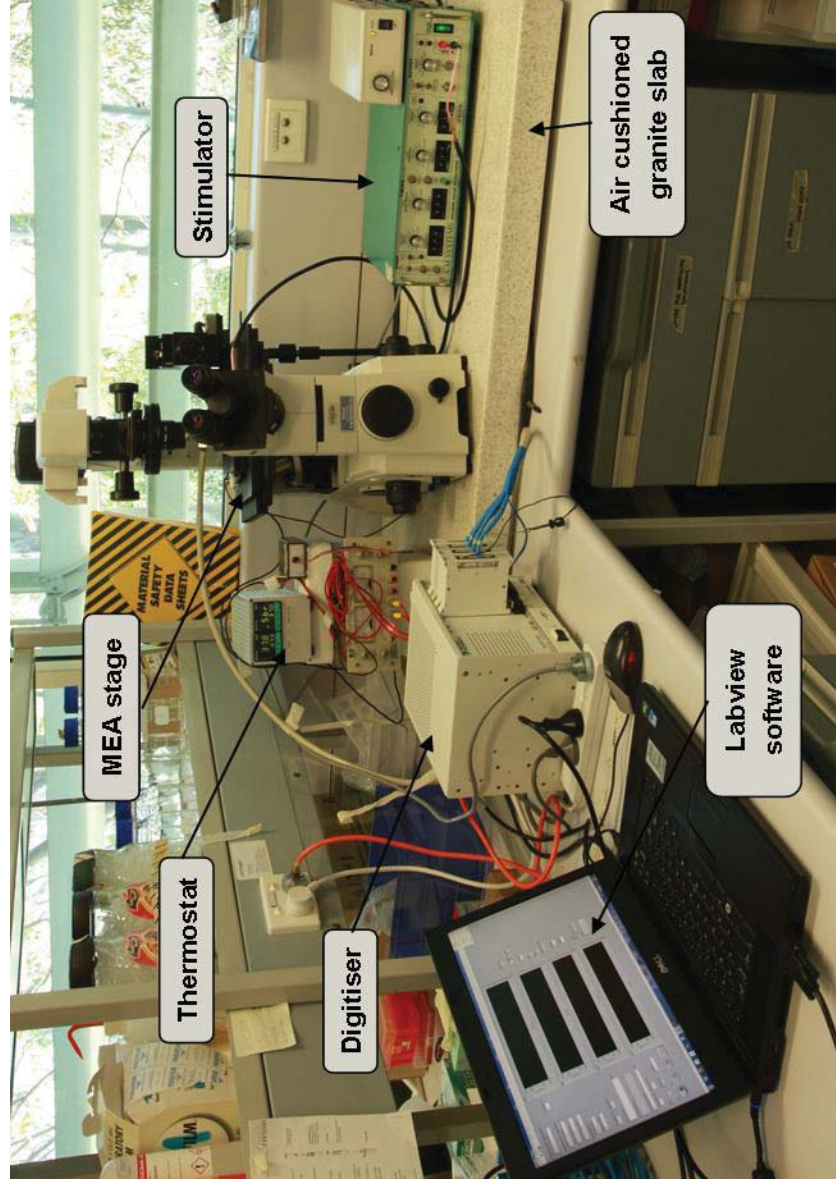


Figure 2.4: MEA recording system.

Signals from the MEA stage were digitised and recorded by the software Labview. A thermostat regulated MEA temperature. Vibration noise was minimised by an air cushioned granite slab.



2.9 *In Vivo* Studies

2.9.1 Anaesthesia, intubation, ventilation, and positioning

Rats were anaesthetised in a custom made Perspex chamber with a mix of oxygen and 5% isoflurane (Aerrane; Baxter Healthcare) supplied via flexible PVC tubing from a small animal anaesthetic machine (The Stinger; Advanced Anaesthesia Specialists). Once unconscious, rats were positioned, dorsal surface downwards, on a custom made intubation board shaped to facilitate neck extension. Direct laryngoscopy was performed by pulling the tongue out with straight serrated forceps (Fine Science Tools) and passing a rigid hippocampal tool (Fine Science Tools) into the pharynx to support the anterior neck tissues. The tubing of an 18 gauge intravenous cannula (Becton, Dickinson and Company) was passed under direct vision between the vocal cords into the trachea using a Seldinger technique. Rats were transferred to a bread board (Ikea) with their dorsal surface downwards. The cannula was subsequently attached with flexible PVC tubing to a small animal ventilator (Harvard Apparatus) set to deliver 2.5 ml tidal volumes at a rate of 70 breaths per minute. The ventilator

received a mix of oxygen and 2% isoflurane from the small animal anaesthetic machine (The Stinger; Advanced Anaesthesia Specialists). Prior to electrophysiology studies and thoracic surgery, upper and lower limbs were held fixed, extended at the shoulders and hips, by rubber bands looped around hooks screwed into the bread board.

2.9.2 Surface electrocardiography

When rats were anaesthetised, unipolar needle electrodes (AD Instruments) were placed subcutaneously at the infra-clavicular and iliac fossa regions bilaterally. Two lead electrocardiograms were generated combining potentials from left upper / right lower and right upper / left lower electrodes pairs. Bio-potentials, sampled at 2 kHz, were amplified with an Octal Bio Amp (AD Instruments) and digitised using a Powerlab 16/30 (AD Instruments) data acquisition system. Data was recorded, via USB, using the Windows based version of Labchart Pro 7 (AD Instruments) running on a Dell laptop. No software filtering was used. All data was analysed in detail offline.

2.9.3 Trans-oesophageal cardiac stimulation and recording

A 5 French octapolar catheter (Biosense Webster) connected to the Octal Bio Amp was passed via the oral cavity into the oesophagus and positioned at the point where recordings from the distal 2 electrodes had the largest atrial electrograms amplitudes. Recordings were made from the distal 2 electrodes only, while stimulation was delivered through the proximal 2 electrodes only. Atria were captured using a constant 60 volt square shaped stimulus of 1 millisecond duration via an isolated pulse stimulator (Model 2100; A-M Systems). Custom designed software installed on a second windows based laptop (Acer) was used to drive the stimulator via its trigger input.

The electrophysiology protocol involved the assessment of atrial refractory periods followed by an attempt to induce atrial fibrillation (AF). Atrial refractory periods were assessed using a drive train of 8 stimuli at a coupling interval of 150ms followed by 1 extra-stimulus. The coupling interval between the drive train and the extra-stimulus started at 120ms and was progressively reduced in 10ms increments down to atrial refractoriness. AF induction was

performed using a single burst of atrial pacing with a 90ms coupling interval for 5 seconds.

2.9.4 Thoracic surgery

A total of 10µg of Buprenorphine hydrochloride (Temgesic; Schering-Plough) and 1mg enrofloxacin (Baytril 50; Bayer Healthcare AG) were separately diluted in 1ml of PBS each and administered subcutaneously by injection. The hair of the anterior chest was moistened with 70% (v/v) ethanol (Fronine), shaved with electric clippers (Remington; Spectrum Brands), and removed. Skin disinfection was performed with 10% w/v Povidine-Iodine solution (Betadine; Sanofi-Aventis) applied for a minimum of 5 minutes prior to skin incision.

Using a scalpel, a horizontal incision of the skin from the ventral midline to the left anterior axillary line was made at the level at which the left apical beat was most prominent to palpation. Blunt dissection with straight haemostats (Fine Science Tools) of the underlying superficial fascia for up to approximately 1cm on both sides of the incision was performed to mobilise the surrounding skin. The muscles of the left chest wall superficial to the ribs and

overlying the area of the left atrial beat were also separated by blunt dissection with straight haemostats (Fine Science Tools). Using curved haemostats (Fine Science Tools), the thoracic cavity was punctured via the intercostal space lying over the area of the left atrial beat. The punctured intercostal muscles were bluntly dissected with the same curved haemostats and a Castroviejo retractor (Roboz) was inserted to hold open the dissected intercostal space. A hole was made in the pericardial sac over the left atrium with curved forceps (Fine Science Tools). Viral vector was applied to the left atrium as described in section 2.3.5. Following viral application and adsorption, the retractor was removed and the rib space closed with a single stitch of 3.0 coated vicryl suture (Ethicon). The skin incision was then closed with a horizontal mattress technique using a 3.0 coated vicryl suture (Ethicon). Drinking water for rats was supplemented with 0.01% enrofloxacin (Baytril 25; Bayer Healthcare AG).

2.9.5 Atrial tissue extraction, preparation, and storage

Prior to atrial extraction, adult rats were euthanized with carbon dioxide in a custom made Perspex chamber for 10 minutes and then weighed. Rats were subsequently laid dorsal surface down

and the chest wall cut open with scissors to the right of the midline. The heart was detached from the mediastinum just above the base and rinsed with PBS and subsequently weighed. The left atrium was then separated from the rest of the heart with a pair of fine scissors and rinsed once with PBS. For histology and immunohistochemistry studies, atria were placed in a vinyl specimen mould (Cryomold; Sakura) filled with Tissue-Tek OCT compound (Sakura). The mould was then frozen with liquid nitrogen and transferred to a -80°C freezer for storage. For protein and mRNA studies, atria were placed in microcentrifuge tubes, frozen in liquid nitrogen and transferred to a -80°C freezer for storage.

2.10 Statistics

Required sample sizes were estimated using nQuery Advisor (Statistical Solutions).

In the entailing *in vivo* research, we wished to detect a mean shift of 2 standard deviations or more in the transduced groups from the mean value observed in the control group. This was equivalent to requiring an effect size of 2 or more due to transduction. In order to detect an effect size of 2 with 80% power, a sample size of 6 per group was required (two sample t-test, 5% significance level, two tailed tests).

Our study of cardiomyocyte cultures required the measurement of conduction velocities on an MEA. Previously, the mean conduction velocity in non-transduced NRVM cultures was measured to be 19.1cm with a standard deviation of 0.6cm/s.⁸³ We expected that the connexin40 mutations would reduce mean conduction velocity to at least 16cm/s with a standard deviation of 0.6cm/s. Hence, a sample size of 6 cultures in each group will have over 80% power to detect a difference in means of 2.0cm/s

assuming that the common standard deviation is 0.6cm/s using a two group t-test with a 0.05 two sided significance level.

Each experimental group obtained equal subject numbers (randomly assigned) from multiple litters in order to minimise the effect of variance between the measurement means of single litters.

All data obtained is expressed as means +/- standard deviation and was assessed using PSAW Statistics 18. Parametric data was analysed with t-tests while non-parametric data (AF durations) were analysed with Mann-Whitney tests. Each mutant study group was compared to the wtCx40 study group.

CHAPTER 3

A System for Assessment of Lentivector Gene Modified Primary Cardiomyocytes

3.1 Introduction and Aims

Despite significant limitations, *in vitro* patch clamp techniques and *in vivo* genetically engineered animal models are the main techniques currently utilised by leading institutions for the functional screening of novel gene mutations identified in patients with cardiac arrhythmias.

While patch clamping is useful for studying action potential characteristics, contradictory results have been obtained depending on the cell type studied. Furthermore, single/dual cell studies fail to consider the modulating effects of extracellular signals often found in a multi-cellular syncytium. Genetically engineered animal models are useful for overcoming these limitations, but are however limited due to secondary

developmental defects. The classic example is the high incidence of congenital malformations associated with alterations in connexin expression.³⁴⁻³⁶ Both techniques are further hampered by high costs and a need for intensive training, experience, and time.

With the above mentioned limitations in mind, electrical assessment of acutely altered, genetically modified cardiomyocyte monolayers presents itself as an attractive alternative for studying such mutations. To date, numerous studies have assessed the effects of lentivector gene modification of cardiomyocyte monolayers with optical mapping, specifically looking at far field potential characteristics, automaticity, and conduction velocities. While extremely effective, optical mapping systems require significant technical support, a large capital investment, and darkroom workspace.

The multi-electrode array system has also been widely employed to assess the properties of cardiomyocyte monolayers. Most notably, using a variety of myocyte origins including atrial cell lines, stem cell derived myocytes, and neonatal rat ventricular myocytes, multi-electrode arrays have been used as a tool for

drug evaluation. Importantly this system is less hampered by the investment limitations of an optical mapping system.

The aim of this study was to validate the ability of a multi-electrode array (MEA) system for studying lentivector gene modified primary cardiomyocytes. We hypothesised that alterations in ion channel expression in primary cardiomyocytes alters monolayer conduction velocities (CV) in a predictable way on an MEA system.

3.2 Methods

3.2.1 Vector packaging and titration

Vector stocks encoding eGFP, the connexin43 internal loop mutant CX43 Δ 8, and the rat inward-rectifier potassium ion channel 2.1 (Kir2.1) were produced using the four plasmid lipofection method as described in sections 2.3.1 to 2.3.3. Titre was assigned to vector stocks by assessing genomic integration of viral DNA following transduction of HEK293T cells as described in section 2.3.4.

3.2.2 Myocyte isolation, transduction and culture

Neonatal rat ventricular myocytes were isolated from 2 to 3 day old Sprague Dawley rat pups as described in section 2.2.3. After isolation, myocytes were separated into a maximum of 4 study groups using 50 ml polypropylene tubes as shown in figure 3.1. Vector transduction of myocytes in suspension at equal multiplicities of infection was performed in the presence of Polybrene 8 μ g/mL as described in section 2.3.5. The non-transduced group received only Polybrene 8 μ g/mL. Following transduction, myocytes were seeded at a density of 220 x 10³

cells/ cm² onto either polystyrene, multi-well plates for transduction optimisation, or onto glass multi-electrode arrays for assessment of myocyte monolayer electrophysiology.

3.2.3 Transduction optimisation

To assess transduction efficiencies and toxicity, bright field and fluorescence microscopic assessment at a magnification of 20X was performed of cultures plated onto polystyrene plates after eGFP transduction at multiplicities of infection (MOI) of 1, 5, 25, 50, and 75. The capture ability of cultures to stimulation with 30µA pulses of 1ms duration at differing MOI's was also assessed.

3.2.4 Multi-electrode array studies

Transduced eGFP control monolayers were initially assessed for their level of transduction. If transduction efficiency was lower than 95% in any culture, all cultures within the experiment were discarded and section 3.2.2 repeated. If fluorescent assessment was satisfactory, all monolayers were next assessed for confluency with bright field microscopy. All non-confluent cultures were discarded, prior to electrophysiological assessment.

Following placement of MEA's within the MEA stage, MEA culture wells were sealed with a coverslip and the culture temperature maintained at 37°C for a minimum of 5 minutes prior to further assessment. Spontaneous beating frequency was assessed with bright field microscopy. If the beat frequency of an individual culture was greater than 2Hz, the culture was discarded. Conduction velocity assessment was then performed as described in sections 2.8.1 to 2.8.3. In brief, all remaining cultures were stimulated with square shaped 30 μ A current pulses of 1ms duration at a frequency of 2 Hz. Monolayer capture was assessed with bright field microscopy, followed by recording of monolayer field potentials via the multi-electrode array system. The software CEPAS was then used to generate isochronal maps of each culture and calculate the velocity of far field potential propagation.

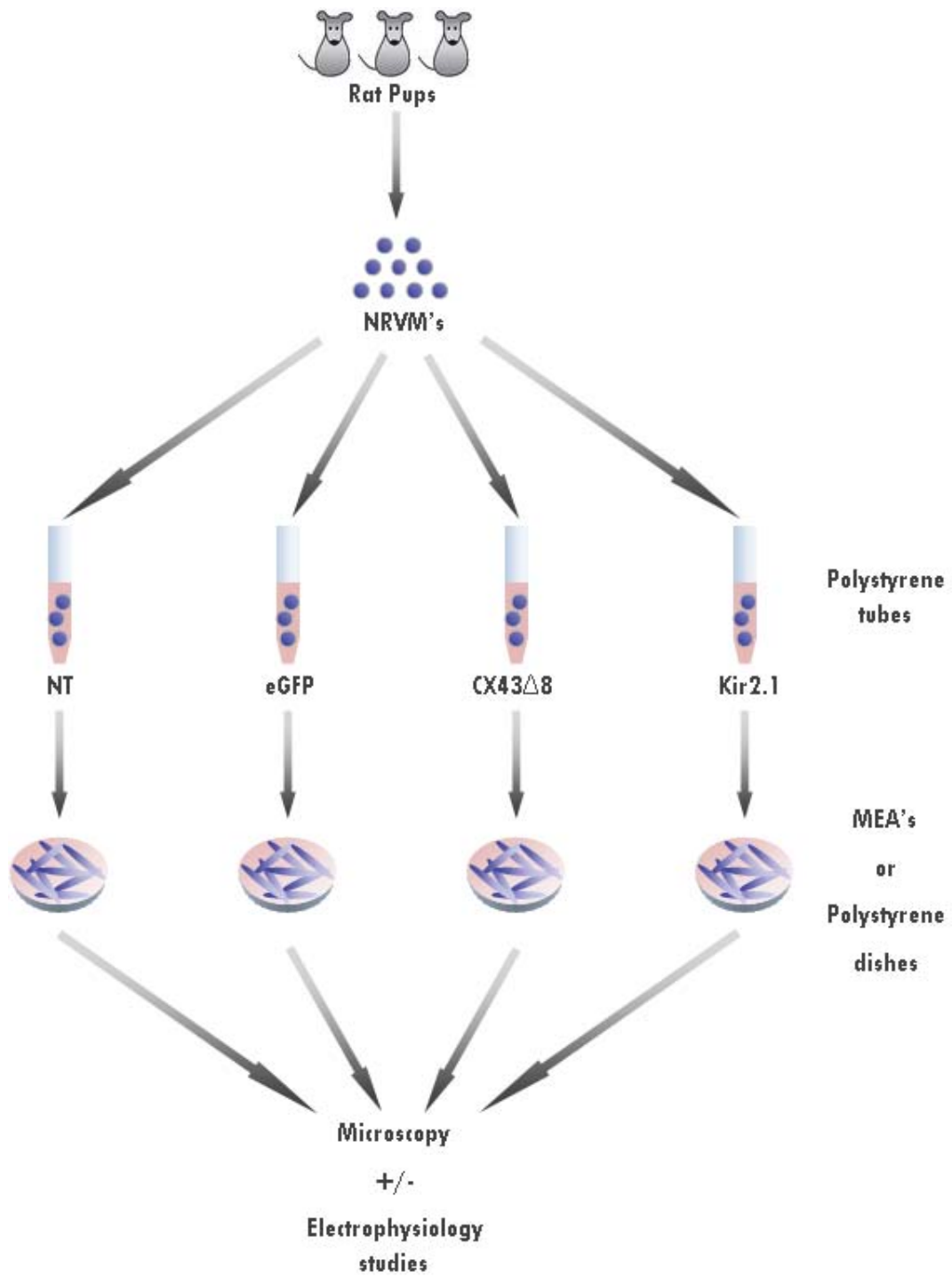


Figure 3.1: NRVM's study flow diagram. (NT - Non-transduced)

3.3 Results

3.3.1 Optimal multiplicity of infections

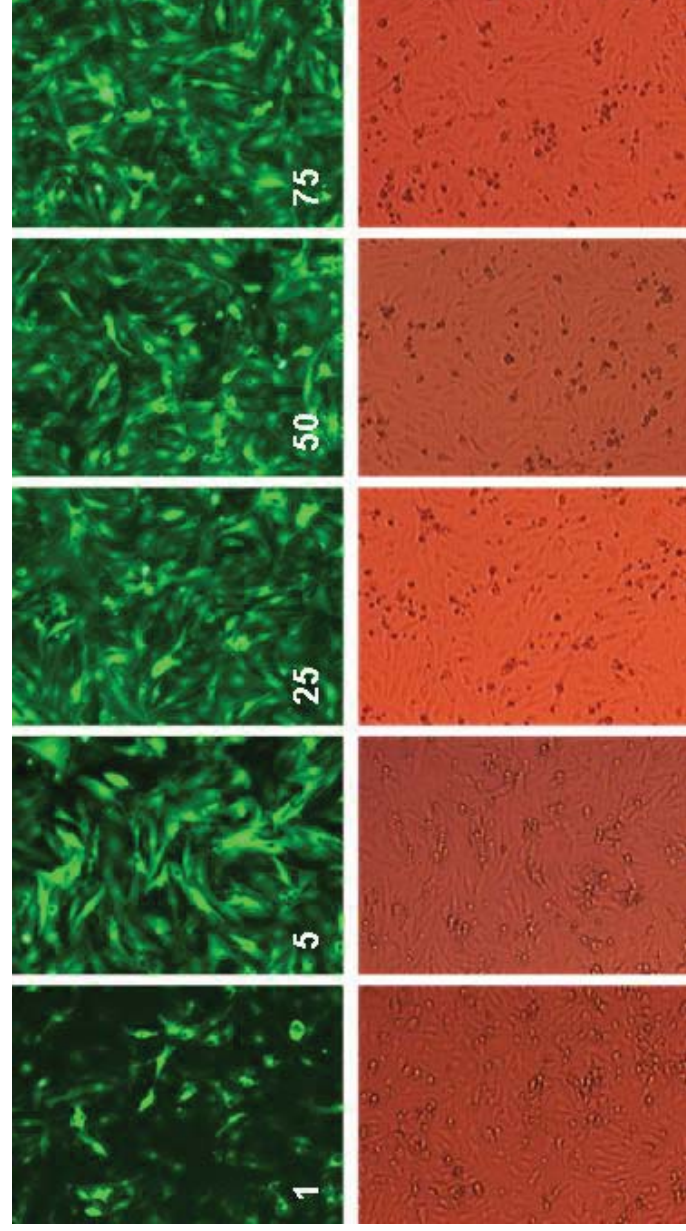
Bright field and fluorescent micrographs taken approximately 96 hours following plating of NRVM's after transduction at multiplicities of infection of 1, 5, 25, 50, and 75 are shown in figure 3.2. Transduction efficiency falls below 95% at an MOI of 1. At all higher MOI's, transduction efficiency remains above 95% by visual inspection. At these levels of transduction, culture confluency remains at 100%, and by visual inspection, there was no visible toxicity due to the level of virus transduced or eGFP expressed.

3.3.2 Culture capturability

As shown in table 3.1, at least half of all eGFP transduced cultures were captured at all MOI's tested. Beat frequency was however higher than non-transduced controls at MOI's of 100 and 75, indicating toxicity from either virus or eGFP. Monolayers belonging to the CX43 Δ 8 group failed to capture at MOI's above 25. In addition, non-coordinated spontaneous contractions of

Figure 3.2: Transduction efficiency of eGFP transduced cultures

Top row shows fluorescent microscopy: Green represent eGFP expression. Transduction efficiency of NRVM's remains above 95% till the MOI falls below 5. **Bottom row** shows bright field microscopy: Cultures remain confluent at all MOI's. (MOI for each culture displayed within fluorescence images)



myocytes with a fibrillatory appearance were observed at these higher MOI's. Taking the results of the eGFP and CX43 Δ 8 groups into consideration, monolayers belonging to the KIR2.1 group were subsequently assessed only at an MOI of 25. All cultures within this group possessed a beat frequency less than 1Hz, and were captured when stimulated. Figure 3.3 demonstrates a transduction efficiency of greater than 95% in monolayers transduced with eGFP at a multiplicity of infection of 25 along with a good far field potential detected during stimulation. Hence all subsequent conduction velocity assessments were performed at an MOI of 25.

3.3.3 Isochronal maps and conduction velocities

Isochronal maps, which represent the distance travelled by a propagating action potential wave front over fixed time intervals, were generated for each monolayer. In cultures with a slower than usual conduction velocity, less distance is travelled during each consecutive isochrone and hence isochronal narrowing or crowding is observed. The opposite is observed in monolayers with faster than usual conduction velocities where isochrones are wider due to the greater distance travelled during a fixed time

interval. Figure 3.4 demonstrates representative isochronal maps from each of the 4 study groups. Isochrones of the non-transduced map are generally equal in width and the mean conduction velocity for the group is 22.0 ± 1.1 cm/s. Compared to non-transduced cultures, the eGFP group possessed mildly narrower isochrones and this translated to a mildly slower mean group conduction velocity of 19.3 ± 1.7 cm/s. Compared to both the non-transduced and eGFP groups, the KIR2.1 group possessed markedly wider isochrones with a much faster mean group conduction velocity of 27.6 ± 1.2 cm/s. The CX43 Δ 8 group possessed marked crowding of isochrones compared to all other groups with a mean group conduction velocity of 8.0 ± 3.5 cm/s. Mean conduction velocities of all transduced groups were significantly different compared to non-transduced monolayers as shown in figure 3.5 and the direction and magnitude of conduction velocity changes were consistent with the results of published optical mapping studies.

Table 3.1: Monolayer capturability and beat frequency

Mean spontaneous beat frequency of monolayers and proportion of monolayers captured within non-transduced controls and at different multiplicities of infection for transduced groups are shown. (Fib - fibrillatory appearing spontaneous contractile activity; NA - not assessed)

MOI	NT		eGFP		CX43Δ8		Kir2.1	
	Cultures captured	Mean beat frequency	Cultures captured	Mean beat frequency	Cultures captured	Mean beat frequency	Cultures captured	Mean beat frequency
25	27/27	< 1Hz	7/8	< 1Hz	6/7	< 1Hz	6/6	< 1Hz
50			4/5	< 1Hz	0/5	Fib	NA	NA
75			3/6	1 - 2 Hz	0/5	Fib	NA	NA
100			3/6	1 - 2 Hz	0/4	Fib	NA	NA

Figure 3.3: eGFP fluorescence of an NRVM monolayer on an MEA

Greater than 95% transduction was achieved at an MOI of 25. The insert (bottom left corner) demonstrates good amplitude of a far field potential detected at electrode 25 during stimulation.

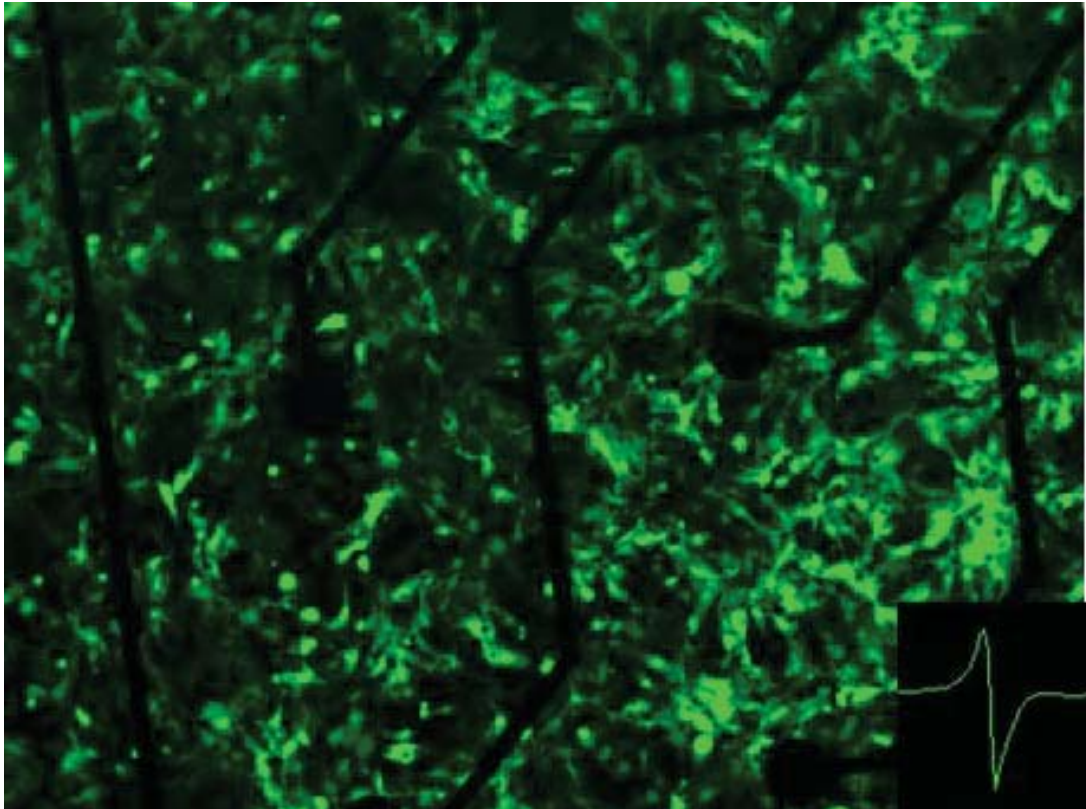


Figure 3.4: Representative Isochronal maps

Representative isochronal maps and mean conduction velocities of each of the 4 study groups.

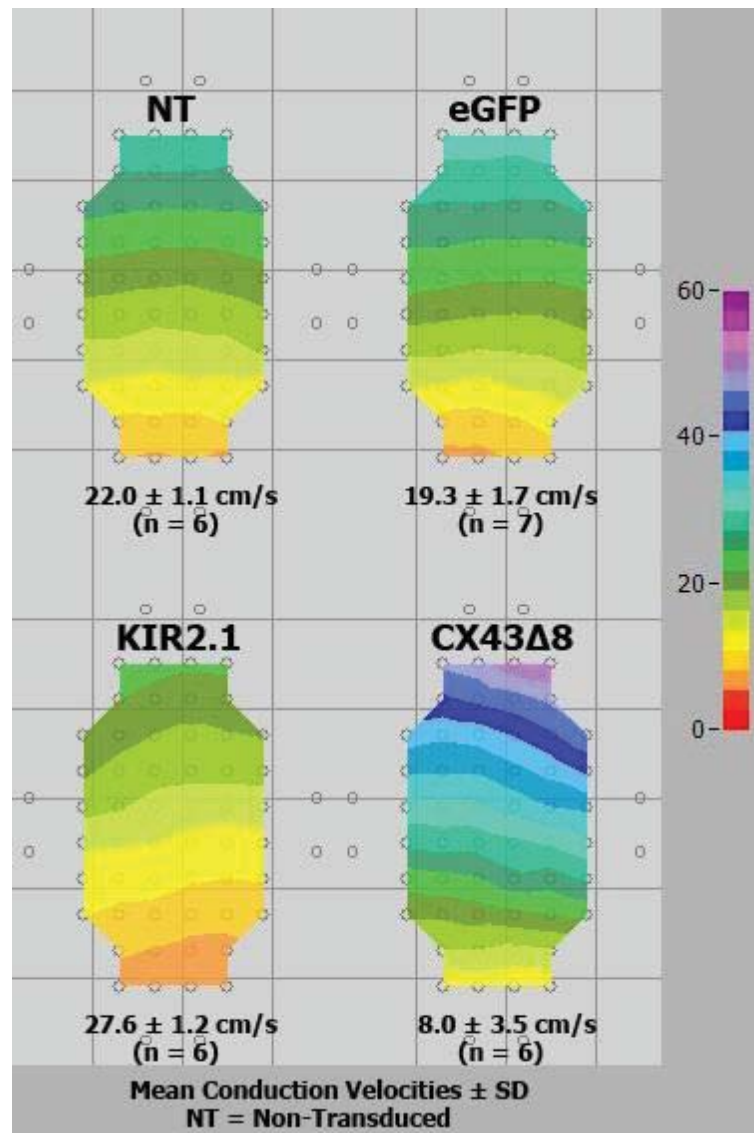
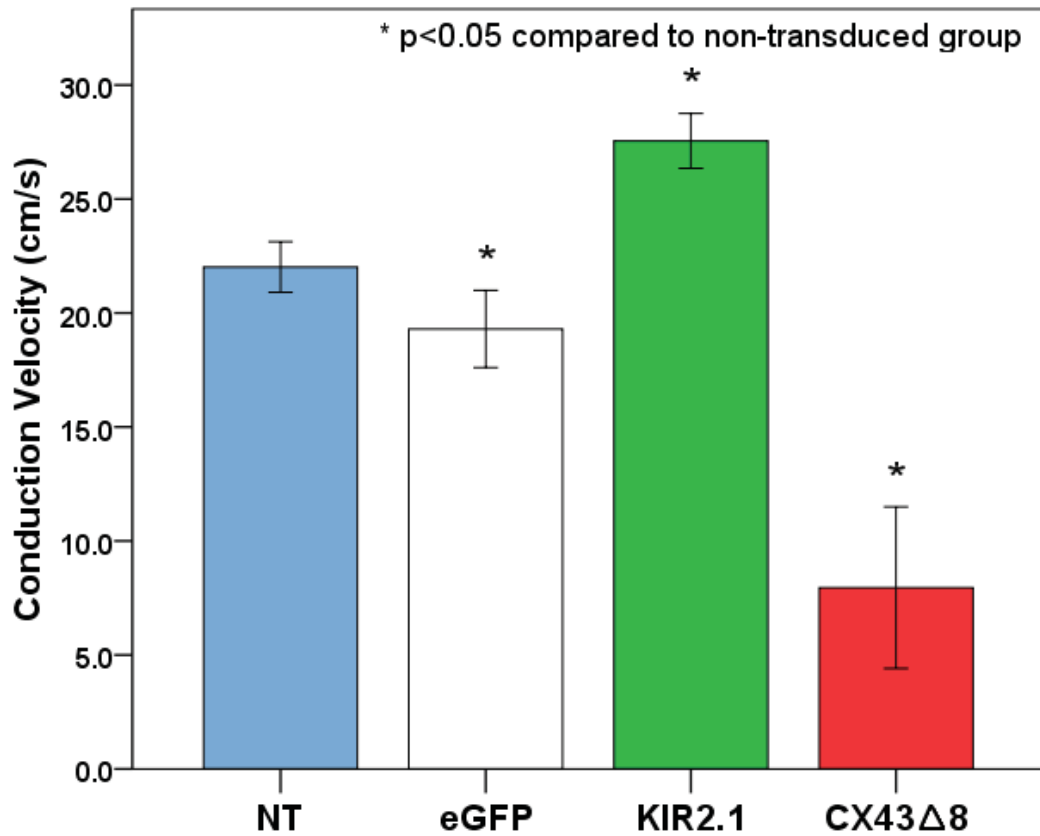


Figure 3.5: Graphical representation of mean conduction velocities.

Conduction velocities of all transduced groups are significantly different to non-transduced controls.



3.4 Discussion

These results demonstrate that the multi-electrode array system is a reliable method for studying lentivector gene modified primary cardiomyocytes. In particular, transduction of monolayers to express eGFP, KIR2.1, or CX43 Δ 8 resulted in predictable changes in conduction velocity when measured on an MEA. Hence the multi-electrode array system would be a useful tool to study the functional significance of disease related gene mutations.

3.4.1 Assessing conduction velocities and capturability

Propagation velocity is determined by the rate of passive transfer of ions between both zones. This in turn is determined by drivers of passive ion transfer and resistors to this process. The main drivers are action potential amplitude and speed of action potential generation which is determined by fast sodium channels (I_{Na} rapid current). The main resistors are intra-cellular cytoplasmic resistance and inter-cellular gap junction resistance.

The resistance of the central aqueous pore of cell-cell coupled connexons is inversely proportional to its conductance capacity.¹⁸

3.4.1.1 Characteristics of KIR2.1 over expression

While the channel Kir2.1 is predominately responsible for the late phase of action potential repolarisation, studies have demonstrated that over expression not only shortens action potential duration but also increases sodium channel availability.⁸⁴ Hence over expression is expected to increase myocyte conduction velocities, a phenomenon that has previously been demonstrated with optical mapping of lentivector modified cardiomyocyte monolayers.⁸³

3.4.1.2 Characteristics of CX43 Δ 8 over expression

The connexin43 loop mutant CX43 Δ 8 has been shown to exert a dominant negative effect on endogenous connexin43 (Cx43) in myocytes resulting in slowing of myocyte conduction when assessed with optical mapping.⁸⁵ In addition, we have shown that at a multiplicity of infection of 50, CX43 Δ 8 is capable of precipitating a degree of cardiomyocyte uncoupling supportive of fibrillatory type contractile activity in monolayers. This effect was

not observed within the eGFP group at the same MOI level suggesting that the disorganised contraction is secondary to endogenous connexin interference rather than viral toxicity. A pro-arrhythmic effect of the CX43 Δ 8 was also observed by Nakagami et al., where rapid pacing of NRVM cultures transduced with CX43 Δ 8 produced spiral wave re-entrant arrhythmias.⁸⁶

3.4.1.3 Characteristics of eGFP over expression

An expected mild slowing of conduction secondary to eGFP expression was observed, the degree of which is consistent with prior optical mapping data.⁸³ Although the mechanism for slowing has yet to be elucidated, existing studies point towards both an interference effect on connexin expression and a reduction in sodium channel availability, possibly through an alteration in the levels of repolarising ion channels.

3.4.2 Implications of these findings

With the advent of genome wide sequencing, and the rapid identification of novel gene mutations, there is a clear need for inexpensive high throughput functional screening to delineate between functionally significant mutations and simple

polymorphisms. Our study clearly demonstrates that the multi-electrode array system is able to accurately assess the functional effects of lentivector gene modified cardiomyocyte monolayers.

Our results in combination with the recent development of cheap disposable polyimide based multi-electrode arrays using printable circuit board technology ideally positions the MEA system as a diagnostic tool suitable for the functional screening of mutations within myocytes.

CHAPTER 4

The Human Connexin40 Mutations P88S, G38A, and A96S Alter Primary Cardiomyocyte Coupling and Conduction

4.1 Introduction and Aims

Germ-line (A96S) and somatic mutations (G38A, P88S) of connexin40 (Cx40) have been identified within the atria of patients with a history of idiopathic atrial fibrillation (AF).¹⁰ Immunohistochemistry for Cx40 on atrial tissue from patients with somatic mutations revealed a mosaic pattern of abnormal gap junction expression and intracellular accumulation. Furthermore, immunofluorescence of transfected N2A cells revealed that the germ-line mutation, while appearing to form normal gap junctions, caused abnormal intracellular accumulation of Cx40. N2A cells transfected with each of the three mutants were found to have markedly reduced gap junction conductances when compared to

wild-type connexin40. In addition, co-transfection of wild-type connexin40 (wtCx40) and connexin43 (Cx43) along with either P88S or A96S into oocytes revealed a dominant negative effect of each mutant on gap junctional conductance. The results suggested that each mutant was pathogenic. Interpretation of the results of these functional studies are however limited. Firstly gap junction naïve cell lines were used to assess each mutation. A variety of studies have demonstrated that connexins are subject to a variety of post translational modifications, something that is likely dependant on the cell type used. This may explain why the same lab has since demonstrated conflicting conductance alterations between N2A cells and oocytes during the assessment of a somatic Cx43 mutation. Hence connexins should ideally be studied within their native context, that is within cardiomyocytes. Secondly, the validity of the oocyte voltage clamping studies has been questioned given the presence of large variations in baseline conductances of Cx40 only transfected controls. In particular, while the amount of wtCx40 cRNA injected into each oocyte was kept constant, mean conductance of coupled oocytes between experiments varied by approximately 20 μ S. Finally, dual whole cell studies fail to consider the modulating effects of extracellular signals found within a myocyte syncytium. Hence we aimed to

characterise the phenotype of primary cardiomyocyte cultures following somatic gene transfer of Cx40 mutations. We hypothesised that if pathogenic, each Cx40 mutant should result in conduction slowing.

4.2 Methods

4.2.1 Vector packaging and titration

Vector stocks encoding eGFP, wild-type Cx40, and the three mutant connexin40's P88S, G38A, and A96S were produced using the four plasmid lipofection method as described in section 2.3.1 to 2.3.3. Titre was assigned to vector stocks by assessing genomic DNA integration of viral DNA following transduction of HEK293T cells as described in sections 2.3.4.1 to 2.3.4.3.

4.2.2 Myocyte isolation, transduction and culture

Neonatal rat ventricular myocytes were isolated from 2 to 3 day old Sprague Dawley rat pups as described in sections 2.2.3. After each isolation, cardiomyocytes were separated into a maximum of 6 study groups using 50 ml polypropylene tubes as shown in figure 4.1. Vector transduction of cardiomyocytes in suspension at equal multiplicities of infection was performed in the presence of Polybrene 8µg/mL as described in section 2.3.5. The non-transduced group received Polybrene 8µg/mL without viral vector. Following transduction, cardiomyocytes were seeded at a density of 220×10^3 cells/cm² onto polystyrene plates for immunoblotting,

4 well chamber slides (Nunc) for immunofluorescence and polyimide multi-electrode arrays for the assessment of cardiomyocyte electrophysiology.

4.2.3 Multi-electrode array studies

Transduced eGFP control monolayers were initially assessed for their level of transduction. If transduction efficiency was lower than 95% in any culture, all cultures within the experiment were discarded and section 4.2.2 repeated.

Following placement in the MEA stage, culture wells were sealed with the stimulation electrode apparatus and the culture temperature maintained at 37°C for a minimum of 5 minutes prior to further assessment. If the beat frequency of an individual culture was greater than 2Hz, the culture was discarded. Conduction velocity assessment was performed as described in sections 2.8.1 to 2.8.3. In brief, cultures were stimulated at a frequency of 2 Hz with square shaped 30 μ A current pulses of 1ms duration.

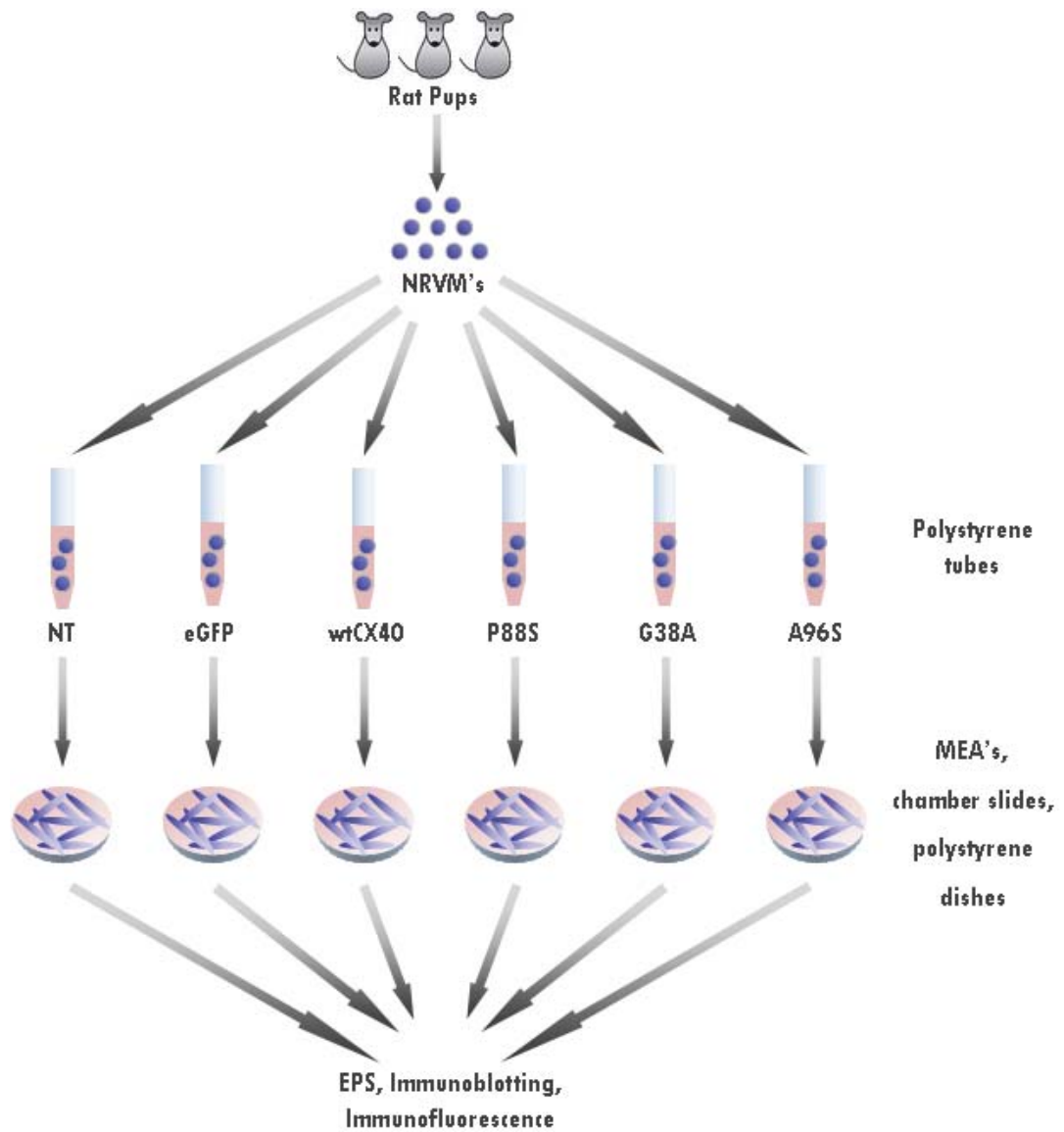


Figure 4.1: NRVM study flow diagram.

Following isolation from rat pups, NRVM's were separated into 6 groups and transduced in suspension (except for the non-transduced group). Cultures were analysed 96 hours post plating.

Monolayer capture was assessed with recording of monolayer field potentials via the multi-electrode array system shown in figure 3.2. The software CEPAS was then used to generate isochronal maps of each culture and calculate the velocity of far field potential propagation.

4.2.5 Immunoblotting

Myocytes were collected for protein extraction and quantification at approximately 96 hours post plating as described in section 2.6.2 and 2.6.3. Once prepared, protein samples underwent immunoblotting as described in section 2.6.3. In brief, samples were subject to electrophoretic separation on 4-12% Bis-Tris gradient gels, followed by membrane transfer using the iBlot gel transfer system. Membranes were washed and incubated with primary antibodies for either Cx40 or Cx43, followed by secondary incubation. The chemiluminescence system was used to produce immunoblot images of the probed protein bands.

4.2.6 Immunofluorescence

Co-immunostaining was commenced at approximately 96 hours post plating as outlined in section 2.4.3. Chamber slides were

gently washed, fixed with 4% (w/v) paraformaldehyde, permeabilised with 0.05% (v/v) Triton X-100, and blocked with goat serum. Slides were co-incubated with primary antibodies for Cx40 and Cx43, followed by co-incubation with secondary antibodies for the respective rabbit and mouse primary antibodies. Slides were cover slip mounted with the aid of Prolong Gold anti-fade reagent containing the DAPI nuclear stain. Fluorescent images were acquired using an Olympus FV 1000 confocal laser scanning microscope as detailed in section 2.4.4.

4.3 Results

Table 4.1 summarises the results of Cx43 and Cx40 expression within each study group along with their effect on conduction velocity. Both the NT and eGFP groups possessed similar membranous Cx43 levels and lacked membranous Cx40. Conduction velocity was mildly reduced within the eGFP group. While the wtCX40 and A96S groups possessed similar membranous Cx43 to that of the NT group, there was also membranous Cx40 expression. Compared to the NT group, conduction velocity was moderately reduced within the wtCX40 group and greatly reduced within the A96S group. Membranous expression of Cx43 within the P88S group was reduced compared to the NT group, and almost absent within the G38A group. Membranous Cx40 was absent within the P88S group and sparse within the G38A group. Conduction velocity was moderately reduced within the P88S group. There was no capture of G38A cultures on stimulation.

Table 4.1: Summary of Cx43 / Cx40 levels and conduction velocities for each group.

Transgene	Total Cx43	Total Cx40	Membranous Cx43	Membranous Cx40	Conduction velocity
NT	++++	+	++++	0	++++
eGFP	++++	+	++++	0	+++
wtCX40	++++	++++	++++	++++	++
A96S	++++	++++	++++	++++	+
P88S	++++	++++	++	0	++
G38A	+	++++	+	+	No Capture

4.3.1 Isochronal maps and conduction velocities

Isochronal maps, which represent the distance travelled by a propagating action potential wave front over fixed consecutive time intervals, were generated for each monolayer. Figure 4.2 demonstrates representative isochronal maps from each of the 6 study groups ($n = 6$ within each group). In cultures with a slower than usual conduction velocity, less distance is travelled during consecutive isochrones and hence isochronal narrowing or crowding is observed. The opposite is observed in monolayers with faster than usual conduction velocities where isochrones are wider due to the greater distance travelled during a fixed time interval. Isochrones within the non-transduced map are generally equal and the mean conduction velocity for the group is 20.1 ± 1.8 cm/s. Compared to non-transduced cultures, the eGFP group possessed mildly narrower isochrones and this translated to a mildly slower mean group conduction velocity of 18.3 ± 2.1 cm/s. Compared to the non-transduced monolayers, the wtCX40 group possessed a significantly slower mean group conduction velocity of 14.1 ± 1.2 cm/s ($p < 0.05$). Isochrones were markedly crowded within the A96S mutant group (Figure 4.2), translating to a significantly slower group mean conduction velocity of 8.4 ± 2.1

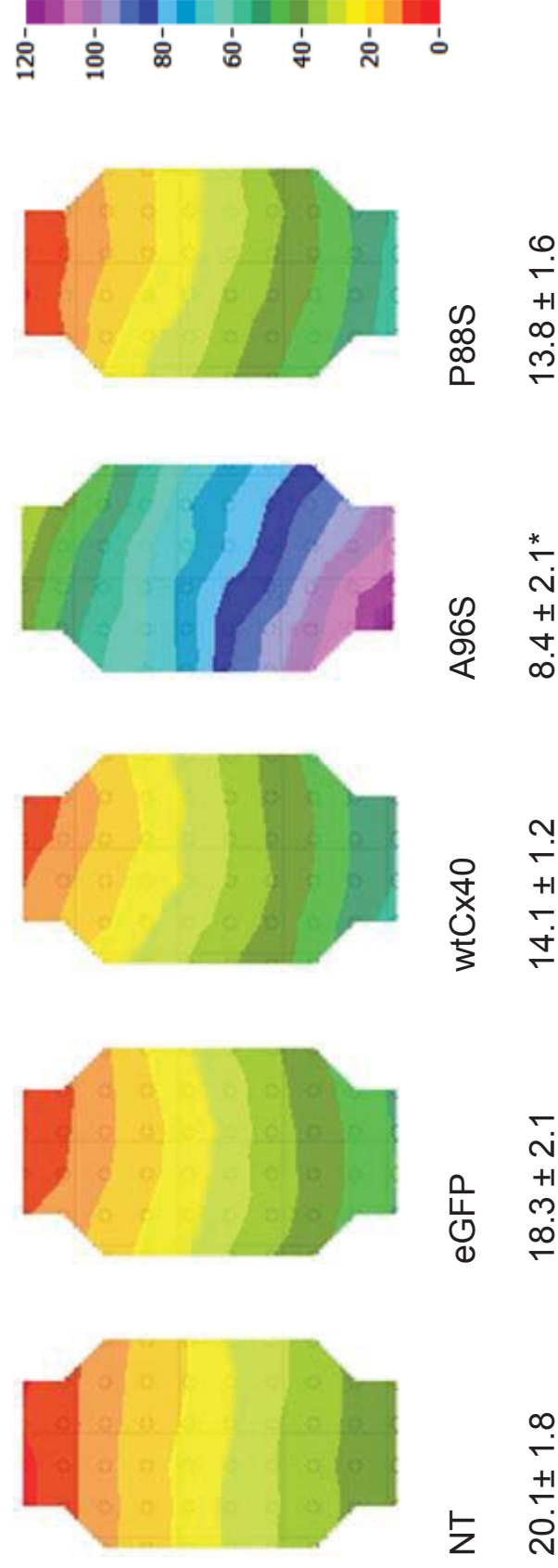
cm/s when compared to wtCx40 monolayers ($p < 0.05$) as shown in Figure 4.3. Interestingly, the P88S mutant group had almost similar spaced isochrones compared to the wtCX40 group and a mean group conduction velocity of 13.8 ± 1.6 cm/s. All G38A mutant transduced cultures possessed spontaneous fibrillatory type myocyte contractile activity and were not capturable with stimulation even after escalating the current amplitude slowly up to a maximum of 1mA and pulse duration up to 2ms.

4.3.2 Immunofluorescence and immunoblotting

Only wtCX40 and A96S monolayers expressed abundant membranous Cx40 (red signal) as shown in the confocal images of co-immunostained monolayers in figure 4.4. Membranous expression of Cx40 within the G38A group was sparse and within the P88S group absent. Intracellular Cx40 expression was evident within P88S monolayers. While the wtCX40 and A96S groups contained similar levels of membranous Cx43 expression, monolayers expressing P88S and G38A possessed markedly reduced membranous Cx43 expression with almost complete abolishment in the latter. Areas of possible membranous

Figure 4.2: Representative isochronal maps and mean conduction velocities.

The isochronal map from the A96S group appears crowded and is consistent with the significantly slower mean conduction velocity of the group when compared to the wtCx40 group ($p < 0.05$). There was no capture of monolayers transduced to express G38A. (n = 6 within each group)



* $p < 0.05$ compared to wtCx40

Figure 4.3: Graphical representation of conduction velocities.

A bar graph of the mean conduction velocity of each transduction group. Conduction velocities within the A96S group are clearly slower compared to the wtCX40 group.

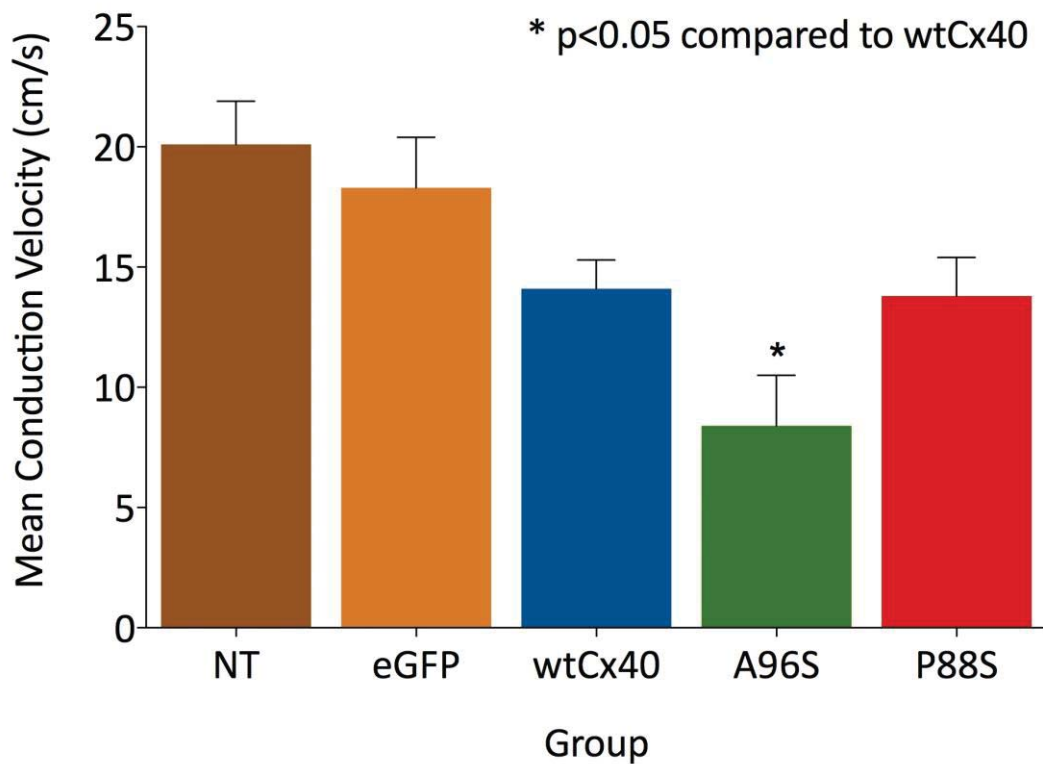


Figure 4.4: Co-Immunostaining of NRVM cultures.

Co-immunostaining for Cx40 (red) and Cx43 (green) in NT and eGFP, wtCX40, P88S, G38A and A96S transduced cultures. Yellow signal identifies areas of possible co-localisation of Cx40 and Cx43. Nuclei labelled blue with DAPI.

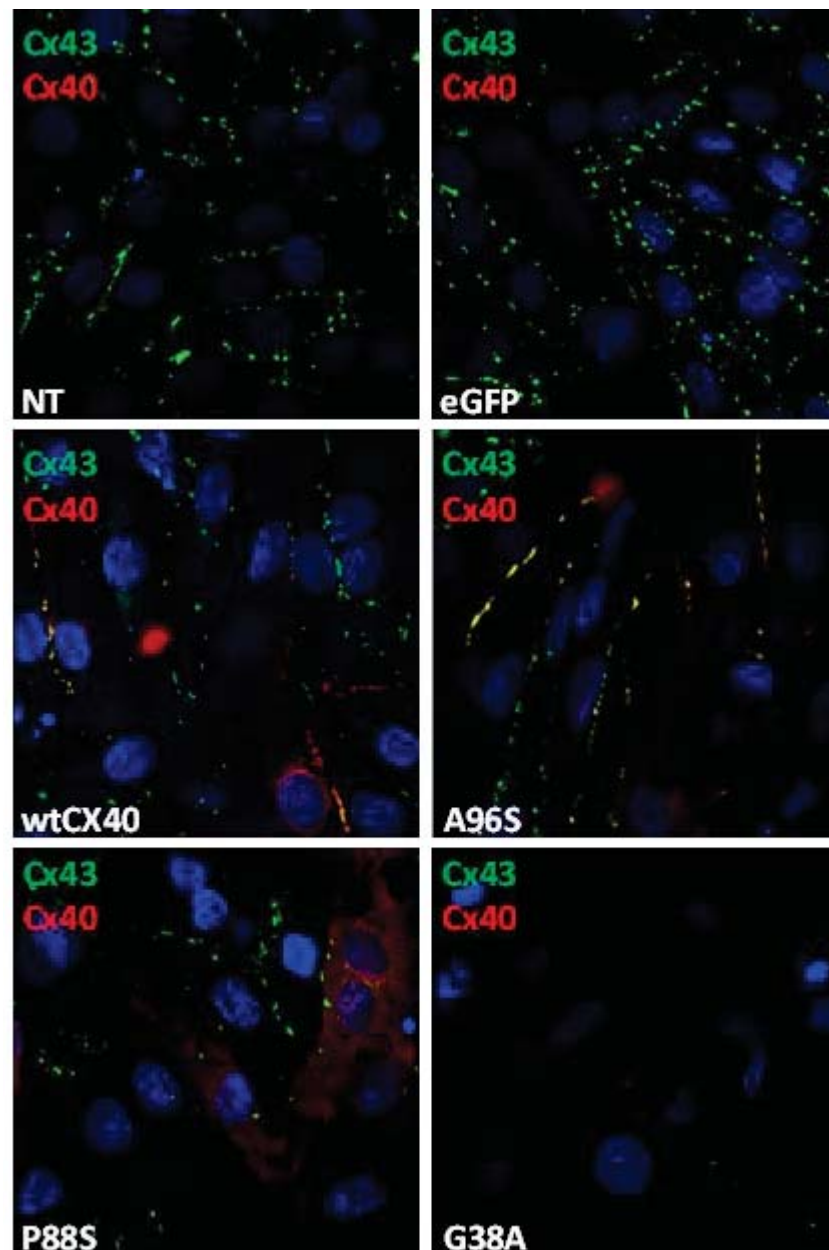


Figure 4.5: Immunoblots for connexin 40 expression in NRVM's.

Immunoblots and densitometry for Cx40 normalised to β -tubulin and expressed relative to the non-transduced group. Cx40 over expression is seen within NRVM's from each group (n = 1 for each group).

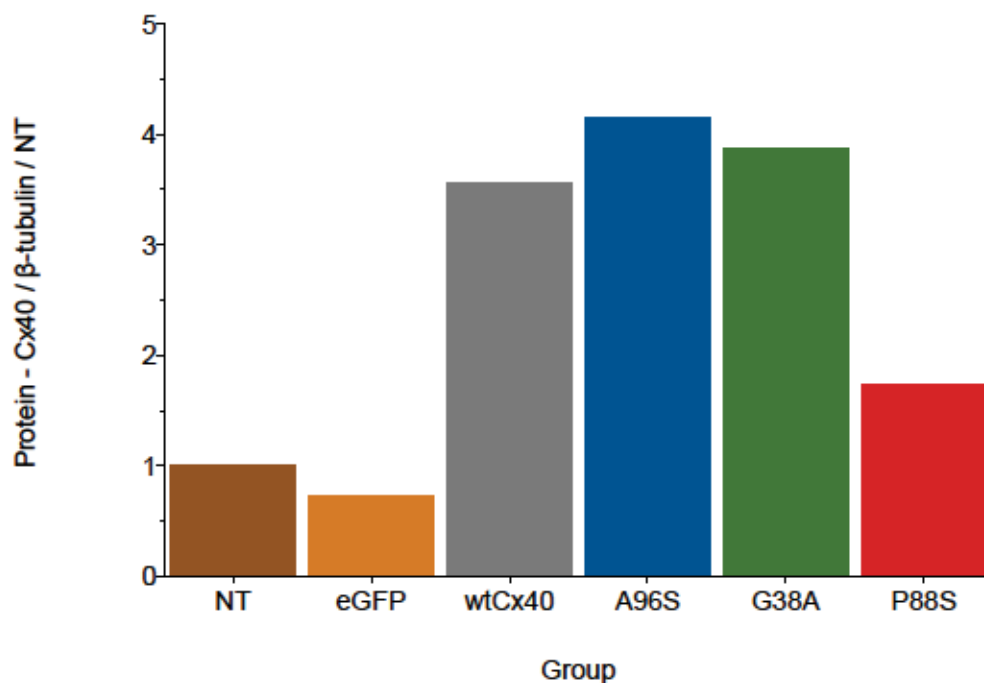
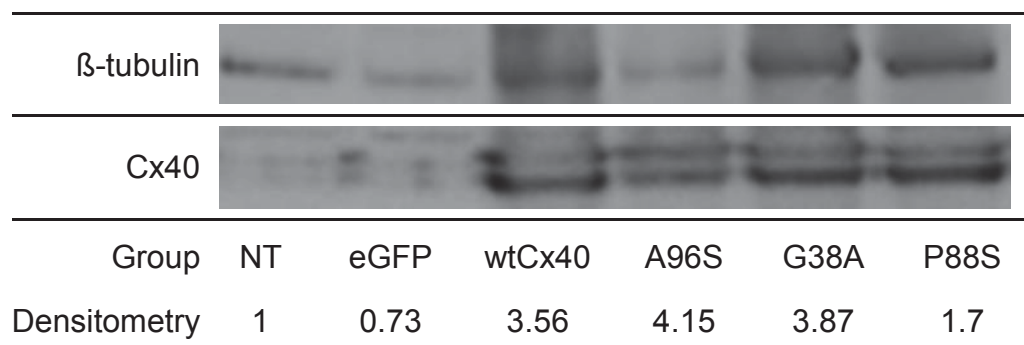
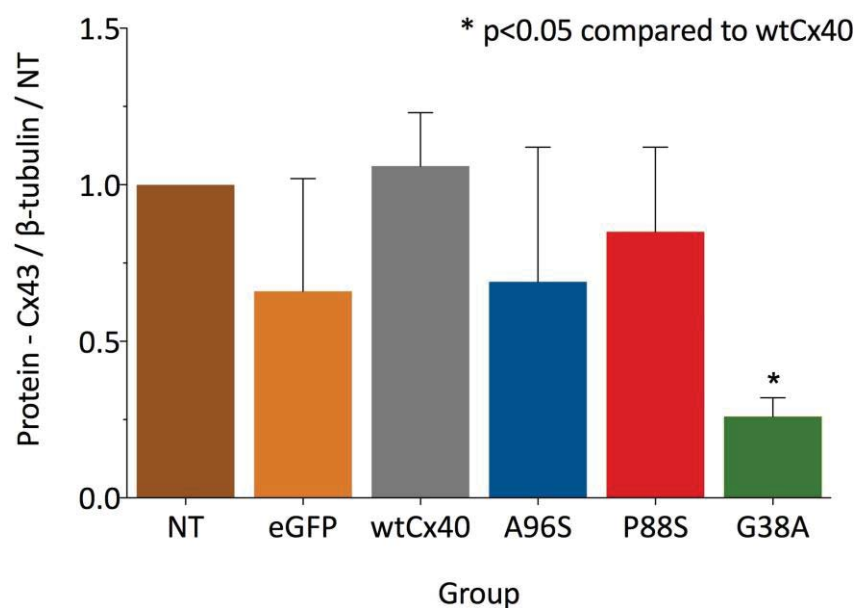
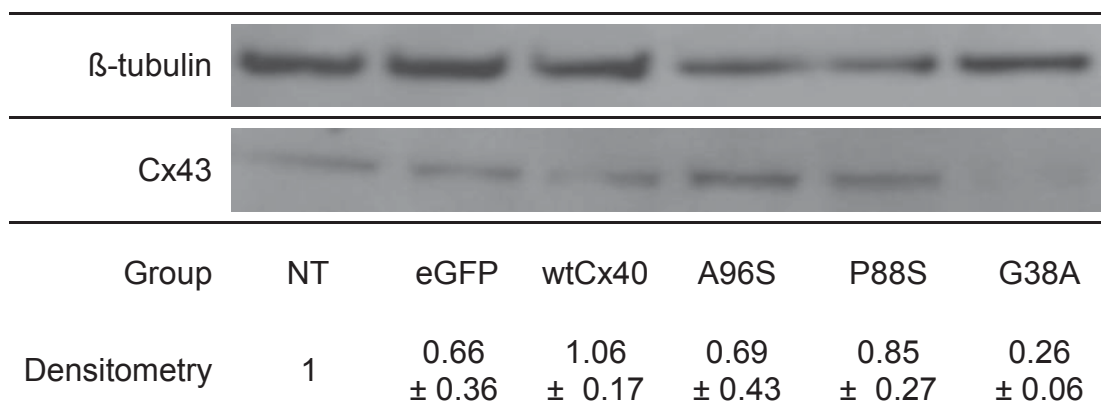


Figure 4.6: Immunoblots for connexin 43 expression in NRVM's.

Immunoblots and densitometry for Cx43 normalised to β -tubulin and expressed relative to the non-transduced group. Significantly reduced Cx43 expression is seen within NRVM's from the G38A group when compared to the wtCX40 group ($p < 0.05$; $n = 3$ for all groups).



co-localisation of Cx40 and Cx43 within wtCX40 and A96S monolayers were evidenced by yellow signal. Immunoblotting confirmed significant Cx40 expression within wtCx40 and mutant Cx40 transduced cardiomyocytes as shown in figure 4.5. Furthermore, immunoblotting for Cx43 revealed an almost complete absence within the G38A group as shown in figure 4.6.

4.4 Discussion

Our results have for the first time confirmed that a significant electrophysiological functional impairment is imparted to cardiomyocytes by the Cx40 mutations G38A, and A96S. The results have also provided an insight into the mechanism by which all three investigated Cx40 mutations may be pathogenic.

4.4.1 Characteristics of wild-type Connexin40

The co-localisation appearance of wtCX40 with native Cx43 at the cell membrane suggests that the formation heteromeric connexons is responsible for the conduction slowing observed within wtCX40 transduced cultures. These findings are consistent with previous NRVM optical mapping studies which demonstrated that wtCX40 transduction resulted in conduction slowing whilst co-expression of wtCX40 with a Cx43 siRNA knockdown vector increased conduction velocities.⁸⁷

4.4.2 Characteristics of the G38A Connexin40

Mutation

The sparse membranous expression of Cx40 in G38A monolayers means that the formation of heteromeric heterotypic channels with reduced conductances is an unlikely explanation for the conduction impairment observed. Instead, myocyte uncoupling itself due to an almost complete absence of membranous Cx43 is the likely cause for the fibrillatory contractile activity of G38A transduced monolayers. The reduction in membranous Cx43 is paralleled by a reduction in total cellular Cx43 indicating that the G38A mutant interferes with the production process and/or intracellular trafficking of Cx43.

4.4.3 Characteristics of the A96S Connexin40

Mutation

Given that the A96S mutant expresses at the cell membrane and appears to co-localise with membranous Cx43 on fluorescent microscopy, conduction slowing is likely mediated through the formation of heterotypic heteromeric channels. The greater degree of conduction slowing compared to wtCx40 indicates that

the A96S mutation may either have a dominant negative effect on Cx43 function or alter the ratio of Cx40 to Cx43 within gap junctions.

4.4.4 Characteristics of the P88S Connexin40

Mutation

Although our studies revealed similar impairments of conduction velocities between monolayers transduced with either wtCx40 or P88S when compared to eGFP controls, the mechanisms by which this is achieved is clearly different. WtCx40 depends on the development of heteromeric heterotypic channels while P88S likely depends on Cx43 knock down to achieve conduction slowing. The lack of conduction velocity differences between P88S and wtCx40 in combination with the immunofluorescence studies demonstrates a lack of sensitivity of the MEA system when differing mechanisms of conduction slowing are present.

4.4.5 Other considerations

Sodium and potassium channels, both of which contribute to the cardiac action potential, have been shown to co-localise with

Cx43 at the intercalated discs.^{88, 89} Voltage clamping studies of Cx43-null neonatal myocytes have revealed no differences in action potential characteristics when compared to wild-type myocytes.^{90, 91} Hence the membranous reduction in Cx43 observed within P88S and G38A monolayers is unlikely to have had an effect on the expression of sodium and potassium channels within these groups. The occurrence and significance of sodium and potassium channel co-localisation with Cx40 is unknown however. Hence an alteration in sodium and potassium channel expression may still be possible within all three Cx40 mutant groups. Nevertheless, if alterations in sodium and potassium channel expression were to have occurred to different degrees within each monolayer group, this would be further support of a pathogenic role for these mutations.

Neonatal rat ventricular myocytes undergo further differentiation during the process of isolation and culture. In addition to an *in vitro* environment, this differentiation process lacks the electrical, mechanical, and humoral regulatory factors found within an *in vivo* environment. Although action potential characteristics between cultured neonatal myocytes and intact cardiac myocytes are similar, gap junction distribution is diffuse and immature within

neonatal myocyte cultures.⁹² Hence *in vivo* confirmation of the functional impairment imparted to intact cardiomyocytes by the Cx40 mutations and their propensity to induce arrhythmia is still required.

Despite the limitations of neonatal myocyte cultures, the results further demonstrate that the MEA system in combination with immunofluorescence can be a useful screening tool for assessing the functional significance of mutations prior to embarking on more costly and labour intensive *in vivo* investigations.

CHAPTER 5

***In Vivo* Somatic Atrial Gene Transfer of Human Connexin40 Mutations Increases the Propensity for Arrhythmia**

5.1 Introduction and aims

We previously demonstrated that the connexin40 (Cx40) mutations A96S and G38A alter the electrophysiological properties of cardiomyocytes. While the use of neonatal cardiomyocyte cultures demonstrated a reduction in endogenous connexin43 (Cx43) expression following P88S transduction, there was a failure of the multi-electrode array system to discriminate conduction slowing due to myocyte uncoupling from that of heterotypic heteromeric channel formation hypothesized to occur with wild-type Cx40 (wtCX40) transduced cultures.

Furthermore, the altered differentiation process of neonatal myocytes compared to intact tissue may have altered the impact that each mutation had on cellular electrophysiology. Hence *in vivo* confirmation of the functional impairment imparted to intact cardiomyocytes by the Cx40 mutations and their propensity to induce arrhythmia is needed.

In vivo models have been used extensively to elucidate the roles of connexins in electrical conduction and atrial fibrillation (AF). Results have been difficult to interpret due to the inherent limitations of the models used. Genetically engineered models are plagued by congenital malformations, while human biopsy studies suffer from the lack of appropriate disease state controls. A “chicken and egg” scenario exists with AF induced animal models. In particular, does the induction process directly change connexin expression to precipitate AF, or are the observed changes in connexin expression due the occurrence of AF.

More recently, two studies have utilised a gene therapy approach to assess the role of connexins in AF. Utilising adenoviral mediated gene transfer both studies were able to demonstrate a reduced vulnerability to AF after Cx43 overexpression.^{62, 63}

Hence we aimed to characterise the phenotype of rat hearts following expression of the Cx40 mutations by somatic gene transfer. We hypothesised that if pathogenic, each Cx40 mutant should result in conduction slowing and increase the propensity for atrial arrhythmia.

5.2 Methods

A total of 5 study groups were used as shown in Figure 5.1. The first 2 groups were transduced to express either eGFP or wtCX40 while the last three were transduced to express A96S, P88S, or G38A. Each group used a total of 6 adult Sprague Dawley rats. Studies were performed as outlined in Figure 5.2.

5.2.1 Vector packaging and titration

Vector stocks encoding eGFP, wtCx40, and the three mutant connexin40's P88S, G38A, and A96S were produced using the four plasmid lipofection method as described in sections 2.3.1 to 2.3.3. Titre was assigned to vector stocks by assessing genomic DNA integration of viral DNA following transduction of HEK293T cells as described in sections 2.3.4.1 to 2.3.4.3.

5.2.2 Left atrial transduction

Left atrial transduction was performed as described in sections 2.9.4 and 2.3.6. In brief, rats were anesthetized with 2% isoflurane, and the left atrium exposed via a left thoracotomy.

Figure 5.1: *In vivo* study groups

A total of 5 groups were studied. The eGFP and wtCX40 groups acted as controls. Three groups were transduced to express either the P88S, G38A, or A96S connexin40 mutation.

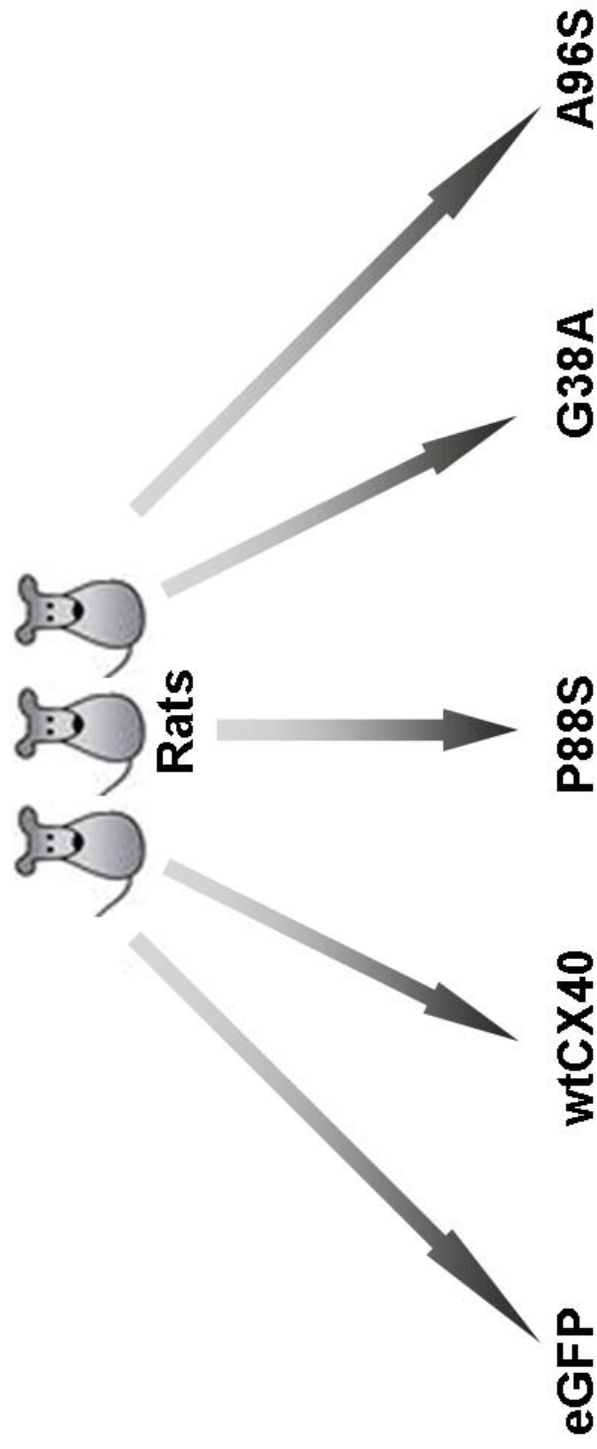
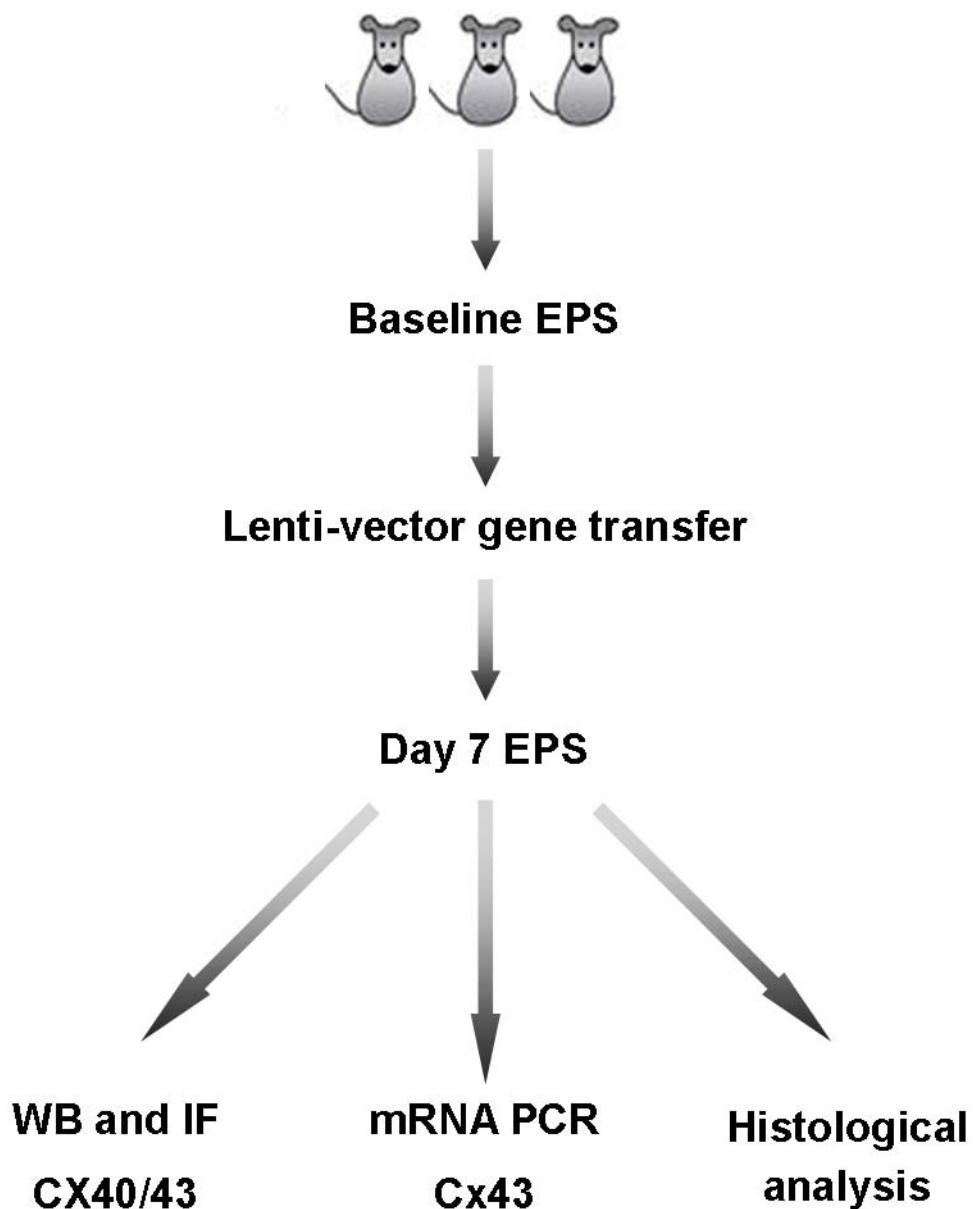


Figure 5.2: *In vivo* study protocol

All rats underwent a baseline electrophysiology study (EPS) followed by left atrial transduction. EPS was re-performed at day 7 followed by removal of the left atrium. Atria were probed for Cx40 and Cx43 protein levels, Cx43 mRNA levels, and inflammation and fibrosis with histological analysis.



A transduction gel mix consisting of 10^8 lentivector genomes, 20% (wt/vol) Pluronic F127, 0.5% (wt/vol) Trypsin, and polybrene (160 μ g/mL) was applied to the left atrium and allowed to adsorb for 20 minutes prior to closure of the thoracotomy.

5.2.3 Electrophysiology studies

Electrophysiology studies were performed as described in section 2.9.1, 2.9.2, and 2.9.3. In brief, recordings were made using subcutaneous needle electrodes while stimulation was performed with trans-oesophageal pacing. Stimulation used both programmed stimulation and atrial burst pacing. Programmed stimulation used an 8 beat drive train with a coupling interval of 150ms followed by 1 extra-stimulus down to refractoriness. Burst pacing used a coupling interval of 90ms for a duration of 5s.

5.2.4 Morphometric studies

All rats were weighed prior to each electrophysiology study. In addition, hearts were extracted and weighed before dissecting off the left atria.

5.2.5 Immunoblotting

Left atria were excised and stored following day 7 electrophysiology studies as described in section 2.9.5. Protein was extracted from atria and quantified as described in sections 2.6.2 and 2.6.3. Once prepared, protein samples underwent immunoblotting as described in section 2.6.3. In brief, samples were subjected to electrophoretic separation in 4-12% Bis-Tris gradient gels, followed by membrane transfer using the iBlot (Invitrogen) gel transfer system. Membranes were washed and incubated with primary antibodies for either Cx40 or Cx43, followed by secondary incubation. The chemiluminescence system was used to produce immunoblot images of the probed protein bands.

5.2.6 Immunofluorescence

Left atria were excised and stored following day 7 electrophysiology studies as described in section 2.9.5. Atria were then cryostat sectioned and subjected to immunostaining as described in section 2.4. In brief, sections were gently washed, fixed with 4% (w/v) paraformaldehyde, permeabilised with 0.05%

(v/v) Triton X-100, and blocked with goat serum. Slides were incubated with primary antibodies to either Cx40 or Cx43, followed by incubation with their respective secondary antibodies. Slides were cover slip mounted with the aid of Prolong Gold anti-fade reagent containing the DAPI nuclear stain. Fluorescent images were acquired using either a Leica DMIL wide field fluorescent microscope or an Olympus FV 1000 confocal laser scanning microscope.

5.2.7 Haematoxylin and Eosin staining

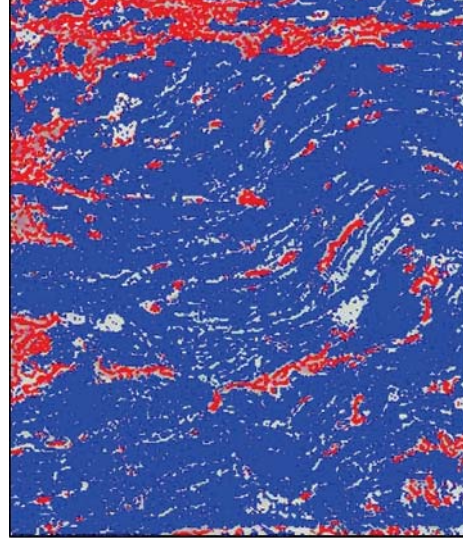
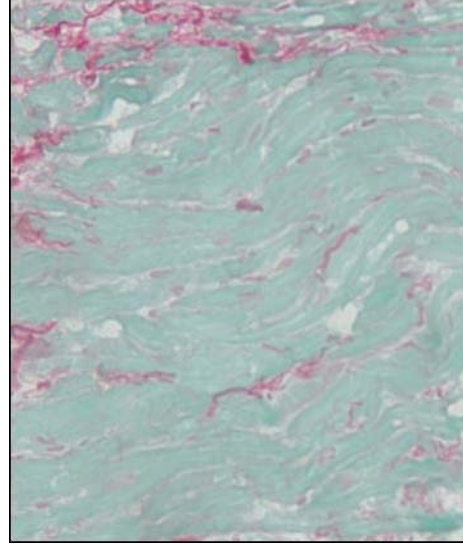
Fresh atrial tissue sections were produced as described in section 2.4.2. Haematoxylin and eosin staining was performed as described in section 2.5.1. Following image acquisition as described in section 2.5.3, images were blindly assessed for the level of inflammation by two independent observers. The scoring system used to grade inflammation is as follows. 1 - absent, 2 - occasionally present, 3 - $\leq 50\%$ affected, 4 - 50% to 90% affected, 5 - $\geq 90\%$ presence.

5.2.8 Picro-Sirius Red staining

Picro-Sirius red staining of atrial tissue was performed as described in section 2.5.2. Following image acquisition as described in section 2.5.3, images were processed (as shown in figure 5.3) with custom made software designed to objectively identify the total pixel area occupied by collagen (red) and the total pixel area occupied by the remaining tissue (green). The ratio of the area of collagen to the area of collagen plus remaining tissue was used to calculate the percentage fibrosis within each image.

Figure 5.3: Image processing of Picro-Sirius Red tissue staining

Representative images from an atrial section showing Picro-Sirius Red staining on the left (collagen coloured red, remaining tissue coloured green) and a software processed image on the right (collagen identified as red, remaining tissue identified as blue). The formula $(\text{red pixels} \times 100) / (\text{red pixels} + \text{blue pixels})$ was used to calculate the percentage fibrosis within processed images.



10,481 Red Pixels
86,494 Blue Pixels
10.8% fibrosis

5.3 Results

There were no significant differences in heart weight, body weight, and heart weight to body weight ratios between eGFP and wtCx40 groups (shown in Table 5.1). In addition, there was no significant difference in all three parameters between mutant Cx40 and wtCx40 groups.

5.3.1 Electrophysiology studies

Electrophysiology studies revealed a significant prolongation of P wave duration in the A96S, G38A, and P88S groups compared to the wtCx40 group as shown in Figure 5.4. In addition, P wave prolongation was associated with bifid P wave formation. The P wave duration was similar between the non-transduced, eGFP, and wtCx40 groups. Figure 5.5 demonstrates that both sinus rhythm and AF following burst pacing can be clearly distinguished. The duration of induced AF was significantly prolonged within all 3 mutant Cx40 groups when compared to the wtCx40 group as shown in Figure 5.6. There was no significant difference in AF duration between non-transduced, eGFP, and wtCx40 groups.

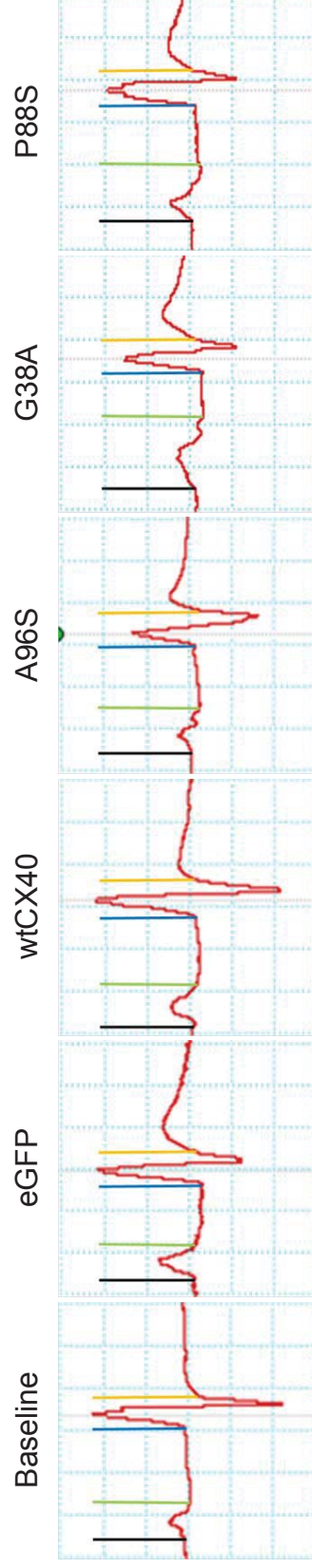
Table 5.1: Morphometric Characteristics.

Mean heart weights, mean body weights, and mean heart to body weight ratios are shown for each group. There was no significant difference between wtCx40 and eGFP groups. Furthermore, there was no significant difference in all parameters between mutant and wtCx40 groups.

	eGFP (n=6)	wtCx40 (n=6)	A96S (n=6)	G38A (n=6)	P88S (n=6)
Heart Weight (g)	0.92 ± 0.08	0.95 ± 0.12	0.92 ± 0.07	0.97 ± 0.05	0.93 ± 0.10
Body Weight (g)	214 ± 8.8	217 ± 6.8	214 ± 6.2	220 ± 3.9	213 ± 7.6
Heart / Body Weight (%)	0.43 ± 0.05	0.44 ± 0.05	0.43 ± 0.04	0.44 ± 0.02	0.44 ± 0.06

Figure 5.4: Representative Subcutaneous Electrocardiograms during Sinus Rhythm.

P waves are delimited by vertical lines in each ECG. Group mean P wave durations are displayed below the ECG's. Mean P wave durations for the A96S, G38A, and P88S groups are significantly prolonged compared to the wtCx40 group. Rats within the G38A and P88S groups were more likely to possess bifid P waves compared to the wtCx40 group.

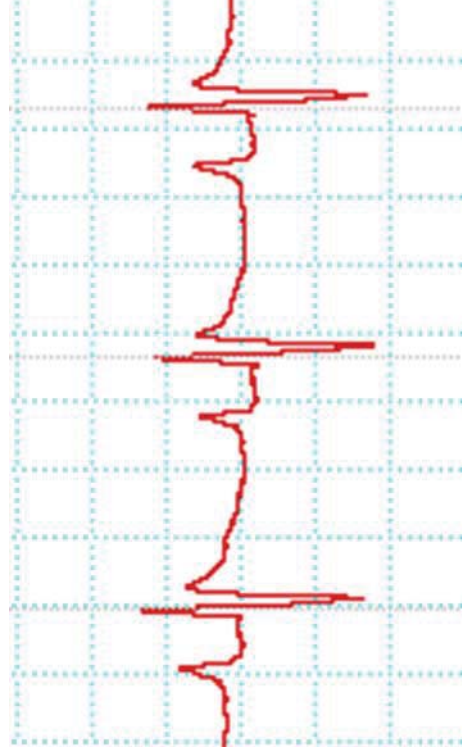


P (ms)	22.6 ± 2.6	21.9 ± 1.3	23.9 ± 2.2	26.4 ± 1.8*	34.2 ± 1.9*	29.0 ± 1.8*
Bifid P waves	0/30	0/6	0/6	3/6	5/6*	4/6*
PR (ms)	50.0 ± 5.0	52.6 ± 4.4	54.3 ± 3.8	55.0 ± 6.0	55.4 ± 5.3	50.6 ± 7.7
QRS (ms)	22.8 ± 2.2	24.3 ± 1.2	24.5 ± 2.2	22.9 ± 1.0	26.1 ± 2.8	23.9 ± 1.6

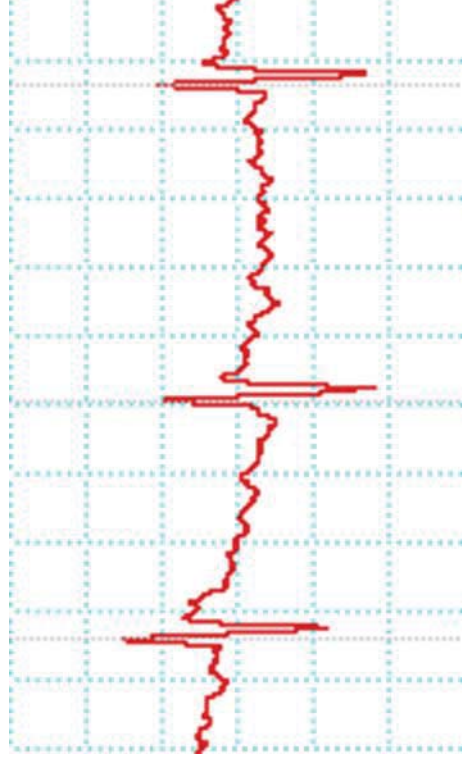
* p < 0.05 compared to wtCx40

Figure 5.5: Sinus Rhythm versus Atrial Fibrillation.

A) Representative subcutaneous electrograms during sinus rhythm and AF. During AF, there is a lack of P waves, fibrillation of the baseline, and irregularly irregular R-R intervals.



Sinus rhythm



Atrial fibrillation

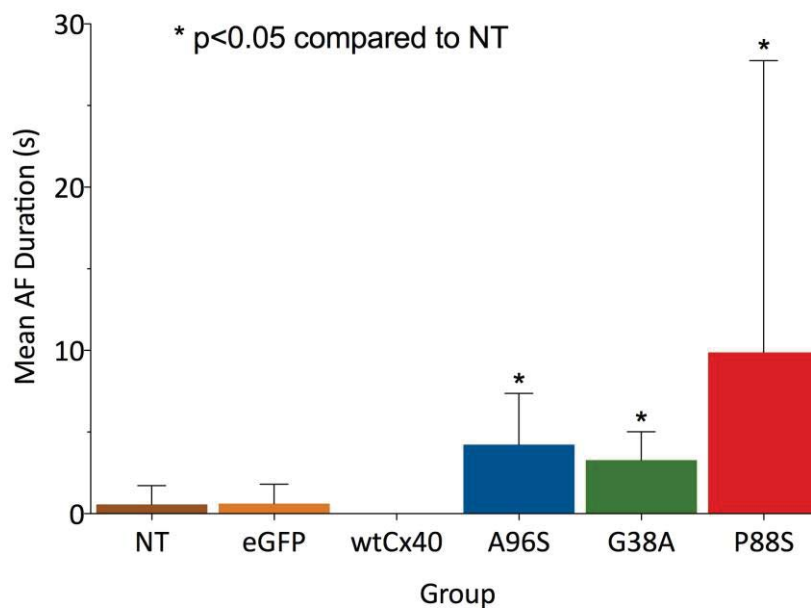
Figure 5.6: Mean durations of atrial fibrillation

A) Mean durations of AF within each group. B) Bar graph of mean durations of induced AF showing significantly longer durations in the A96S, G38A, and P88S groups when compared to the wtCx40 group (*p<0.01).

A)

Baseline	eGFP	wtCx40	A96S	G38A	P88S
0.6 ± 1.2	0.6 ± 1.3	0	4.2 ± 3.14*	3.3 ± 1.7*	9.9 ± 17.9*

B)



5.3.2 Immunofluorescence

Immunofluorescence for Cx40 revealed membranous expression within the wtCx40 and A96S groups as shown in Figure 5.7. Membranous Cx40 expression was however absent within the P88S and G38A groups. Non-transduced and eGFP transduced hearts did not express membranous Cx40.

Immunofluorescence for Cx43 revealed a marked reduction in membranous expression within the G38A and P88S groups when compared to the wtCx40 group as shown in Figure 5.8. Similar levels of membranous expression were observed between the non-transduced, eGFP, wtCx40, and A96S groups.

5.3.3 Immunoblotting

Immunoblotting of tissue lysates revealed increased Cx40 within left atria transduced to express wild-type or mutant Cx40 as shown in Figure 5.9. Quantitative densitometry revealed a greater level of expression within the wtCx40 and mutant groups compared to non-transduced and eGFP groups. Immunoblotting of tissue lysates also revealed increased Cx43 expression within

Figure 5.7: Immunofluorescence of atrial tissue sections for Cx40.

Cx40 is represented by red signal (arrows). Nuclei are stained blue. Cx40 is expressed at the intercalated discs in the wtCx40 and A96S groups.

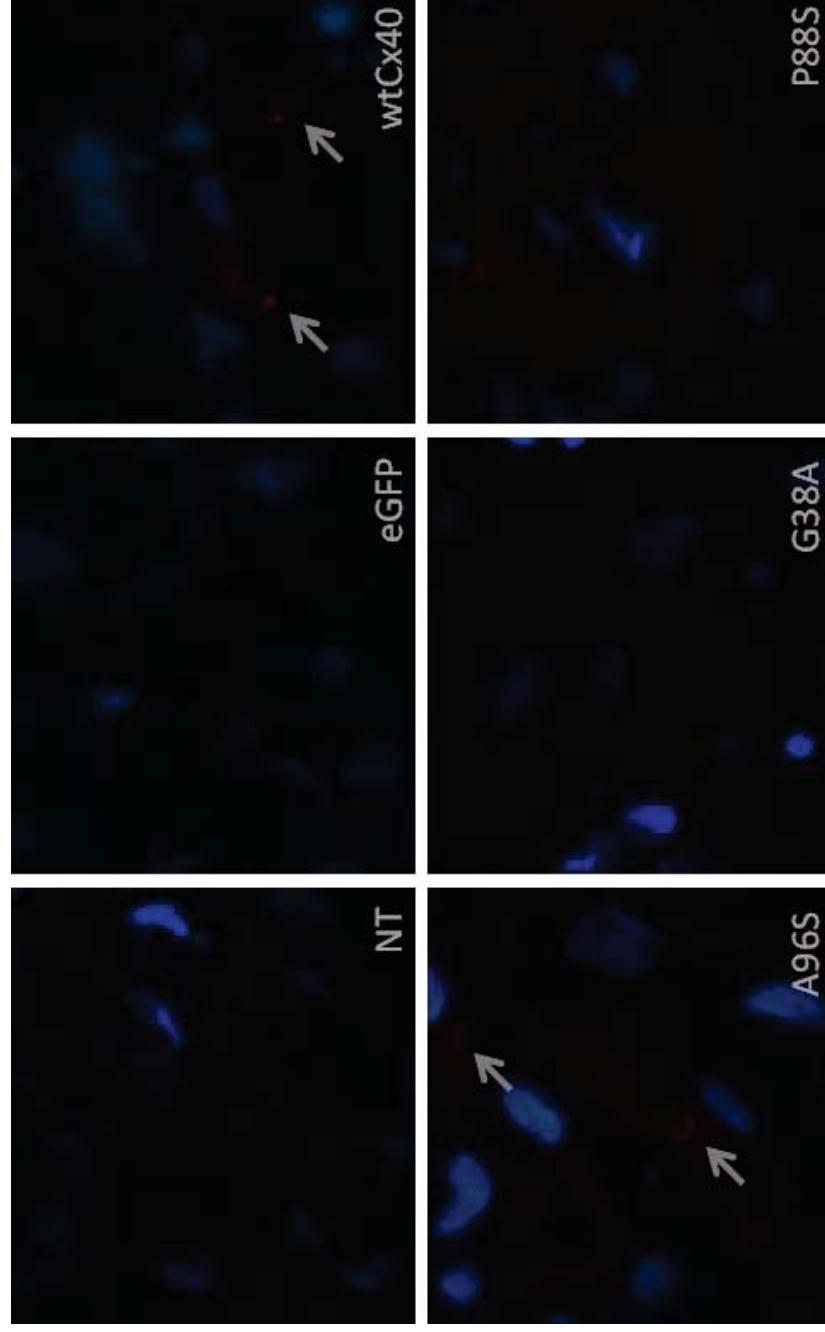


Figure 5.8: Immunofluorescence of atrial tissue sections for Cx43.

Cx43 is represented by green signal. Nuclei are stained blue. Membranous Cx43 expression is markedly reduced within the G38A and P88S groups.

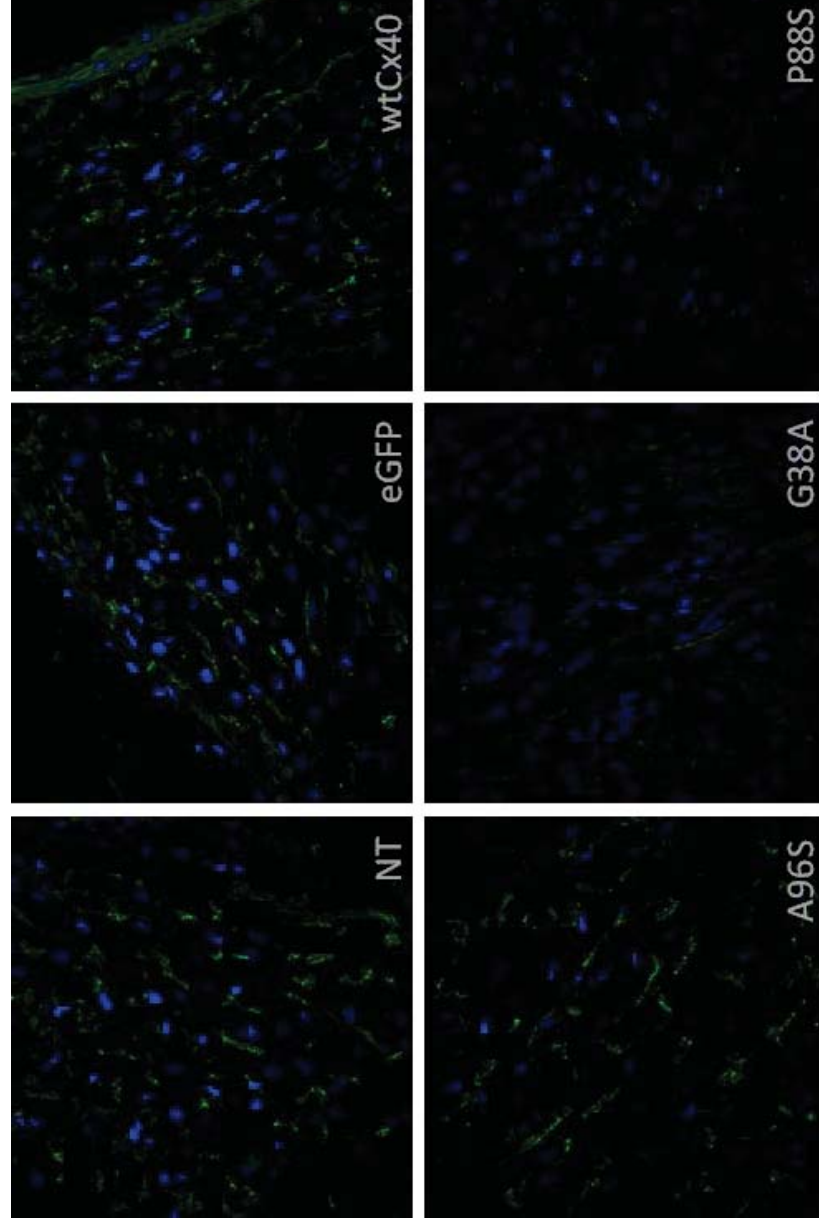




Figure 5.9: Immunoblots for left atrial Cx40 expression

Immunoblots and densitometry for Cx40 normalised to β -tubulin and expressed relative to the non-transduced group. Cx40 over expression is seen within left atria of groups transduced to express a wild-type or a mutant Cx40 (n = 1 for each group).

β -tubulin						
Cx40						
Group	NT	eGFP	wtCx40	A96S	G38A	P88S
Densitometry	-	0.72	4.21	6.50	3.06	1.29

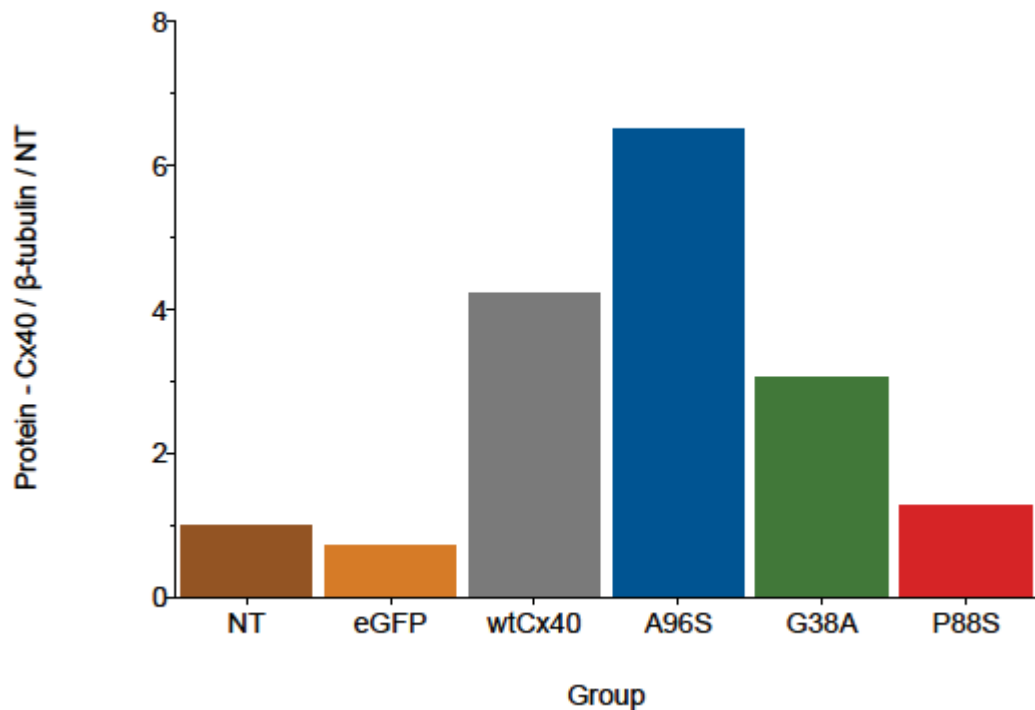


Figure 5.10: Immunoblots for left atrial Cx43 expression.

Immunoblots and densitometry for Cx43 normalised to β -tubulin and expressed relative to the non-transduced group. Significantly increased Cx43 expression is seen within left atria from the P88S group when compared to the wtCx40 group ($p < 0.05$; $n = 3$ for all groups).

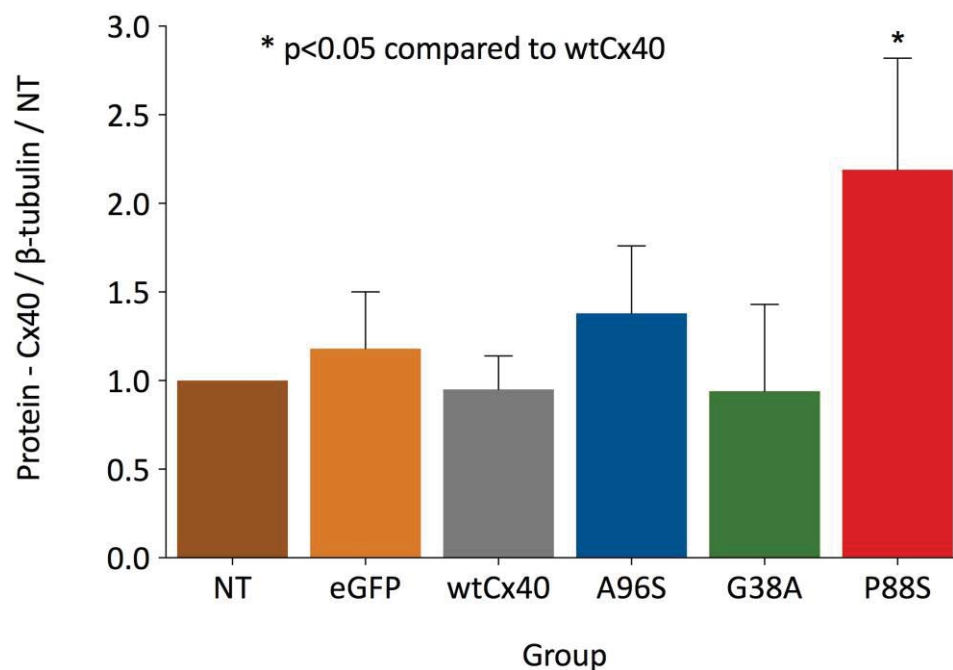
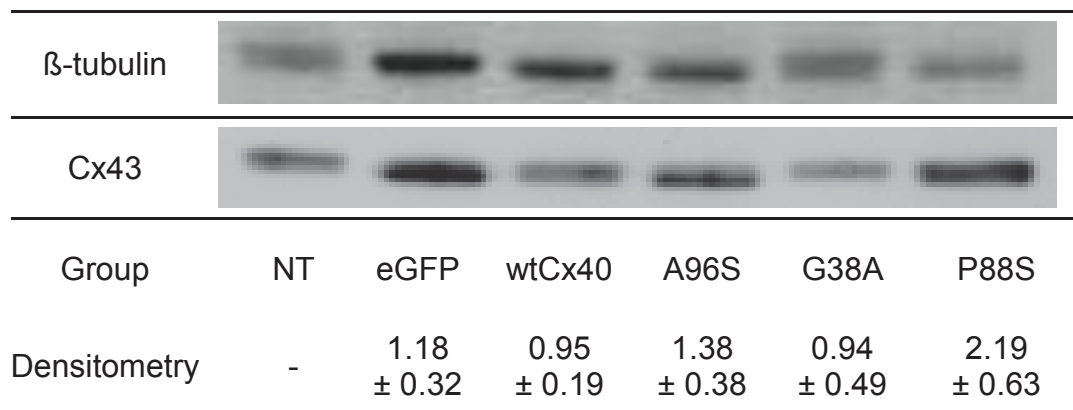
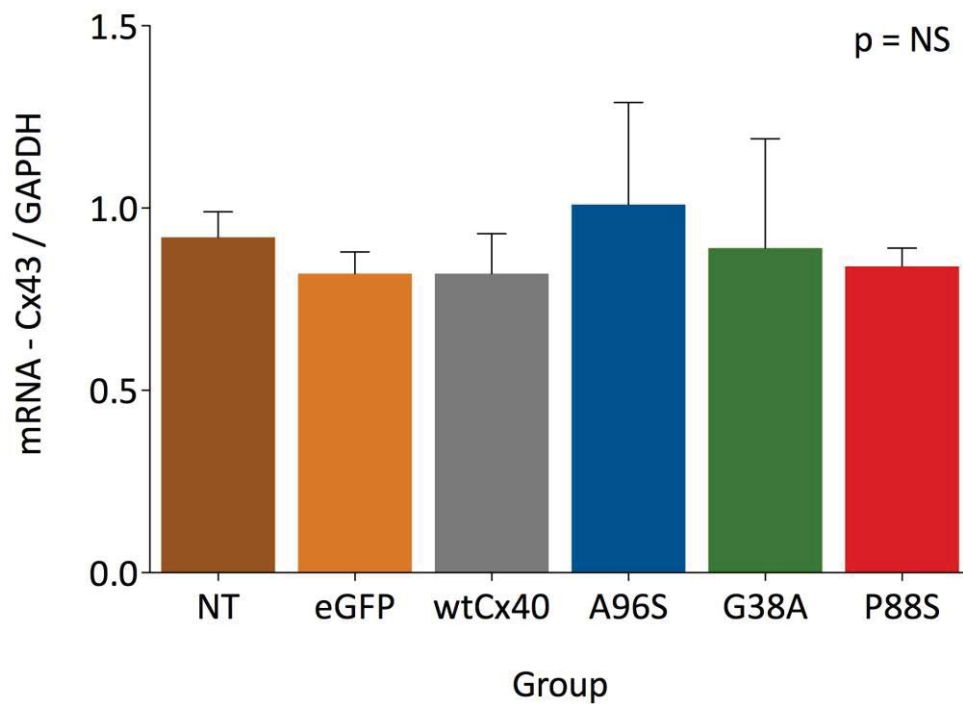


Figure 5.11: Quantitative PCR for Cx43 mRNA.

Cx43 mRNA levels normalised to GAPDH mRNA within atrial tissue for each study group. There was no significant difference in each of the mutant groups when compared to the wtCx40 group. (n=3 for all groups)

NT	eGFP	wtCx40	A96S	G38A	P88S
0.92 ± 0.07	0.82 ± 0.06	0.82 ± 0.11	1.01 ± 0.28	0.89 ± 0.30	0.84 ± 0.05



the P88S group when compared to the wtCx40 transduced group as shown in Figure 5.10. Cx43 levels were similar between the G38A and wtCx40 groups.

5.3.4 Connexin43 mRNA

There was no significant difference in the left atrial Cx43 mRNA levels of each mutant Cx40 group when compared to the wtCx40 group as shown in Figure 5.11.

5.3.4 Inflammation and fibrosis

Inflammation scores of left atrial sections stained with haematoxylin and eosin were similar between wild-type and all mutant Cx40 groups as shown in Figure 5.12. Furthermore, there was no significant difference in levels of fibrosis between wild-type and mutant Cx40 groups as shown in Figure 5.13.

Figure 5.12: Haematoxylin and eosin stains of atrial tissue

Representative left atrial tissue sections stained with haematoxylin and eosin from each of the study groups and non-transduced atria. Inflammation score from 96 images within each group is provided (mean \pm SD). No significant difference is observed between means of the A96S, G38A, and P88S groups when compared to wtCX40.

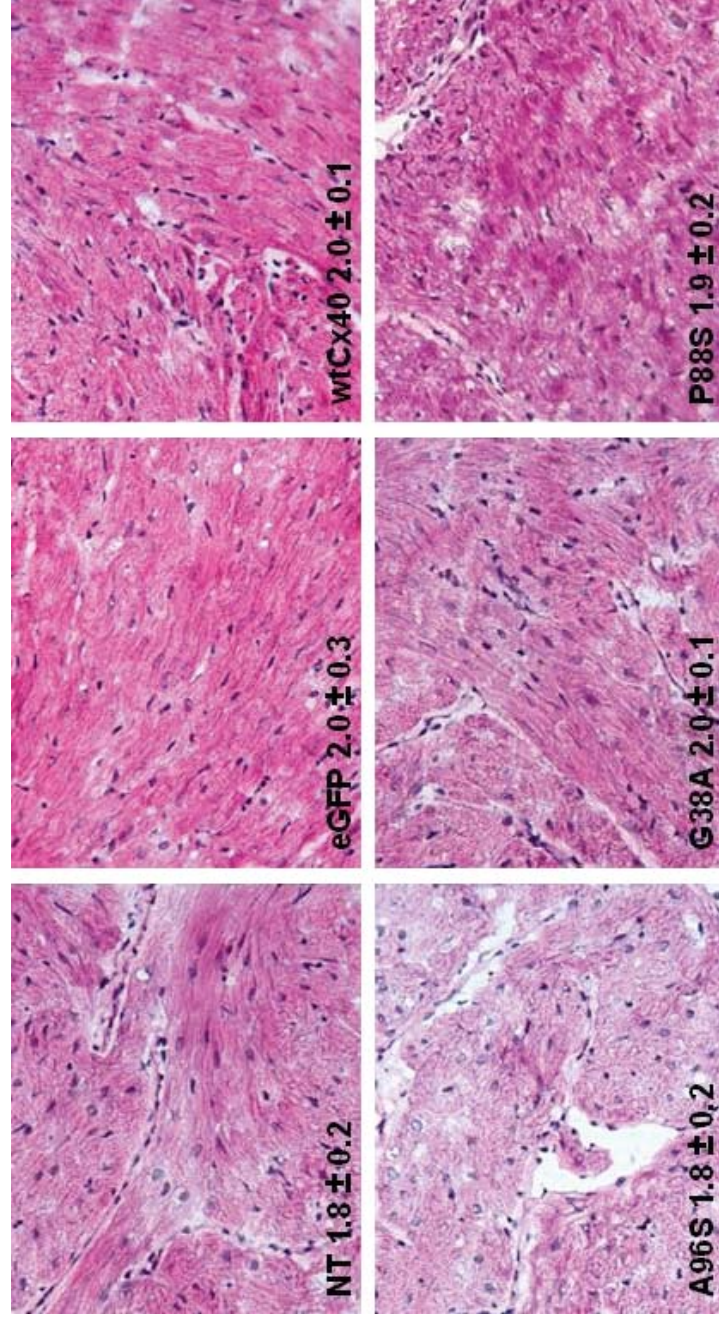
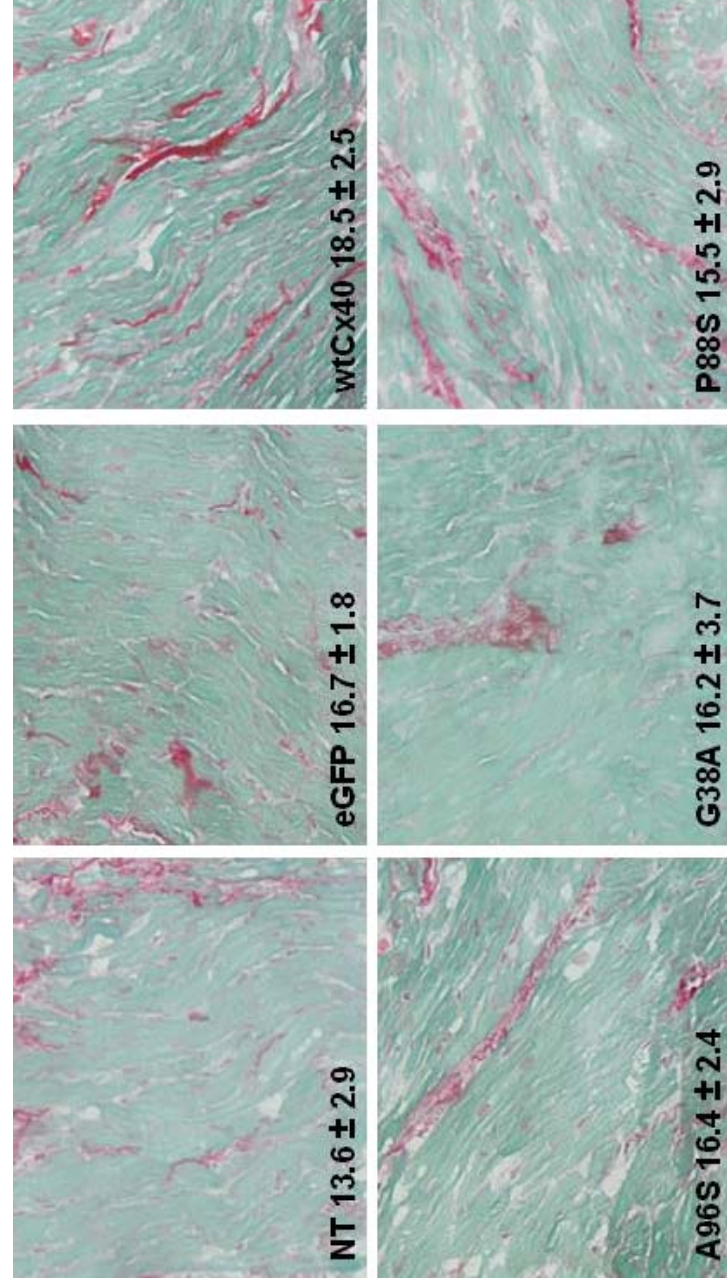


Figure 5.13: Pico Sirius Red stains of atrial tissue

Representative left atrial tissue sections stained with Pico Sirius Red from each of the study groups and non-transduced atria. Percentage fibrosis from 96 images within each group is provided (mean \pm SD). No significant difference is observed between means of the A96S, G38A, and P88S groups when compared to wtCX40.



5.4 Discussion

For the first time, we have clearly demonstrated the pathogenicity of the Cx40 mutations A96S, G38A, and P88S within an *in vivo* model. In addition to precipitating conduction slowing, all three mutations also result in an increased propensity for AF.

5.4.1 *In vivo* characteristics of A96S, P88S, and G38A

Given the consistency of our immunofluorescence studies between atrial tissue and neonatal cardiomyocyte cultures, the mutations P88S and G38A likely exert their effects by reducing native Cx43 myocyte coupling while the mutation A96S likely co-localises with connexin43 in gap junction channels to mediate conduction slowing.

The observed parameters of left atrial conduction slowing (P wave prolongation and bifid morphology) caused by A96S, P88S, and G38A within the left atrium are consistent with the results from our primary cardiomyocyte cultures. Such findings are also commonly seen in patients with left atrial enlargement. While echocardiographic or MRI assessment for left atrial enlargement in our rats was not performed, the absence of significant

inflammatory and fibrotic changes between wild-type and mutant Cx40 groups in combination with conduction slowing on our MEA studies makes this possibility unlikely.

Interestingly immunoblotting detected no change in overall cellular levels of Cx43 within the G38A group and an increase within the P88S group. This was surprising given the reduction in observed membranous expression of Cx43 and the lack of increased intracellular expression with immunofluorescence. In addition, Cx43 mRNA levels were similar between all study groups. It is likely that Cx40 and Cx43 share the same intracellular machinery for production. Hence P88S and G38A may be inducing conformational changes within Cx43. Such changes may cause steric hindrance, rendering the epitope inaccessible to our anti-Cx43 antibody on immunofluorescence. The denaturation process involved with sodium dodecyl sulfate polyacrylamide gel electrophoresis (SDS-PAGE), which utilises a detergent, heat, and reducing agent, may remove this inaccessibility.⁹³

5.4.2 *In vivo* characteristics of wild-type connexin40

The lack of left atrial conduction slowing and resistance to AF induction following wtCx40 transduction was unexpected, particularly given the demonstration of conduction slowing within primary cardiomyocyte cultures. The *in vivo* results of wtCx40 are however consistent with a recent study that transduced porcine atria with wtCx40.⁶³ In that study, wtCx40 reduced the vulnerability of porcine atria to pacing induced AF. The mechanism behind the reduced vulnerability of atria to AF following Cx40 gene transfer is unclear. One possibility is that wild-type Cx40 fails to form heterotypic heteromeric channels *in vivo*, an effect that may speed up conduction. Alternatively, the level of transduction achieved within our study may not have been high enough to result in significant conduction slowing from the formation of heterotypic heteromeric channels. Hence the presence of a Cx40 mutation (such as A96S) with a negative dominant effect on Cx43 function is also required to tip the balance towards conduction slowing. Other possible mechanisms include alterations in the phosphorylation status of both Cx40 and Cx43 and alterations in the availability of sodium channels.

5.4.3 Other considerations

Sodium channels, which contribute to the cardiac action potential, have been shown to co-localise with Cx43 at the intercalated discs.^{88, 89} The occurrence and significance of sodium channel co-localisation with Cx40 is unknown however. While Cx43-null cardiomyocytes possess similar action potential characteristics to wild-type cardiomyocytes, the effects of Cx40 alterations have not been studied.^{90, 91} Hence an alteration in sodium channel expression may also contribute to some of the conduction slowing observed. Nevertheless, alterations in sodium channel expression would not act to exclude each mutant as pathogenic.

The transgenes used within this study utilised a lentivector to facilitate transduction and a tissue non-specific CMV promoter to drive expression. Hence non-cardiomyocytes (predominately fibroblasts), which constitute more than 50% of the cells in an adult rat heart, would have expressed Cx40.^{94, 95} Although no evidence exists for fibroblast-myocyte coupling within the native heart outside of the sino-atrial node, transduced fibroblasts may have coupled with transduced cardiomyocytes within the setting of our study and modulated myocyte action potential propagation.^{96,}

⁹⁷ The indirect *in vivo* findings of conduction slowing (longer P wave durations) within the atria for each of the studied Cx40 groups were however consistent with our *in vitro* studies making this possibility less likely.

5.4.4 Implications of somatic mutations

Familial AF is considered a monogenic disorder with an autosomal dominant pattern of inheritance. Non-familial AF however, which represents the majority of cases of AF, is considered primarily a polygenic disorder.^{98, 99} The existence of functional somatic mutations however provides an alternative explanation for the otherwise lack of identification of causative mutations in the setting of non-familial AF. Further support for a possible larger role of somatic mechanisms in the generation of atrial arrhythmias is the existence of electrical rotors or focal drivers of AF identified in most patients with AF.¹⁰⁰ It is quite possible that the substrates supporting these rotors are secondary to localised areas of somatic mutation.

Given the mosaic nature of expression of somatic mutations within the atria, no technique currently exists that could conclusively

diagnose a somatic mutation as a precipitant for AF within a patient. This is of particular concern as we enter into the era of human cardiac gene therapy.¹⁰¹

The rescue of porcine atrial myocardium from pacing induced AF after over expression of wild-type Cx43 in combination with an absence of detrimental ventricular arrhythmias, suggests that a “blanket” approach of Cx43 up regulation in all patients with idiopathic AF may be a possible therapeutic strategy. This would bypass the need for confirming the presence of a somatic mutation in patients with AF. Studies with a large animal model, and a more clinically relevant viral vector such as an adeno-associated virus, is however required to further assess the therapeutic and safety profile of this approach.

CHAPTER 6

Summary and General Discussion

With an aging population and an increasing prevalence of atrial fibrillation (AF), an imperative exists to elucidate the mechanisms underpinning arrhythmogenesis. The ability of connexins to influence cardiac conduction has long been recognised as described within section 1.2. Results of studies into the roles connexin isotypes and mutations play in cardiac conduction and arrhythmogenesis have however been conflicting, largely owing to the models used for study. The technique of somatic gene transfer presented itself as a unique method for overcoming some of the technical limitations of these models. To date, only 3 other studies have utilised somatic gene transfer techniques in an attempt to understand the functional significance of connexins, each with their own limitations.^{62, 63, 102} The contents of this thesis in this regard, describe an innovative approach for using such techniques to understand the role of connexin mutations in atrial physiology and AF.

6.1 *In Vitro* Ion Channel Screening Systems

6.1.1 Summary

Tissue conduction velocity is determined by drivers and resistors to action potential conduction. The main drivers of conduction include the action potential amplitude and speed of action potential generation (determined by fast sodium channels) while the main resistors are intracellular cytoplasmic resistance and intercellular resistance (determined by the quantity and functional characteristics of connexons located at gap junctions). Traditionally, studies into the role of ion channel mutations in cardiac diseases have utilised voltage clamping techniques (single or dual cell) or cell culture mapping^{10, 55, 103, 104}. Voltage clamping techniques fail to consider the modulating extracellular effects of a multicellular system. Cell culture studies have used cells from genetically engineered animal models and thus are likely subject to some of the confounding effects and limitations.

The validation of somatic gene transfer techniques combined with the multi-electrode array (MEA) system within this thesis (Chapter 3) shows that this technique can be used to assess ion channels that affect both action potential characteristics and intercellular

communication. This novel and fundamental work provides a sound basis upon which this technology can be further applied to the functional characterisation of the rapidly accumulating list of identified ion channel mutations. With the advent of inexpensive printable circuit board (PCB) technology for MEA production¹⁰⁵ and induced pluripotent stem cell (IPS) technologies¹⁰⁶, successful clinical transition of this work has the potential to provide a personalised diagnostic service.¹⁰⁷

6.1.2 Limitations

6.1.2.1 Measurement of cellular electrical activity

The methodological limitations of this study system, while not detracting from the strength of the central observation of conduction velocity, do constrain complete assessment of cellular electrical activity. In particular, far field potentials represent an indirect gross spatiotemporal measurement of surrounding cellular action potentials. Hence while changes in far field potentials resemble alterations in a patient's surface electrocardiogram (such as QT duration), they are less sensitive compared to the cellular action potential.¹⁰⁷ Hence complete characterisation of ion channel function in the setting of a mutation is best performed with

patch clamping techniques until higher resolution technologies can be validated.

6.1.2.2 NRVM cellular electrophysiology

It is well established that gap junction distribution is diffuse and immature within neonatal rat ventricular myocyte (NRVM) cultures.⁹² In addition, NRVM's undergo further differentiation during isolation and culture, a process that lacks the electrical, mechanical, and humoral regulatory factors found within an *in vivo* environment. Hence although being cardiomyocytes, the NRVM ion channel expression profile is likely neither that of a mature atrial or ventricular myocyte. Consequently there are bound to be false positive and false negative results when compared to mature myocytes in an *in vivo* setting.

6.1.2.3 Protein interactions and toxicity

It is clear that NRVM's are highly sensitive to non-physiological manipulations and require gentle and careful processing. While lentivirus has been shown to not adversely affect NRVM function for up to at least 10 days, function is sensitive to the type of protein overexpressed.^{83, 85} Hence careful optimisation is required

for each type of ion channel before mutational screening can be performed.

6.1.3 Future Directions

6.1.3.1 MEA technology

With the advent of printable circuit board technology, the cost of manufacturing an MEA has dropped to less than a dollar (Australian). As a result, it is now feasible to produce MEA chips customised for the purpose of high throughput mutational screening. Although electrode size, number, and density are confined in part by resolution limitations of conventional PCB technology, advances have been made in the adaptation of other electronic technologies such as complementary metal–oxide–semiconductor (CMOS) chips for the purpose of MEA studies. With a spatiotemporal resolution in excess of 4000 electrodes within an approximate area of 7mm², the electrophysiological data that stands to be gleaned is immense.¹⁰⁸

6.1.3.2 Cellular technologies

Cardiomyocytes produced from induced pluripotent stem (IPS) cells have shown great promise for personalised medicine, with their successful use for medication optimisation in patients with channelopathies. From a mutational screening point of view, they provide the perfect context for ion channel study on an MEA, and in the setting of germline mutations obviate the need for viral vectors.¹⁰⁷ Unfortunately at this point in time, IPS technology is within its infancy and a great deal remains to be elucidated about the differentiation pathways involved before high throughput screening can be performed.

6.2 Connexin Mutations and Conduction

6.2.1 Summary

Fibrillatory conduction within the atrium occurs when a re-entrant circuit of very short cycle length drives tissue faster than which 1:1 conduction can occur.¹⁰⁹ Re-entrant circuits require the presence of unidirectional block and alterations in conduction velocity.¹¹⁰ Both connexin40 (Cx40) and connexin43 (Cx43) have been shown to modulate conduction velocity as described in section 1.2. The novel mutant Cx40 studies of Chapter 4 show that when each mutant is co-expressed with endogenous Cx43, they modulate conduction velocity in a manner different to that of wild-type Cx40.

Using an acute somatic gene transfer technique, the Cx40 mutants A96S, P88S, and G38A were characterised as loss of function mutants with slowing of conduction in MEA studies. The loss of function imparted to gap junctions differed mechanistically between each mutant.

The ramifications of these results are 2 fold. Firstly they provide an insight into how 'real world' germline and somatic mutations

might give rise to substrate supportive of AF. Secondly they highlight the mutational screening benefit of the MEA system in a 'real world' scenario.

6.2.2 Limitations

6.2.2.1 Somatic mutations and *in vitro* implications

The majority of mutations identified within the various channelopathies have an autosomal dominant pattern of inheritance.¹¹¹ In this setting, the combination of *in vitro* confirmation of channel impairment, phenotype/genotype correlations, and co-segregation studies are sufficient to confirm any given mutation as pathogenic. Given the focal nature of cardiac somatic mutations however, phenotype/genotype correlations are more difficult, requiring prior electrophysiological mapping of re-entrant circuits (rotors) within the atria. Furthermore, co-segregation studies are not possible. Hence the loss of function demonstrated with the P88S and G38A somatic Cx40 mutations while significant, does not have the corroborative support of genotype/phenotype correlations and co-segregation studies to implicate them as the definitive cause of AF within the patients in which they were identified.

6.2.2.2 Germline mutations and *in vitro* implications

Traditional voltage clamping studies of germline mutations in ion channels responsible for action potential generation often reveal a gain or loss of function that can be directly correlated with ECG characteristics such as QT prolongation or shortening. *In vitro* studies of the germline mutation A96S while revealing reduced gap junction conductance¹⁰ and alterations in conduction velocity cannot be directly correlated with the phenotype of AF. A phenotype suggestive of atrial conduction slowing however, namely P wave prolongation, was identified in the patient with an A96S mutation and his 2 sons, both of whom also carried the mutation.¹⁰ A more extensive familial screen was not mentioned to comment on definite co-segregation of this finding. Both sons were not afflicted with AF. The A96S allele was also identified within 1 out of 170 asymptomatic controls giving a population allele frequency of 0.3%. Although high when compared to mutations responsible for channelopathies such as long QT syndrome (>0.04%), the allele frequency was not helpful given the small sample size of the control group and the higher population prevalence of AF compared to other channelopathies. Furthermore, the relatively young (48 year old) control carrier

could go on to develop AF as they age. The Exome Variant Server Database for population allele frequencies did not contain data regarding the A96S Cx40 allele at the time of writing this thesis.¹¹²

6.2.3 Future Directions

Bearing in mind the interpretative limitations of *in vitro* studies, *in vivo* studies are required to determine whether the functional impairment imparted to gap junctions by mutations is able to create a substrate supportive of AF. Acute somatic gene transfer using a direct topical approach for viral delivery to a small rodent heart would be the ideal *in vivo* model. Such a model would circumvent the congenital limitations associated with genetically engineered models. Furthermore, a topical approach for viral delivery to the atria would minimise the potential for lethal ventricular arrhythmias due to ventricular transduction. Other advantages of a small animal model include the need for only small quantities of virus for transduction, ease of manipulation and handling, and convenience of housing and animal care.

6.3 Connexin Mutations and Arrhythmia

6.3.1 Summary

Review of the anatomy of the atrium reveals 4 specialised conduction paths (inter-atrial tract, internodal tracts - anterior, middle, and posterior) for rapid impulse propagation from the SA node to the left atrium and AV node.¹¹³ It would be expected then that should atrial activation originate from an ectopic re-entrant focus of short cycle length (such as one possibly caused by a somatic connexin mutation), the atria would have a reduced ability to conduct in a 1:1 manner and hence an increased vulnerability for AF. If conduction slowing is also impaired by a germline connexin mutation, then complex patterns of atrial activation with more severe conduction block might also be expected in the setting of an ectopic re-entrant focus. Of note, Bagwe and co-workers demonstrated complex atrial activation with conduction block during a relatively slow ectopic atrial rhythm in Langendorff-perfused Cx40 knock-out hearts, an effect that resolved with ablation of the ectopic foci (section 1.2.2.1).

We previously demonstrated that the Cx40 somatic mutations A96S, P88S, and G38A imparted a loss of function to gap

junctions with conduction slowing in NRVM cultures. Within Chapter 5, we have gone on to show that gap junction loss of function is capable of producing a tissue substrate that is supportive of AF. Using acute somatic gene transfer to the left atrium via a topical route of administration, we demonstrated an increased propensity for inducible AF following atrial transduction with each of the Cx40 mutations.

The ramifications of these findings are four fold: firstly they confirm a role for connexins in the pathogenesis of idiopathic AF, secondly they strengthen the evidence for somatic mutations in general as a cause for idiopathic AF, thirdly they represent the first *in vivo* non-genetically engineered genotype-phenotype correlations ever performed for a mutation identified in a patient with AF, and lastly they raise the possibility of a wider role of somatic mutations in the generation of all types of cardiac arrhythmias.

6.3.2 Limitations

6.3.2.1 Mechanisms: From cells to arrhythmia

The mechanism behind which conduction slowing causes AF in the setting of acute gene transfer to a rat atrium remains to be elucidated. Whether AF induction was a result of an inability of the left atrium to conduct in a 1 to 1 fashion from our stimulation protocol or whether transduction has given rise to a re-entrant circuit via an area of mosaic expression is not known. In addition, the rat myocardium is clearly different from humans with respect to size, ECG characteristics, and ion channel expression. Hence results that may be significant within a rat heart may not necessarily be so within a human heart. Lastly, non-specific cellular transduction was performed within rat atria. Hence transduced non-myocytes may have played a role in modulating impulse propagation and altered the propensity for AF.

6.3.3. Future Directions

Given the inherent limitations of Chapter 5, further evaluation within a large animal model is required. Acute somatic gene transfer should be performed both focally and globally throughout

the atria to understand how both focal somatic mutations and diffuse germline mutations may give rise to AF. With a larger sized heart, it becomes possible to map the atrium using standard electrophysiological techniques as used in humans. In addition, the impact of radiofrequency ablation would be readily assessable. Finally, assessment of the therapeutic benefits of mutant allele knockdown and/or overexpression of either Cx40 or Cx43 is needed prior to moving to therapeutic clinical trials.

6.4 Connexin Mutations and Atrial Arrhythmia – Final Comments

The clinically relevant studies hereto described within this thesis provide the first glimpses into the role somatic mutations may play within the intact heart. In addition to confirming the findings of previous studies (section 1.2) with respect to the ability of connexins to modulate impulse propagation, they also represent the first ever *in vivo* non-genetically engineered genotype-phenotype correlations for AF.

Large animal models using similar somatic gene transfer techniques, clinically relevant targeted viral vectors, and electrophysiological mapping are now required to better understand the mechanisms behind which impairment of conduction precipitates AF and to determine the best strategy for a genetic cure. Armed with such information, a rational targeted approach to human therapy becomes feasible, particularly as we move into an era of gene therapy.

Lastly, as IPS cell and organ generation technologies progress, it will become feasible to apply the techniques used within this

thesis directly to human cells and tissue, bypassing the need for animal studies.

CHAPTER 7

Bibliography

1. Go AS, Hylek EM, Phillips KA, Chang Y, Henault LE, Selby JV, Singer DE. Prevalence of diagnosed atrial fibrillation in adults: National implications for rhythm management and stroke prevention: The anticoagulation and risk factors in atrial fibrillation (atria) study. *JAMA*. 2001;285:2370-2375
2. Feinberg WM, Blackshear JL, Laupacis A, Kronmal R, Hart RG. Prevalence, age distribution, and gender of patients with atrial fibrillation. Analysis and implications. *Arch Intern Med*. 1995;155:469-473
3. Australian bureau of statistics 2011, population by age and sex, regions of australia, 2011, cat. No. 3235.0, abs, canberra.
4. Australian bureau of statistics 2009, australian social trends, march 2009, cat. No. 4102.0, abs, canberra.
5. Wolf PA, Abbott RD, Kannel WB. Atrial fibrillation as an independent risk factor for stroke: The framingham study. *Stroke*. 1991;22:983-988
6. Benjamin EJ, Wolf PA, D'Agostino RB, Silbershatz H, Kannel WB, Levy D. Impact of atrial fibrillation on the risk of death: The framingham heart study. *Circulation*. 1998;98:946-952
7. Hylek EM, Evans-Molina C, Shea C, Henault LE, Regan S. Major hemorrhage and tolerability of warfarin in the first year of therapy among elderly patients with atrial fibrillation. *Circulation*. 2007;115:2689-2696
8. Cappato R, Calkins H, Chen SA, Davies W, Iesaka Y, Kalman J, Kim YH, Klein G, Packer D, Skanes A. Worldwide survey on the methods, efficacy, and safety of catheter

ablation for human atrial fibrillation. *Circulation*. 2005;111:1100-1105

9. Kanagaratnam P, Cherian A, Stanbridge RD, Glenville B, Severs NJ, Peters NS, Kanagaratnam P, Cherian A, Stanbridge RDL, Glenville B, Severs NJ, Peters NS. Relationship between connexins and atrial activation during human atrial fibrillation. *Journal of Cardiovascular Electrophysiology*. 2004;15:206-216
10. Gollob MH, Jones DL, Krahn AD, Danis L, Gong XQ, Shao Q, Liu X, Veinot JP, Tang AS, Stewart AF, Tesson F, Klein GJ, Yee R, Skanes AC, Guiraudon GM, Ebihara L, Bai D. Somatic mutations in the connexin 40 gene (*gja5*) in atrial fibrillation. *N Engl J Med*. 2006;354:2677-2688
11. Thibodeau IL, Xu J, Li Q, Liu G, Lam K, Veinot JP, Birnie DH, Jones DL, Krahn AD, Lemery R, Nicholson BJ, Gollob MH. Paradigm of genetic mosaicism and lone atrial fibrillation: Physiological characterization of a connexin 43-deletion mutant identified from atrial tissue. *Circulation*. 2010;122:236-244
12. Zimmer DB, Green CR, Evans WH, Gilula NB. Topological analysis of the major protein in isolated intact rat liver gap junctions and gap junction-derived single membrane structures. *The Journal of biological chemistry*. 1987;262:7751-7763
13. Sohl G, Willecke K. Gap junctions and the connexin protein family. *Cardiovasc Res*. 2004;62:228-232
14. Laird DW. Life cycle of connexins in health and disease. *Biochem J*. 2006;394:527-543
15. Fallon RF, Goodenough DA. Five-hour half-life of mouse liver gap-junction protein. *The Journal of cell biology*. 1981;90:521-526
16. Laird DW, Puranam KL, Revel JP. Turnover and phosphorylation dynamics of connexin43 gap junction

- protein in cultured cardiac myocytes. *Biochem J.* 1991;273(Pt 1):67-72
17. Beardslee MA, Laing JG, Beyer EC, Saffitz JE. Rapid turnover of connexin43 in the adult rat heart. *Circ Res.* 1998;83:629-635
 18. Berne RM, Levy MN. Cardiovascular physiology. 2001:312
 19. Neyton J, Trautmann A. Single-channel currents of an intercellular junction. *Nature.* 1985;317:331-335
 20. Veenstra RD, DeHaan RL. Measurement of single channel currents from cardiac gap junctions. *Science.* 1986;233:972-974
 21. Burt JM, Spray DC. Single-channel events and gating behavior of the cardiac gap junction channel. *Proc Natl Acad Sci U S A.* 1988;85:3431-3434
 22. Traub O, Eckert R, Lichtenberg-Frate H, Elfgang C, Bastide B, Scheidtmann KH, Hulser DF, Willecke K. Immunochemical and electrophysiological characterization of murine connexin40 and -43 in mouse tissues and transfected human cells. *Eur J Cell Biol.* 1994;64:101-112
 23. Valiunas V, Weingart R, Brink PR. Formation of heterotypic gap junction channels by connexins 40 and 43. *Circ Res.* 2000;86:E42-49
 24. Cottrell GT, Burt JM. Heterotypic gap junction channel formation between heteromeric and homomeric cx40 and cx43 connexons. *Am J Physiol Cell Physiol.* 2001;281:C1559-1567
 25. Cottrell GT, Wu Y, Burt JM. Cx40 and cx43 expression ratio influences heteromeric/ heterotypic gap junction channel properties. *American journal of physiology. Cell physiology.* 2002;282:C1469-1482
 26. Davis LM, Kanter HL, Beyer EC, Saffitz JE. Distinct gap junction protein phenotypes in cardiac tissues with disparate

- conduction properties. *J Am Coll Cardiol.* 1994;24:1124-1132
27. Gros D, Jarry-Guichard T, Ten Velde I, de Maziere A, van Kempen MJ, Davoust J, Briand JP, Moorman AF, Jongsma HJ. Restricted distribution of connexin40, a gap junctional protein, in mammalian heart. *Circ Res.* 1994;74:839-851
 28. Spach MS, Heidlage F, Dobler PC. The dual nature of anisotropic discontinuous conduction in the heart. *In cardiac electrophysiology: From cell to bedside.* 2000:213-221
 29. Spach MS, Heidlage JF, Dolber PC, Barr RC. Changes in anisotropic conduction caused by remodeling cell size and the cellular distribution of gap junctions and na(+) channels. *J Electrocardiol.* 2001;34 Suppl:69-76
 30. Saffitz JE, Kanter HL, Green KG, Tolley TK, Beyer EC. Tissue-specific determinants of anisotropic conduction velocity in canine atrial and ventricular myocardium. *Circ Res.* 1994;74:1065-1070
 31. Hoyt RH, Cohen ML, Saffitz JE. Distribution and three-dimensional structure of intercellular junctions in canine myocardium. *Circ Res.* 1989;64:563-574
 32. Luke RA, Saffitz JE. Remodeling of ventricular conduction pathways in healed canine infarct border zones. *J Clin Invest.* 1991;87:1594-1602
 33. Peters NS, Coromilas J, Severs NJ, Wit AL. Disturbed connexin43 gap junction distribution correlates with the location of reentrant circuits in the epicardial border zone of healing canine infarcts that cause ventricular tachycardia. *Circulation.* 1997;95:988-996
 34. Gu H, Smith FC, Taffet SM, Delmar M. High incidence of cardiac malformations in connexin40-deficient mice. *Circ Res.* 2003;93:201-206
 35. Kirchhoff S, Kim JS, Hagendorff A, Thonnissen E, Kruger O, Lamers WH, Willecke K. Abnormal cardiac conduction and

morphogenesis in connexin40 and connexin43 double-deficient mice. *Circ Res.* 2000;87:399-405

36. Ya J, Erdtsieck-Ernste EB, de Boer PA, van Kempen MJ, Jongsma H, Gros D, Moorman AF, Lamers WH. Heart defects in connexin43-deficient mice. *Circ Res.* 1998;82:360-366
37. Simon AM, Goodenough DA, Paul DL. Mice lacking connexin40 have cardiac conduction abnormalities characteristic of atrioventricular block and bundle branch block. *Curr Biol.* 1998;8:295-298
38. Delorme B, Dahl E, Jarry-Guichard T, Marics I, Briand JP, Willecke K, Gros D, Theveniau-Ruissy M. Developmental regulation of connexin 40 gene expression in mouse heart correlates with the differentiation of the conduction system. *Dev Dyn.* 1995;204:358-371
39. Kirchhoff S, Nelles E, Hagendorff A, Kruger O, Traub O, Willecke K. Reduced cardiac conduction velocity and predisposition to arrhythmias in connexin40-deficient mice. *Curr Biol.* 1998;8:299-302
40. Hagendorff A, Schumacher B, Kirchhoff S, Luderitz B, Willecke K. Conduction disturbances and increased atrial vulnerability in connexin40-deficient mice analyzed by transesophageal stimulation. *Circulation.* 1999;99:1508-1515
41. Verheule S, van Batenburg CA, Coenjaerts FE, Kirchhoff S, Willecke K, Jongsma HJ. Cardiac conduction abnormalities in mice lacking the gap junction protein connexin40. *J Cardiovasc Electrophysiol.* 1999;10:1380-1389
42. Bagwe S, Berenfeld O, Vaidya D, Morley GE, Jalife J. Altered right atrial excitation and propagation in connexin40 knockout mice. *Circulation.* 2005;112:2245-2253
43. Urthaler F, Krames BL, James TN. Selective effects of pentobarbital on automaticity and conduction in the intact canine heart. *Cardiovasc Res.* 1974;8:46-57

44. Kass DA, Hare JM, Georgakopoulos D. Murine cardiac function: A cautionary tail. *Circ Res*. 1998;82:519-522
45. Thomas SA, Schuessler RB, Berul CI, Beardslee MA, Beyer EC, Mendelsohn ME, Saffitz JE. Disparate effects of deficient expression of connexin43 on atrial and ventricular conduction: Evidence for chamber-specific molecular determinants of conduction. *Circulation*. 1998;97:686-691
46. Morley GE, Vaidya D, Samie FH, Lo C, Delmar M, Jalife J. Characterization of conduction in the ventricles of normal and heterozygous cx43 knockout mice using optical mapping.[see comment]. *Journal of Cardiovascular Electrophysiology*. 1999;10:1361-1375
47. Eloff BC, Lerner DL, Yamada KA, Schuessler RB, Saffitz JE, Rosenbaum DS. High resolution optical mapping reveals conduction slowing in connexin43 deficient mice. *Cardiovasc Res*. 2001;51:681-690
48. Fogoros RN. Electrophysiologic testing. 2006:296
49. Waldo AL, Waldo AL. Mechanisms of atrial fibrillation. *Journal of Cardiovascular Electrophysiology*. 2003;14:S267-274
50. Tamaddon HS, Vaidya D, Simon AM, Paul DL, Jalife J, Morley GE. High-resolution optical mapping of the right bundle branch in connexin40 knockout mice reveals slow conduction in the specialized conduction system. *Circ Res*. 2000;87:929-936
51. Guerrero PA, Schuessler RB, Davis LM, Beyer EC, Johnson CM, Yamada KA, Saffitz JE. Slow ventricular conduction in mice heterozygous for a connexin43 null mutation. *J Clin Invest*. 1997;99:1991-1998
52. Zhou J, Jeron A, London B, Han X, Koren G. Characterization of a slowly inactivating outward current in adult mouse ventricular myocytes. *Circ Res*. 1998;83:806-814

53. Gutstein DE, Morley GE, Tamaddon H, Vaidya D, Schneider MD, Chen J, Chien KR, Stuhlmann H, Fishman GI. Conduction slowing and sudden arrhythmic death in mice with cardiac-restricted inactivation of connexin43. *Circ Res*. 2001;88:333-339
54. Leaf DE, Feig JE, Vasquez C, Riva PL, Yu C, Lader JM, Kontogeorgis A, Baron EL, Peters NS, Fisher EA, Gutstein DE, Morley GE, Leaf DE, Feig JE, Vasquez C, Riva PL, Yu C, Lader JM, Kontogeorgis A, Baron EL, Peters NS, Fisher EA, Gutstein DE, Morley GE. Connexin40 imparts conduction heterogeneity to atrial tissue. *Circ Res*. 2008;103:1001-1008
55. Beauchamp P, Yamada KA, Baertschi AJ, Green K, Kanter EM, Saffitz JE, Kleber AG. Relative contributions of connexins 40 and 43 to atrial impulse propagation in synthetic strands of neonatal and fetal murine cardiomyocytes. *Circ Res*. 2006;99:1216-1224
56. Elvan A, Huang XD, Pressler ML, Zipes DP. Radiofrequency catheter ablation of the atria eliminates pacing-induced sustained atrial fibrillation and reduces connexin 43 in dogs. *Circulation*. 1997;96:1675-1685
57. van der Velden HM, van Kempen MJ, Wijffels MC, van Zijverden M, Groenewegen WA, Allessie MA, Jongsma HJ. Altered pattern of connexin40 distribution in persistent atrial fibrillation in the goat. *Journal of cardiovascular electrophysiology*. 1998;9:596-607
58. van der Velden HM, Ausma J, Rook MB, Hellemons AJ, van Veen TA, Allessie MA, Jongsma HJ. Gap junctional remodeling in relation to stabilization of atrial fibrillation in the goat. *Cardiovasc Res*. 2000;46:476-486
59. Guerra JM, Everett THt, Lee KW, Wilson E, Olgin JE, Guerra JM, Everett THt, Lee KW, Wilson E, Olgin JE. Effects of the gap junction modifier rotigaptide (zp123) on atrial conduction and vulnerability to atrial fibrillation. *Circulation*. 2006;114:110-118

60. Shiroshita-Takeshita A, Sakabe M, Haugan K, Hennan JK, Nattel S, Shiroshita-Takeshita A, Sakabe M, Haugan K, Hennan JK, Nattel S. Model-dependent effects of the gap junction conduction-enhancing antiarrhythmic peptide rotigaptide (zp123) on experimental atrial fibrillation in dogs. *Circulation*. 2007;115:310-318
61. Rossman EI, Liu K, Morgan GA, Swillo RE, Krueger JA, Gardell SJ, Butera J, Gruver M, Kantrowitz J, Feldman HS, Petersen JS, Haugan K, Hennan JK, Rossman EI, Liu K, Morgan GA, Swillo RE, Krueger JA, Gardell SJ, Butera J, Gruver M, Kantrowitz J, Feldman HS, Petersen JS, Haugan K, Hennan JK. The gap junction modifier, gap-134 [(2s,4r)-1-(2-aminoacetyl)-4-benzamido-pyrrolidine-2-carboxylic acid], improves conduction and reduces atrial fibrillation/flutter in the canine sterile pericarditis model. *J Pharmacol Exp Ther*. 2009;329:1127-1133
62. Bikou O, Thomas D, Trappe K, Lugenbiel P, Kelemen K, Koch M, Soucek R, Voss F, Becker R, Katus HA, Bauer A. Connexin 43 gene therapy prevents persistent atrial fibrillation in a porcine model. *Cardiovasc Res*. 2011;92:218-225
63. Igarashi T, Finet JE, Takeuchi A, Fujino Y, Strom M, Greener ID, Rosenbaum DS, Donahue JK. Connexin gene transfer preserves conduction velocity and prevents atrial fibrillation. *Circulation*. 2012;125:216-225
64. Kanagaratnam P, Rothery S, Patel P, Severs NJ, Peters NS. Relative expression of immunolocalized connexins 40 and 43 correlates with human atrial conduction properties. *J Am Coll Cardiol*. 2002;39:116-123
65. Ryu K, Li L, Khrestian CM, Matsumoto N, Sahadevan J, Ruehr ML, Van Wagoner DR, Efimov IR, Waldo AL. Effects of sterile pericarditis on connexins 40 and 43 in the atria: Correlation with abnormal conduction and atrial arrhythmias. *Am J Physiol Heart Circ Physiol*. 2007;293:H1231-1241
66. Beardslee MA, Lerner DL, Tadros PN, Laing JG, Beyer EC, Yamada KA, Kleber AG, Schuessler RB, Saffitz JE.

Dephosphorylation and intracellular redistribution of ventricular connexin43 during electrical uncoupling induced by ischemia. *Circ Res.* 2000;87:656-662

67. Dupont E, Ko Y, Rothery S, Coppen SR, Baghai M, Haw M, Severs NJ. The gap-junctional protein connexin40 is elevated in patients susceptible to postoperative atrial fibrillation. *Circulation.* 2001;103:842-849
68. Polontchouk L, Haefliger JA, Ebel B, Schaefer T, Stuhlmann D, Mehlhorn U, Kuhn-Regnier F, De Vivie ER, Dhein S. Effects of chronic atrial fibrillation on gap junction distribution in human and rat atria. *J Am Coll Cardiol.* 2001;38:883-891
69. Kostin S, Klein G, Szalay Z, Hein S, Bauer EP, Schaper J. Structural correlate of atrial fibrillation in human patients. *Cardiovasc Res.* 2002;54:361-379
70. Nao T, Ohkusa T, Hisamatsu Y, Inoue N, Matsumoto T, Yamada J, Shimizu A, Yoshiga Y, Yamagata T, Kobayashi S, Yano M, Hamano K, Matsuzaki M. Comparison of expression of connexin in right atrial myocardium in patients with chronic atrial fibrillation versus those in sinus rhythm. *Am J Cardiol.* 2003;91:678-683
71. Kanagaratnam P, Cherian A, Stanbridge RD, Glenville B, Severs NJ, Peters NS. Relationship between connexins and atrial activation during human atrial fibrillation. *J Cardiovasc Electrophysiol.* 2004;15:206-216
72. Gaborit N, Steenman M, Lamirault G, Le Meur N, Le Bouter S, Lande G, Leger J, Charpentier F, Christ T, Dobrev D, Escande D, Nattel S, Demolombe S. Human atrial ion channel and transporter subunit gene-expression remodeling associated with valvular heart disease and atrial fibrillation. *Circulation.* 2005;112:471-481
73. Wetzel U, Boldt A, Lauschke J, Weigl J, Schirdewahn P, Dorszewski A, Doll N, Hindricks G, Dhein S, Kottkamp H. Expression of connexins 40 and 43 in human left atrium in

atrial fibrillation of different aetiologies. *Heart*. 2005;91:166-170

74. Rucker-Martin C, Milliez P, Tan S, Decrouy X, Recouvreur M, Vranckx R, Delcayre C, Renaud JF, Dunia I, Segretain D, Hatem SN. Chronic hemodynamic overload of the atria is an important factor for gap junction remodeling in human and rat hearts. *Cardiovasc Res*. 2006;72:69-79
75. Sinno H, Derakhchan K, Libersan D, Merhi Y, Leung TK, Nattel S. Atrial ischemia promotes atrial fibrillation in dogs. *Circulation*. 2003;107:1930-1936
76. Freshney RI. *Culture of animal cells*. Chicester: John Wiley and Sons Ltd; 2010.
77. Zufferey R, Nagy D, Mandel RJ, Naldini L, Trono D. Multiply attenuated lentiviral vector achieves efficient gene delivery in vivo. *Nat Biotechnol*. 1997;15:871-875
78. Zufferey R, Dull T, Mandel RJ, Bukovsky A, Quiroz D, Naldini L, Trono D. Self-inactivating lentivirus vector for safe and efficient in vivo gene delivery. *J Virol*. 1998;72:9873-9880
79. Dull T, Zufferey R, Kelly M, Mandel RJ, Nguyen M, Trono D, Naldini L. A third-generation lentivirus vector with a conditional packaging system. *J Virol*. 1998;72:8463-8471
80. Zufferey R, Donello JE, Trono D, Hope TJ. Woodchuck hepatitis virus posttranscriptional regulatory element enhances expression of transgenes delivered by retroviral vectors. *J Virol*. 1999;73:2886-2892
81. Zennou V, Petit C, Guetard D, Nerhbass U, Montagnier L, Charneau P. Hiv-1 genome nuclear import is mediated by a central DNA flap. *Cell*. 2000;101:173-185
82. Sastry L, Johnson T, Hobson MJ, Smucker B, Cornetta K. Titering lentiviral vectors: Comparison of DNA, rna and marker expression methods. *Gene Ther*. 2002;9:1155-1162

83. Sekar RB, Kizana E, Smith RR, Barth AS, Zhang Y, Marban E, Tung L. Lentiviral vector-mediated expression of gfp or kir2.1 alters the electrophysiology of neonatal rat ventricular myocytes without inducing cytotoxicity. *Am J Physiol Heart Circ Physiol.* 2007;293:H2757-2770
84. Milstein ML, Musa H, Balbuena DP, Anumonwo JM, Auerbach DS, Furspan PB, Hou L, Hu B, Schumacher SM, Vaidyanathan R, Martens JR, Jalife J. Dynamic reciprocity of sodium and potassium channel expression in a macromolecular complex controls cardiac excitability and arrhythmia. *Proc Natl Acad Sci U S A.* 2012;109:E2134-2143
85. Kizana E, Chang CY, Cingolani E, Ramirez-Correa GA, Sekar RB, Abraham MR, Ginn SL, Tung L, Alexander IE, Marban E. Gene transfer of connexin43 mutants attenuates coupling in cardiomyocytes: Novel basis for modulation of cardiac conduction by gene therapy. *Circ Res.* 2007;100:1597-1604
86. Nakagami T, Tanaka H, Dai P, Lin SF, Tanabe T, Mani H, Fujiwara K, Matsubara H, Takamatsu T. Generation of reentrant arrhythmias by dominant-negative inhibition of connexin43 in rat cultured myocyte monolayers. *Cardiovasc Res.* 2008;79:70-79
87. Kizana E, Foster DB, Sekar RB, Tung L, Marban E. Abstract 504: Co-expression of connexin40 or 45 slows connexin43-dependent conduction. *Circulation.* 2007;116:87-88
88. Cohen SA. Immunocytochemical localization of rh1 sodium channel in adult rat heart atria and ventricle. Presence in terminal intercalated disks. *Circulation.* 1996;94:3083-3086
89. Mays DJ, Foose JM, Philipson LH, Tamkun MM. Localization of the kv1.5 k+ channel protein in explanted cardiac tissue. *J Clin Invest.* 1995;96:282-292
90. Wang L, Feng ZP, Kondo CS, Sheldon RS, Duff HJ. Developmental changes in the delayed rectifier k+ channels in mouse heart. *Circ Res.* 1996;79:79-85

91. Johnson CM, Green KG, Kanter EM, Bou-Abboud E, Saffitz JE, Yamada KA. Voltage-gated na⁺ channel activity and connexin expression in cx43-deficient cardiac myocytes. *J Cardiovasc Electrophysiol*. 1999;10:1390-1401
92. Peters NS, Severs NJ, Rothery SM, Lincoln C, Yacoub MH, Green CR. Spatiotemporal relation between gap junctions and fascia adherens junctions during postnatal development of human ventricular myocardium. *Circulation*. 1994;90:713-725
93. Waehneltd TV. Sodium dodecyl sulfate in protein chemistry. *Biosystems*. 1975;6:176-187
94. Barth AS, Kizana E, Smith RR, Terrovitis J, Dong P, Leppo MK, Zhang Y, Miake J, Olson EN, Schneider JW, Abraham MR, Marban E. Lentiviral vectors bearing the cardiac promoter of the na⁺-ca²⁺ exchanger report cardiogenic differentiation in stem cells. *Mol Ther*. 2008;16:957-964
95. Nag AC. Study of non-muscle cells of the adult mammalian heart: A fine structural analysis and distribution. *Cytobios*. 1980;28:41-61
96. Ongstad EL, Gourdie RG. Myocyte-fibroblast electrical coupling: The basis of a stable relationship? *Cardiovasc Res*. 2012;93:215-217
97. Gaudesius G, Miragoli M, Thomas SP, Rohr S. Coupling of cardiac electrical activity over extended distances by fibroblasts of cardiac origin. *Circ Res*. 2003;93:421-428
98. Liu X, Wang F, Knight AC, Zhao J, Xiao J. Common variants for atrial fibrillation: Results from genome-wide association studies. *Hum Genet*. 2012;131:33-39
99. Xiao J, Liang D, Chen YH. The genetics of atrial fibrillation: From the bench to the bedside. *Annu Rev Genomics Hum Genet*. 2011;12:73-96
100. Narayan SM, Krummen DE, Shivkumar K, Clopton P, Rappel WJ, Miller JM. Treatment of atrial fibrillation by the

ablation of localized sources: Confirm (conventional ablation for atrial fibrillation with or without focal impulse and rotor modulation) trial. *J Am Coll Cardiol*. 2012;60:628-636

101. Jessup M, Greenberg B, Mancini D, Cappola T, Pauly DF, Jaski B, Yaroshinsky A, Zsebo KM, Dittrich H, Hajjar RJ. Calcium upregulation by percutaneous administration of gene therapy in cardiac disease (cupid): A phase 2 trial of intracoronary gene therapy of sarcoplasmic reticulum ca²⁺-atpase in patients with advanced heart failure. *Circulation*. 2011;124:304-313
102. Greener ID, Sasano T, Wan X, Igarashi T, Strom M, Rosenbaum DS, Donahue JK. Connexin43 gene transfer reduces ventricular tachycardia susceptibility after myocardial infarction. *Journal of the American College of Cardiology*. 2012;60:1103-1110
103. Priori SG, Pandit SV, Rivolta I, Berenfeld O, Ronchetti E, Dhamoon A, Napolitano C, Anumonwo J, di Barletta MR, Gudapakam S, Bosi G, Stramba-Badiale M, Jalife J. A novel form of short qt syndrome (sqt3) is caused by a mutation in the *kcnj2* gene. *Circ Res*. 2005;96:800-807
104. Bennett PB, Yazawa K, Makita N, George AL, Jr. Molecular mechanism for an inherited cardiac arrhythmia. *Nature*. 1995;376:683-685
105. Giovangrandi L, Gilchrist KH, Whittington RH, Kovacs GTA. Low-cost microelectrode array with integrated heater for extracellular recording of cardiomyocyte cultures using commercial flexible printed circuit technology. *Sensor Actuat B-Chem*. 2006;113:545-554
106. Takahashi K, Tanabe K, Ohnuki M, Narita M, Ichisaka T, Tomoda K, Yamanaka S. Induction of pluripotent stem cells from adult human fibroblasts by defined factors. *Cell*. 2007;131:861-872
107. Matsa E, Rajamohan D, Dick E, Young L, Mellor I, Staniforth A, Denning C. Drug evaluation in cardiomyocytes derived

from human induced pluripotent stem cells carrying a long qt syndrome type 2 mutation. *Eur Heart J.* 2011;32:952-962

108. Frey U, Sanchez-Bustamante CD, Ugniwenko T, Heer F, Sedivy J, Hafizovic S, Roscic B, Fussenegger M, Blau A, Egert U, Hierlemann A. Cell recordings with a cmos high-density microelectrode array. *Conf Proc IEEE Eng Med Biol Soc.* 2007;2007:167-170
109. Waldo AL. Mechanisms of atrial fibrillation. *J Cardiovasc Electrophysiol.* 2003;14:S267-274
110. Kleber AG, Rudy Y. Basic mechanisms of cardiac impulse propagation and associated arrhythmias. *Physiol Rev.* 2004;84:431-488
111. Ackerman MJ, Priori SG, Willems S, Berul C, Brugada R, Calkins H, Camm AJ, Ellinor PT, Gollob M, Hamilton R, Hershberger RE, Judge DP, Le Marec H, McKenna WJ, Schulze-Bahr E, Semsarian C, Towbin JA, Watkins H, Wilde A, Wolpert C, Zipes DP. Hrs/ehra expert consensus statement on the state of genetic testing for the channelopathies and cardiomyopathies this document was developed as a partnership between the heart rhythm society (hrs) and the european heart rhythm association (ehra). *Heart Rhythm.* 2011;8:1308-1339
112. Exome variant server, nhlbi go exome sequencing project (esp), seattle, wa (url: <http://evs.gs.washington.edu/evs/>) [aug 2012 accessed].
113. Catalano JT. *Guide to ecg analysis.* Philadelphia: Lippincott; 2002.